USING ELECTRICAL RESISTANCE TOMOGRAPHY (ERT) AND COMPUTATIONAL FLUID DYNAMICS (CFD) TO STUDY THE MIXING OF YIELD-PSEUDOPLASTIC FLUIDS IN THE SMX STATIC MIXER

By

Sinthuran Jegatheeswaran

B.Eng. Ryerson University, Toronto, Canada, 2014

A Thesis

Presented to Ryerson University

in Partial Fulfillment of Requirements for the Degree of

Master of Applied Science

in the Program of Chemical Engineering

Toronto, Ontario, Canada, 2016

ABSTRACT

Sinthuran Jegatheeswaran

Using electrical resistance tomography (ERT) and computational fluid dynamics (CFD) to study the mixing of yield-pseudo plastic fluids in the SMX static mixer

MASc, Chemical Engineering, Ryerson University, Toronto, 2016

In this study, both electrical resistance tomography (ERT) and computational fluid dynamics (CFD) were employed to study the performance of the SMX static mixer in the mixing of a secondary fluid in a yield-pseudo plastic primary fluid. Using ERT, the effects of the primary fluid rheology, the primary fluid flow rate, and the secondary fluid type (Newtonian and non-Newtonian) were investigated. A CFD model was then developed for the fluid mixing in the SMX static mixer and was validated using the experimental pressure drop and the ERT mixing index measurements. Using the validated CFD flow model, the effects of the primary/secondary flow ratio and the secondary fluid viscosity on the mixing performance of the SMX static mixer were analyzed. The results from this study revealed that the SMX static mixer was effective for the mixing of highly viscous fluids especially at a lower primary/secondary flow ratio.

ACKNOWLEDGEMENTS

I would like to express my sincere gratitude and appreciation to my supervisors, Dr. Farhad Ein-Mozaffari and Dr. Jiangning Wu, for their guidance and motivation for this work.

I also want to be thankful to all the staff and technicians, especially Ali Hemmati and Daniel Boothe for their support in designing and implementing my experimental setup.

I also would like to acknowledge the advice and helpful suggestion of my friends in the Fluid Mixing Technology Laboratory at Ryerson University.

Dedicated to my mom (Viji), dad (Jega), and my supervisor (Dr.Farhad Ein-Mozaffari)

for their encouragement in the pursuit of excellence and

success in my life

TABLE OF CONTENTS

LIST OF TABLES

LIST OF FIGURES

NOMENCLATURE

A	Surface area of the ith electrode (cm^2)
CoV	Coefficient of variance
$\bar{C}$	Average concentration for a homogenous mixture (kg/m^3)
C_m	Concentration measured in a quadrant (kg/m^3)
$C_{is}(x)$	Standardized concentration value at location x (kg/m^3)
$C_i(x)$	Concentration value at location x (kg/m^3)
C	Right Cauchy-Green strain tensor
Ci_i	Local conductivity measurement (mS/cm)
$\bar{Ci}$	Average conductivity (mS/cm)
$\bar{\bar{D}}$ or $\frac{\partial v_z}{\partial r}$	Shear rate (s^{-1})
D	Diameter of the pipe (m)
D_m	Molecular diffusivity (m^2/s)
$E\ (\vartheta)$	Exit age distribution function
F	Deformation gradient tensor
$F\ (\vartheta)$	Cumulative curve
g	Gravitational acceleration (m/s^2)
$G(r|r_0)$	Green's function
$J(r_0)$	Current source at an internal point, r_0 (mA)
J_i	Current density applied on the ith electrode (mA/cm^2)
K_g	No. of grid points
K	Consistency index $(Pa.s^n)$
K'	Consistency index for local power law parameters $(Pa.s^n)$
I_{disp}	Index of dispersion

ID	Internal Diameter (m)
L_D	Mean length scale
L/D	Length/Diameter (i.e. Aspect ratio)
$\widehat{M}$	Unit vector denoting the direction of particle
M	Number of quadrats
$N\,(h)$	Total number of pairs of data separated by distance h
n	Flow behaviour index
n'	Flow behaviour index for local power law parameters
np	Total number of pixels for each tomography plane
N	Number of electrodes per plane
R_x	Correlogram
r_0	Actual position of the current source (*cm*)
r	Location of the solution to be calculated (*cm*)
T	Transpose
t	Time (*s*)
Δt	Time span
v	Velocity (*m/s*)
$\dot{V}$	Volumetric flow rate (*L/min*)
V	Volume of pipe (*m³*)
$\bar{v}$	Mean velocity (*m/s*)
w	Local mass fraction
X	Initial position of fluid particles
x	Position of particle at varying time
$\bar{x}_1$	Mean value of the PNN distribution
wt%	Weight percent

Greek Letters

σ^2	Variance
γ_x	Variograms
ϕ	Flow map
π	Stretching
φ	Electrical potential
λ	Lyapunov exponent
ϑ	Time (RTD)
τ	Mean residence time
μ_R	Mean value in log-normal distribution model
σ_R	Standard deviation in log-normal distribution model
ρ	Density (kg/m^3)
τ_y	Yield stress (Pa)
ξ	Ratio of yield stress to the wall shear stress
τ_{rz}	Shear stress (Pa)
η	Apparent viscosity (Kg/ms)
τ_w	Shear rate at the wall (s^{-1})
$\dot{\gamma}_{Nw}$	Newtonian shear rate (s^{-1})
$\dot{\gamma}_w$	Non-Newtonian shear rate (s^{-1})

Abbreviations

2D	Two-Dimensions
3D	Three-Dimensions
CFD	Computational Fluid Dynamics
CSR	Complete Spatial Randomness
DAS	Data Acquisition System

ERT   Electrical Resistance Tomography

HPCVL High Performance Computing Virtual Laboratory

LIF   Laser Induced Fluorescence

LBP   Linear Back Projection

PRESTO PREssure STaggering Option

PNN   Point-to-Nearest-Neighbour

RMS   Root Mean Square

RTD   Residence Time Distribution

SIMPLE Semi-Implicit Method for Pressure-Linked Equation

1.INTRODUCTION

Effective mixing of non-Newtonian fluids is often challenging attributing to its inherent complex rheological properties. Complex rheology of non-Newtonian fluids causes non-ideal flows such as channeling, recirculation and dead zones and this non-ideality creates barriers for effective mixing (Patel *et al.,* 2013; Ein-Mozaffari *et al.,* 2003; Ein-Mozaffari *et al.,* 2005). Research studies have been conducted on the continuous flow mixing of non-Newtonian fluids in stirred vessels and Patel *et al.* (2012 and 2015) investigated the effect of fluid rheology, fluid flow rate, impeller geometry, impeller diameter, and impeller speed etc. They reported that non-ideality in non-Newtonian fluid flow increased when the fluid yield stress and feed flow rate were increased. Negligence on this non-ideality behavior could lead to significant errors when designing a unit of mixing operation (Levenspiel, 1998).

Continuous mixing is more preferred over batch mixing as it provides higher production capacity with minimal operation time (Nauman, 2002). Compared to the mechanical agitated system, the static mixers are more appealing to various industrial processes attributing to the minimum consumption of energy intake. Static mixers are motionless mixers which are inserted inside the pipe to alter the fluid flow directions and thus promoting a chaotic mixing behavior. Static mixer creates chaos within the fluid and enhances the fluid mixing process.With the lower investment and operational costs as compared to the mechanical agitator, the practice of static mixers remains competitive (Bauman, 2001; Hobbs, 1997; Junker *et al.*, 1994). Liu *et al.* (2006) reported that shear thinning fluid exhibited a more effective mixing quality in the SMX static mixer compared to the Newtonian fluid. It was also reported that the mixing rate was independent of the primary fluid flowrate for the centerline injection in the SMX static mixer and it was the centerline injection that found to be more effective than the off-center injection (Zalc *et al.,* 2003). Zalc *et al.* (2002) reported that, for Reynolds Number <1, the mixing performance was independent of Reynolds Number for the Newtonian fluid in the SMX static mixer. Lower primary fluid flow rates have been recommended for the effective mixing of viscous fluids in the SMX mixer taken into the consideration of both the mixing rates and the energy requirement (Zalc *et al.,* 2002).

Another research study was conducted on Kenics KM static mixer using Planar Laser Induced Fluorescence (PLIF) method to investigate the effect of primary/secondary stream flow ratio and the effect of superficial velocity of the secondary fluid on the mixing quality of the shear thinning fluid. The fluid was Carbopol 940 which obeys the Herschel-Buckley fluid model. It was reported that, for a higher primary/secondary fluid flow ratio and for a higher velocity of the secondary fluid, a better mixing quality was observed (Alberini *et al*., 2014). The effect of the viscosity ratio between the secondary and the primary fluids on the mixing of these two miscible fluids was studied on the SMX static mixer and the occurrence of the viscous fingering phenomena was reported for the mixing of two miscible fluids with higher viscosity ratio (Ventresca *et al*., 2002; Cao *et al*., 2003). Karoui *et al*. (1998) studied that the higher secondary/primary stream velocity ratio increased the mixing quality of two miscible fluids in the Sulzer SMV static mixer operated under the turbulent flow regime. This research study involved the mixing of a dyed aqueous solution of rhodamine B in water.

Yenjaichon *et al*. (2012) studied the effect of the softwood kraft pulp fibre mass concentration on the mixing quality and reported a poor mixing quality at a higher fibre mass concentration. They employed in-line jet mixing techniques to investigate the effect of the jet velocity, mainstream pipe velocity, and jet-to-pipe diameter.

From the data available in the open literature, a well-defined protocol is not yet fully developed to enhance the in-line mixing operation of the SMX static mixer especially for the yield-pseudoplastic fluids- a type of shear thinning fluids that require a shear stress exceeding the yield stress in order for the fluid deformation. Hence, it is the curiosity of the author to investigate which parameter is more crucial to enhance the mixing of two miscible fluids. Following Alberini's approach (2014) on Kenics KM static mixer, a comprehensive study is conducted on a different type of static mixer, SMX, to investigate the effect of the primary fluid flow rates, secondary/primary velocity ratio, secondary fluid viscosity, and the primary fluid rheology on the mixing of two miscible fluids. This research study will help industries to design an effective in-line mixing operation while lowering the energy requirement. Continuous mixing operation at lower primary flow rates leads to a lower pressure drop. Thus, it requires a lower consumption of energy in order to pump a viscous fluid through the pipe. The mixing performance of the SMX static mixer was investigated experimentally in terms of the mixing index and the pressure drop

measurement. The experimental pressure drop and the mixing index data were then used to validate the CFD flow model. The CFD model was then extensively used to investigate how well a mixing operation could be effectively designed to enhance the mixing of two miscible fluids in the SMX static mixer.

Chapter two provides a brief literature review of the type of commercial static mixers and their applications while elaborating on the mixing characterization tools used to quantify the mixing performance of a static mixer.

Chapter three provides insights into the experimental setup and the operation of the electrical resistance tomography (ERT).

Chapter four offers general information about the computational fluid dynamics (CFD) such as the flow geometry, grid generation, grid independency, and ANSYS Fluent solver settings.

Chapter five discusses the CFD model validation, the results obtained using ERT and CFD, and provides details into the mixing mechanism of the two miscible fluids in the SMX static mixer.

Chapter six summarizes the overall conclusions of this research study and provides recommendations for future work.
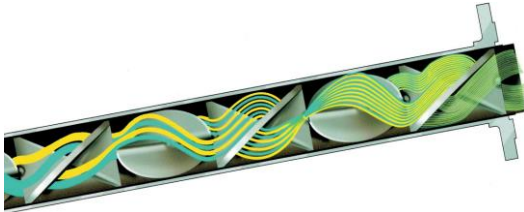
2.LITERATURE REVIEW

2.1 INTRODUCTION

Despite the fact that the design of first static mixer was patented as earliest as 1895, they were only scientifically developed in the 1960's. Nevertheless, it only became available in Europe alone during the 1970's (Anton, 1979). The US developed its first commercial unit called the Kenics Static mixer and filed a patent on 1971, and has been commonly used in wide varieties of industrial process operations (Grout and Devellian, 1974). More than thirty different types of commercial static mixers are available (Thakur, 2003) and each of its kind leads to fluid mixing differently by altering the fluid flow direction. A static mixer is generally effective when the radial mixing is dominant over a shortest flow path as compared to the axial mixing (Fialova *et al*., 1985; Pahl and Muschelknautz, 1982; Baker, 1991; Rader *et al*., 1989).

Static mixer is mostly ideal for continuous flow processes which require short residence time. Unlike dynamic mixers, it could process a wide range of viscosities with a minimum space and maintenance requirements (Myers *et al*., 1997). Since the shear force exerted on fluids is generally lower for static mixers, it is very ideal for industrial processes which are shear-sensitive (Junker *et al*., 1994). Static mixers are often the first choice if the process is continuous attributing to its aforementioned potential benefits. The most commonly used commercial static mixers and its typical applications in industrial settings are highlighted in Table 2.1 and Table 2.2, respectively. This report will highlight the significance of mixing characterization tools reported in the literature for the type of non-Newtonian fluids particularly the power law and yield-pseudoplastic fluids.
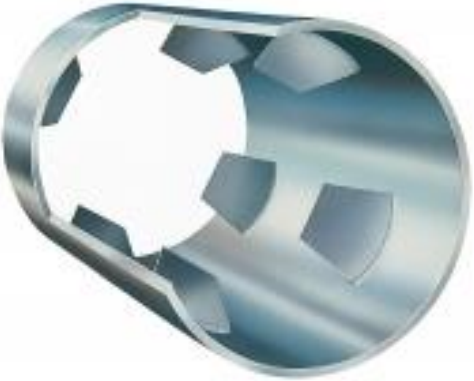
Table 2.1: Types of commercially available static mixers

Company	Static mixers	Description	Mixer Geometry
Lightnin (SPX, 2015) www.spx.com	Series 45 inliner	The helical plate design of this mixer allows a distinct fluid flow that helps achieve desired process results.	

Chemineer (Chemineer) www.chemineer.com	Kenics KM series static mixers	Helical mixing element, patented in early 1970's, directs the fluid flow radially towards the pipe wall and back to the centerline of pipe. It has alternating right- and left-hand elements	

	KMX-V Mixers	It is ideal for demanding mixing applications with wide disparate viscosities or volumetric ratio. It was patented in 2002 and optimized in 2012 for difficult mixing application	

	HEV Mixers	It optimizes the available turbulent energy into an efficient mixing process while inducing vortices around the mixing element edges.	

	Ultra Tab	This type of mixers provide rapid mixing in short distances. Commonly useful in water treatment, desalination plants, and chemical processing applications. It is usually associated with low pressure drop.	

	WVM mixers	It consists of a wall injection point, a pre-distribution tab and banks of trapezoidal shaped mixing elements. Three WVM models A, B and C are available and each model has a different dimensions and spacing of the mixing elements.	

| Sulzer (Sulzer) www.**sulzer**.com | SMX | It has a compact designs and it is ideal for mixing operation with disparate fluid viscosities. It is very suitable for mixing of sensitive products under minimal shear stress. | |

	SMX plus	It is very much similar to a standard SMX mixer except that it lowers the pressure drop by 50% and helps companies save money.	

		SMV	It consists of intersecting corrugated plates and channels that facilitate rapid mixing of any number of additives within the mixing zone. It is suitable for dispersive mixing especially when a higher shear force is required or mass transfer in turbulent flow regime between two immiscible phases.	
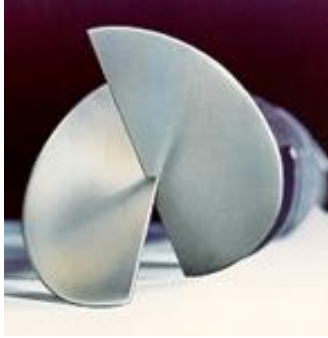
| | SMI | The mixing elements create large counter rotating vortices and thus facilitate efficient mixing over a shorter pipe length. It is mainly available in Europe and Asia. | |

	KVM	This type of mixer is available in the North and South American market. It allows mixing of additives without a sparger and it comes with multiple injection port connections.	

		CompaX	It consists of a highly efficient mixing device with an integrated dosing point into which additive is fed. It allows the lowest possible pressure drop with no clogging. It is typically used in water or wastewater treatment.	

	ISG (Interfacial surface generator)	It consists of individual mixing elements that are stacked in a tubular housing. The fluid exiting one element will enter into the center of the second element and then exits near the wall promoting effective radial mixing.	

| LPD (Low Pressure Drop) | The mixer is made of two inclined semi-elliptical plates opposite to each other. | |
| LLPD (Low-low pressure drop) | | |

KOMAX (Komax System. Inc Mixing by Design) www.komax.com	Sanitary mixer	This mixer helps convert a multiple component input stream into a uniformly blended output. It is ideal in food industries that involves blending of solid materials.	

	Triple action static mixer	Three distinct types of mixing operation are available: Two by Two Division; Cross Current Mixing; Counter-Rotating Vortices and Back-Mixing.	

| | Custody Transfer Mixer | It is typically used in petroleum industry for thorough mixing. | |

Table 2.2: Applications of static mixers

Industry	Application	References
Chemical and Agricultural	Bio diesel production, and ultrafiltration of dairy liquids.	(Thompson and He, 2007; Hiddink *et al.*,1980; Krstić *et al.*, 2006)
Grain Processing	Continuous processing and conversion of starch, and production of ethanol.	(Harvey *et al.*, 1982; Kozyuk, 2011)
Food Processing	Liquid-liquid blending, solid-liquid blending.	(Fellows, 2000)
Mineral Processing	Transporting, mixing and extraction of oil sands	(Cymbalisty,2005)
Pharmaceuticals	Emulsion, and dispersion	(Kiss *et al.*, 2011)
Polymer	Emulsification of liquid-liquid mixtures, mixing of numerous different polymers, and neutralization.	(Siadat *et al.*, 1980; Baker, 1991)
Pulp and Paper	H_2S removal, blending of fluids.	(Bajpai, 1999; Iliuta and Larachi, 2003)
Water and Waste Water Treatment	Continuous polymer feed stream for waste water treatment, waste water disinfection, and transfer of ozone into water.	(Sencza,1984; Boilyky, 1981; Rulyov 1999)

2.2 SIGNIFICANCE OF STATIC MIXERS' GEOMETRY

With wide varieties of static mixers commercially available (Pahl and Muschelknautz, 1982; Cybulski and Wermer, 1986; Myers *et al.,* 1997), the selection of ideal static mixer for a given application depends on how well the desired degree of homogeneity is achieved within a satisfactory power consumption (Mickaily-Huber *et al.*,1996; Li *et al.,* 1998a)**.** Rigorous characterization techniques are essential for highly viscous non-Newtonian fluids due to the possibility for poorly mixed region within the pipe, which leads to lowered product quality (Hobbs and Muzzio, 1997; Hobbs *et al.,* 1998a-c). SMX is generally suitable for this type of highly viscous fluids in the laminar region. However, a higher power consumption is required to overcome the drag force of dense fluid (Baker, 1991; Li *et al.,* 1997; Ottino, 1983). Every static mixer has its own advantages and disadvantages and to compare its mixing performances, a common set of mixing criteria need to be established. Even though Kenics is the most commonly used static mixer, the intrinsic mechanism of fluid mixing is not fully comprehended and, as a result, the substantial pressure drop caused by the helical element often create economic burden to most industrial applications (Seob Song, 2005).

Advanced Computational Fluid Dynamics (CFD) methods have been effectively employed to study the mixing mechanisms of static mixers and recently in 2013, Chen provided insights on static mixers' geometry through his numerical research study on the Kenics static mixer. Since the mixing phenomena becomes incomprehensible due to the complexity of some static mixers' geometry, the mixing characterization becomes difficult and inaccurate (Yang, 2007). Thus, there is incentive to investigate the mechanism of static mixers to enhance the mixing process (Shah and Kale, 1991; Chandra and Kale, 1992; Xu *et al.,* 1997; Pahl and Muschelknautz, 1982; Boss and Czastkiewics, 1982). The Optimal Shape Design (OSD) was first proposed by Mohammadi and Pironneau in 2001 to optimize the mixing performances of static mixers. In 2013, Sarghini *et al*. then extended the work to optimize the shape of HEV and coaxial static mixers using the OSD approach for Newtonian and Non-Newtonian fluids.

Accordingly, the analysis of static mixers' geometry is very critical to understand how it influences the fluid flow in the radial and tangential directions to induce homogenous mixing while minimizing pressure drop. Even though the mixing mechanism of static mixers is still

elusive (Sarghini *et al.,* 2013; Yang, 2007), static mixers have been proven successful in potential applications: gas/gas, gas/liquid, liquid/liquid, liquid/solid, and to some extent solid/solid mixing. Progressive technical development has also been made to employ static mixers as a heat exchanger, convection promoters and even as reactors. The detailed overview of each static mixers' application is briefed in the following section.

2.3 APPLICATIONS OF STATIC MIXERS

2.3.1 GAS-GAS MIXING

Static mixers are most commonly used to mix gases prior to a reaction for a uniform product yield and its distribution. The use of static mixer in nitric acid production plant helps to minimize the deactivation of expensive platinum catalyst used in the process. Similarly, the application of static mixers is very attractive for any gaseous phase chemical reactions which include the production of vinyl chloride, ethylene dichloride, styrene, xylene and maleic anhydride (Baker, 1991). In addition to that, static mixers help to resolve the emission of nitric oxides (NO_x) from catalytic combustion of fuel by alleviating the inhomogeneity in fuel-air mixing prior to combustion (Braun *et al.* 1998).

2.3.2 GAS-LIQUID MIXING

Common applications include the removal of hydrogen sulfide from the gas with sodium hydroxide solution or amines, removal of carbon dioxide with proprietary solvents and dehydration of gases with glycols. Petrochemical industries extensively use static mixers to scrub harmful organic compounds with appropriate solvents, to remove acid gases or to scrub chlorine gas with sodium hydroxide, and to absorb hydrogen fluoride in water (Rader *et al*, 1989). Research findings are proven promising to be applicable in gas absorption towers for the oxidation of activated sludge effluent and for waste water treatment since static mixers enhance the volumetric oxygen transfer coefficients (Hsu *et al.*, 1975; Lee *et al.*, 1971; Hsu, 1974). Waste water treatment plants predominantly use static mixers as it reduces the amount of chemicals such as ozone or chlorine required for coagulation and disinfection (Schulgen *et al.*, 1996; Clark *et al.*, 1994; Amirtharajah and Jones, 1996; Burke, 1996; Latimer and Amirtharajah, 1998; Martin and Galey, 1994; Heindel *et al.*, 1999; McKenna *et al.*, 1986). In parallel to that, static mixers are widely employed in external-loop type airlift bioreactors to enhance the gas-liquid volumetric mass transfer coefficient as most fermentations are oxygen-limited. The gas holdup is increased by 30 to 500% with static mixers while mitigating the liquid superficial velocity. Overall, static mixers are found to be very effective in bioreactors (Blenke, 1979; Onken and Weiland, 1983; Merchuk, 1986; Chisti, 1989; Lin *et al.*, 1976; Stejskal and Potucek, 1985; Bahpaj and Reuss, 1982; Margaritis and Sheppard, 1981; Siegel *et al.*, 1988; Levenspiel, 1972; Gavrilescu *et al.*, 1992; Gavrilescu and Roman, 1993). A new process to reduce membrane

fouling during ultra-filtration was developed. Air was injected through the static mixer to promote turbulence which prevents particles from depositing on the membrane surface. Thus, the permeate flux was improved by 180% due to alleviation of membrane fouling (Derradji *et al*., 2000).

2.3.3 LIQUID-LIQUID MIXING

Clathrate hydrates have created a huge impact as they are significantly useful in the environmental and energy sector. Intensive research activities have been performed on the storage and transportation of natural gas in the form of methane hydrates (Austvik and Loken, 1992; Loren and Austvik, 1993; Saji *et al*.,1995; Saji and Yoshida, 1992; Yamasaki *et al*., 2000; Gudmundsson and Borrehaug, 1996; Ohgaki *et al*., 1994; Khokhar *et al*., 1998). One particular research work employed Kenics static mixer in this application to induce the formation of CO_2 hydrate by mixing liquid CO_2 with water. This technology has proposed a new approach to sequester CO_2 and to mitigate the effect of global warming (Tajma *et al*., 2004).

Most polymer blends are immiscible and it is difficult to mix them homogenously as two phases separate out. Kenics static mixer is used to blend poly (ethylene terephthalate) (PET) and polypropylene (PP) with liquid crystalline polymers (LCP). The degree of dispersion affects the morphology and thus influencing the ultimate mechanical properties of the thermoplastic matrix. Other potential applications include the dispersion of immiscible and less viscous antistatic or antisoiling agent, dispersion of color concentrate, and breakup and dispersion of gel structure from cross-linking or polymer degradation (Paul and Newman, 1978; Sukhadia *et al*.,1992; Grace, 1982). Kenics static mixer is widely used in food applications such as mixing of colors into corn syrup, sugar solution or jelly base, and blending of oils and flavors into tomato paste and ketchups or peanut butter (Bor, 1971). Recent advancement in technology has been made to utilize oil-in-water emulsions induced by SMX static mixer to produce polymeric micro particles, which are vastly used in pharmaceutical industry (Mansour *et al*., 2010; Kiss *et al.,* 2011).

2.3.4 LIQUID-SOLID & SOLID-SOLID MIXING

Food industry uses static mixers to mix dry powders for cake and to mix concentrated coffee extract with aroma. They are often used to blend fragile fruits into yogurt or into whipped topping. Particles of vegetables are blended to make chutneys (Bor, 1971). One of the major concerns with solid-solid mixing is that they tend to agglomerate easily when exposed to moisture in atmosphere. The difference in particle size, density, and shape greatly influence the mixing mechanism (Lacey, 1943; Gyebis and Katai, 1990). Three different types of static mixers such as Kenics, Komacs, and Sulzer SMX were employed to characterize the quality of solid-solid mixing (Bauman, 2001). Other applications include mixing of dry pigments and ink powders, blending of dry clays with cements, mixing lubricants with polymer solids or powdered metals (Thakur, 2003; Baker, 1991).

2.3.5 MIXING WITH REACTION

Static mixers have also been used widely in pharmaceutical industries to help with the synthesis of precursor chemicals. It is prominently used for the synthesis of drug nanoparticles (Dong *et al*., 2010; Douroumis and Fahr, 2006; Gassmann *et al*., 1994). It has also been proven effective for the transesterification reaction to produce biodiesel (Thakur, 2003; Thompson and He, 2007; Frascari, 2008; Somnuk *et al*., 2014). Static mixer, Sulzer SMV, is equipped along with reactor for the continuous hydrogenation of soybean oil with Harshaw Ni catalyst (Rusnac *et al*., 1992). Sulzer SMX static mixing elements are used to enhance heat transfer for the production of hydroxypropyl starch, which finds applications in food and paper industry (Lammers *et al*., 1993). The mass transfer characteristics of the tubular photo bioreactor were investigated using different types of static mixers and such that static mixers have been proven to be a promising method to enhance the productivity of bioreactors (Ugwu *et al*., 2002).

Another study also investigated on the performance of Kenics static mixer on the wall-coated catalytic reactor where static mixer is found effective in enhancing radial mixing for higher reaction conversions (Khinast *et al*., 2003). In another case, SMXL static mixers were used for the polymerization of methyl methacrylate (MMA) and were effective in maintaining good temperature control (Fan *et al*., 2003).

2.3.6 CONVECTION PROMOTERS

Convection promoters simply intensify the velocity fields of fluid molecules while enhancing the movement of fluid material. When fluids are passed into static mixers, their flow patterns are diverted by provoking a certain thrust of fluid movement. By intensifying the magnitude of velocity fields, convective fluid flow is more dominant compared to the diffusion process. Static mixers are widely used as convection promoters in the ultrafiltration of diary liquids as it improves the permeate flux. It is reported that the mass transfer coefficient is increased by a factor of 1.95. The permeate flux is increased by a factor of 2.9 as the concentration polarization is significantly alleviated (Hiddink *et al*.,1980). It has also been used as convection promoters in the hyper filtration of salt solutions, cottage cheese whey, and deproteinized whey. Permeate flux in the ultrafiltration of latex suspension was greatly improved through the use of Kenics static mixer (Vanderwaal *et al*.,1977; Boer *et al*.,1980; Lowe and Durkee, 1971; Thomas *et al*.,1971; (Pitera and Middleman, 1973; Peri and Dunkley, 1971; Copse and Middleman, 1974; Dejmek *et al*.,1974). It is also used in the cross-flow microfiltration of skim milk and helps rectify the issues of membrane fouling and concentration polarization to a significant extent (Krstic *et al*., 2003).

2.4 FUNDAMENTALS OF MIXING

Mixing is a critical operation that alleviates the non-uniformities in the composition of final product and plays a very significant role in chemical reaction or other processes involving mass transfer. Indeed, the wide applicability of static mixers in various industrial processes is very apparent as discussed earlier. For each application, the criterion for mixing performance is different depending on what the intended mixing outcomes are. For blending of gas/solids in liquids or of two miscible liquids, the degree of the spatial distribution of bubbles, solid particles or drops are monitored in the liquid without considering for any size reduction. The spatial distribution is then mapped as a function of position of static mixer element. This is what called as the distributive mixing operation. On the other hand, for the mixing of gas such as Ozone or highly viscous polymer solution into a liquid medium, the disparate change in density or viscosity ratio of the two immiscible fluids causes phase separation. As a result, a huge shear force is required to overcome this opposing force of coalescence. Unlike distributive mixing process, this operation always measure the degree of drop size reduction while ignoring the importance of spatial distribution (Al-Taweel and Walker, 1983; Legrand *et al*., 2001; Grace, 1982; Baker, 1991). This is called as dispersive mixing and the Fig.2.1 and Fig.2.2 graphically illustrate the two distinct mixing operations. The flowchart in Fig.2.3 illustrates the mixing characterization tools of each mixing mechanisms. For the characterization of distributive mixing, the scale of segregation and the intensity of segregation are the most commonly used tools.
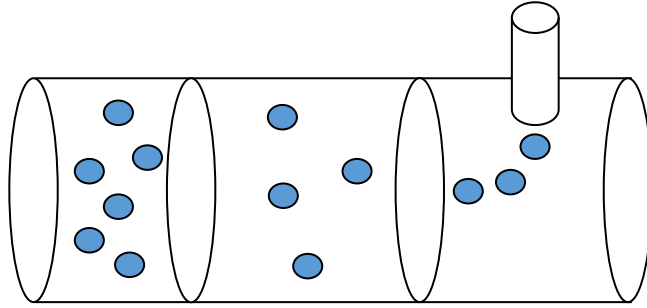
Fig 2.1: Distributive mixing- Measuring the spatial distribution of injected sample
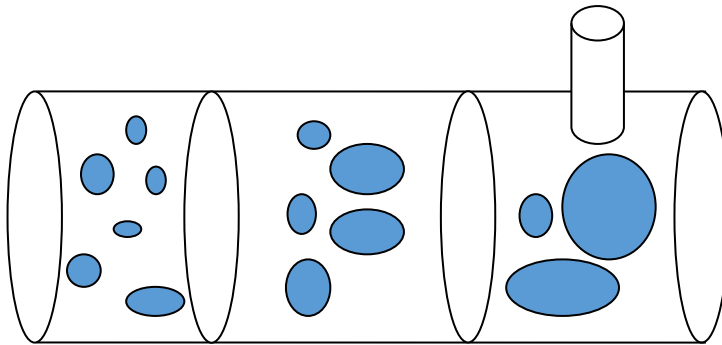
Fig 2.2: Dispersive mixing- Measuring the degree of drop size reduction of the gas or highly viscous fluid added to the liquid medium.
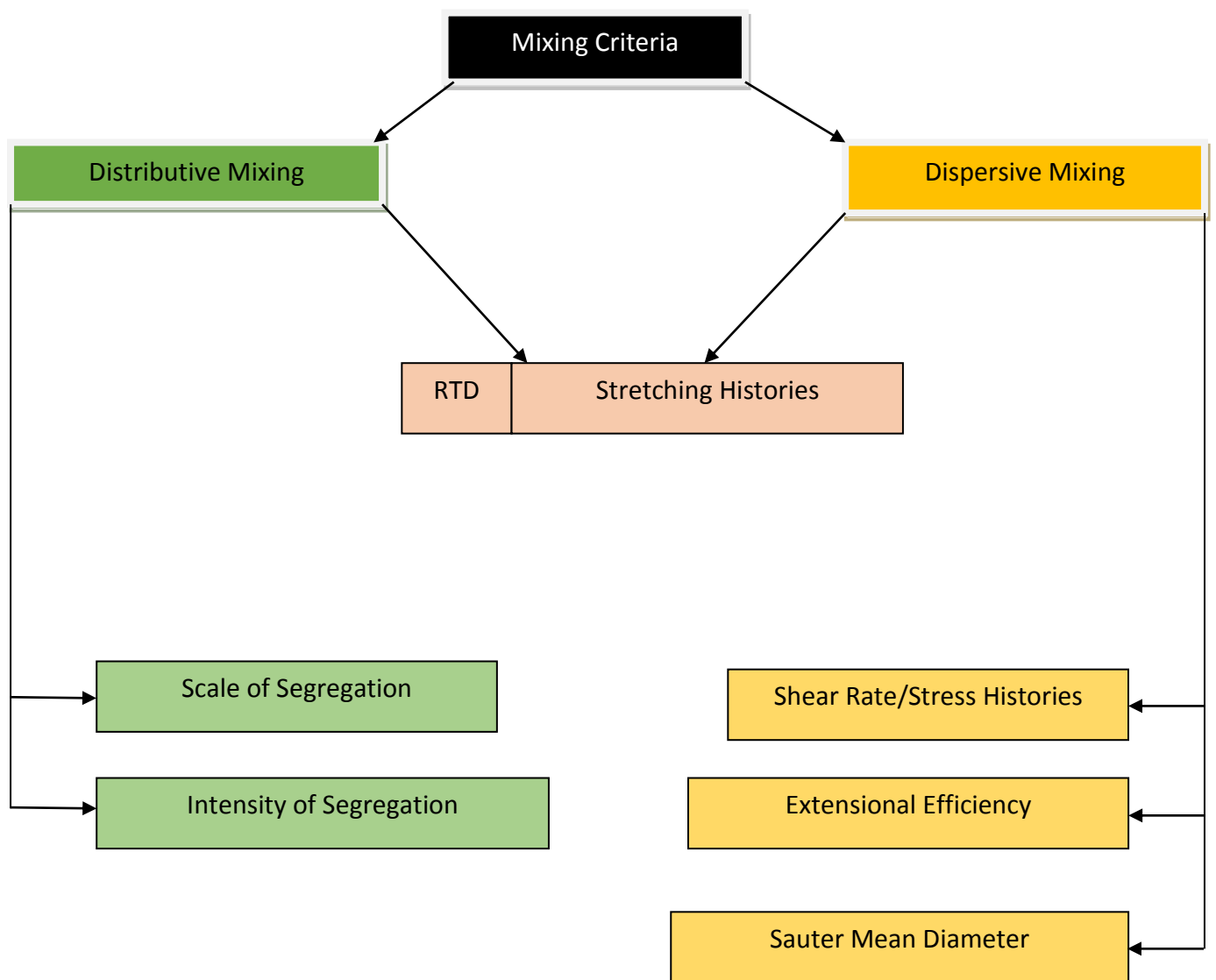
Fig. 2.3: Mixing characterization tools available for dispersive and distributive mixing operations

2.5 MIXING INDEX (OR INTENSITY OF SEGREGATION)

For certain applications, both dispersive and distributive mixing mechanisms exist but one dominates more than the other. For instance, the blending of polymer melt requires the dispersion of highly viscous phase into smaller droplets before being distributed uniformly. Similarly, the injection of ozone for disinfection of water streams involves significant dispersion of ozone gas bubbles followed by the distributive mixing such that ozone is homogenously distributed throughout the entire volume. Even though mixing operation is categorized into two different types, both mechanisms sometimes work co-operatively (Baker, 1991; Ess and Hornsby, 1986).

To understand how well the distribution is evenly spread out, different sampling methods are proposed: quadrats and probes. Each of this sampling method utilizes the concentration data for the computation of the normalized standard deviations of concentration distribution, CoV (Kukukova *et al*., 2008; Diggle, 2003; Reardon and O'Sullivan, 2004). This CoV value signifies how far the mixture is deviated from the desired level of homogeneity. Ideally, the value approaches zero for perfect homogenous mixture. The quadrat is referred to any 2D sample area of arbitrary size and shape. The plane of interest is divided into number of quadrats of same size and shape depending on the level of spatial resolution required for accurate and unbiased analysis. The mean concentration in each quadrat is calculated and repeated for *M* number of quadrats over the plane of interest and correspondingly, the coefficient of variance (CoV) is computed using Equation 2.5.1, where $\bar{C}$ is assumed to be the average concentration for a homogenous mixture:

$$CoV = \frac{\sqrt{\frac{1}{M}\sum_{m=1}^{M}(C_m - \bar{C})^2}}{\bar{C}} \qquad (2.5.1)$$

Similarly, the point probes are used to sample a meaningful number of molecules or tracer particles within its finite sampling area or measurement volume. The probe size should be carefully chosen such that it is small enough to get local data points while holding significant

number of particles, and, at the same time, should not overlap with other probe areas. Equation 2.5.1 is again utilized to compute the CoV for the probe method.

The number of probes, the probe size and location of probe significantly affect the value of CoV and thus will provide misleading information about the mixing quality. It is recommended to use at least 250 probes of size that could identify even the smallest concentration data of interest before beginning experiments or simulations. Otherwise, the CoV value will be affected predominantly by the choice of probe size (Kukukova *et al*., 2008; Clements, 1905; Hessel *et al*., 2003).

Kukukova reported that there was no much different in CoV measurement using probe or quadrat method provided that larger number of probes/quadrats is used to identify the smallest scale of mixing. This signifies the triviality of shape of probes/quadrats. Alternatively, the scale of segregation could be measured using Point-to-Nearest-Neighbour (PNN) distribution which measures the distance x_i from each of the K_g grid points to the nearest of *n* number of particles. A complete spatial randomness (CSR) is assumed such that postulations for each particles to have equal probability of being at any position in a control volume and for being independent of the position of any other particle are asserted. Use of grid points, K_g, approximately equal to $\sqrt{\text{no. of particles}}$ is recommended for optimal spatial resolution for PNN distribution. The shape of PNN distribution reflects on the length of mixing scales. A wide distribution curve indicates clustering while a narrow distribution denotes regular spatial distribution of particles. The index of dispersion shown in equation 2.5.2 measures the deviation from CSR or, in other words, measures the degree of clustering, which is the ratio of variance (σ^2) of the PNN distribution to that of the mean value ($\overline{x}_i$) (Diggle, 2003; Diggle and Matern, 1980; Wong, 2004; McGarvey *et al*., 2005; Kukukova *et al*., 2008; Mead, 1974):

$$I_{disp} = \frac{\sigma^2}{\overline{x}_i} \tag{2.5.2}$$

Since PNN resembles Poisson probability distribution if the particles are randomly distributed, the index of dispersion will be equal to 1 as the variance is equal to its mean for this special case. Accordingly, it will be larger than 1 for clustered distribution and smaller than 1 for a regular distribution of particles.

The PNN method is only suitable for the dimensionless point pattern data, as compared to other sampling methods, and cannot be applicable for concentration data. It evaluates if the system is segregated, clustered or regular distribution of particles by calculating the index of dispersion. The method measures the mixing scales over the whole population and hence enables an accurate depiction of the mixing length scales. However, the method is time consuming for higher grid resolutions, which increases the numbers of particles and the matching of grids needed for those particles. In order for the measurement scale to be independent of time or grid resolution, all PNN distances are normalized with the maximum separation distance between two particles in the plane (Kukukova *et al.*, 2011; Diggle and Matern, 1980).

Other mixing protocols available are correlograms and variograms which utilize the concentration data unlike the PNN method (Danckwerts, 1952). The coefficient of correlation is formulated as below:

$$R_x(h) = \frac{\frac{1}{N(h)}\sum_{N(h)}(C_i(x)-\bar{C})(C_i(x+h)-\bar{C})}{\sigma^2} \tag{2.5.3}$$

where *N(h)* is the total number of pairs of data separated by distance *h*, and $\bar{C}$ and σ^2 are the mean and variance of 2D data set. Similarly, the variogram is calculated using Equation 2.5.4:

$$\gamma_x(h) \equiv \frac{1}{2N(h)}\sum_{N(h)}(C_{is}(x) - C_{is}(x+h))^2 \tag{2.5.4}$$

where C_{is} is the standardized concentration value at location *x*, described in Equation 2.5.5:

$$C_{is}(x) = \frac{C_i(x)-\bar{C}}{\sigma} \tag{2.5.5}$$

The coefficient of correlation is always one when the distance between the pair of data is zero. But, the coefficient falls towards zero as the distance of separation between data pair increases denoting that no correlation exists at this distance. The presence of large-scale segregation is evident if the correlogram crosses zero and reaches a negative value. On the other hand, the physical meaning of variogram shape is exactly opposite to the correlogram. The variograms starts with the value of zero for zero distance of separation and reaches one as the distance of separation increases. Similarly, if variogram exceeds one, then there is a presence of larger segregated region. The correlogram signifies if the correlation between concentration data exists

at the defined distance of separation whilst the variogram depicts the variability between pair of data at that distance:

$$L_D = \int_0^\varepsilon R_x(h)dh \qquad\qquad (2.5.6)$$

As proposed by Danckwerts early in 1952, the integration of the correlogram curve over the distance of separation until the curve crosses zero, gives a mean length scale (L_D) as shown in Equation 2.5.6. One of the limitations with this method is that it does not provide the exact size of the clumps. Danckwerts suggested not using this method for measuring the average length scale if large-scale segregation or periodic patterns in concentration data is present. Hence, this method of analysis is quite unrealistic for addressing any problems in this modern era of mixing research (Kukukova *et al.*, 2011).

In addition to the length of mixing scale (i.e. scale of segregation) and variance in concentration distribution (i.e. intensity of segregation), the third dimension being proposed is the exposure, which measures driving force to reduce segregation. In other words, exposure is defined as the rate of reduction in segregation (Wong, 2002; Wong, 2005).

Early in 1998, Jaffer and Wood engaged a different software package, Sigma Scan/Image measurement to measure perimeter, area, pixel intensity, and striation thickness over the digital image of analysis taken through the laser induced fluorescence (LIF) method. The interface of striations is determined if there are more than 20 units that have different pixel intensities from the neighboring particles of the point of analysis. Again, in 1998, the laser induced fluorescence (LIF) was employed to calculate the concentration variance by translating the fluorescence signal in voltage to the concentration of fluorescence dye, which has direct proportionality (Karoui *et al.*, 1998). The driving force for the reduction in striation thickness could be inferred through the analysis of interfacial area of clumps or the striations and the concentration gradient of the dye or additive tracer.

To understand the driving force for the reduction in striations thickness, the interfacial area available for mass transfer needs to be mathematically expressed. Earlier in 1957, Mohr *et al.*, developed a relationship between striation thickness and shear rate. With respective to the velocity distribution, both the rate of shear and time during which shear is applied, can both be

specified for any location in a laminar flow system. Equation 2.5.7 unveils the relationship between velocity gradient and the shear rate as follows:

$$\overline{\overline{D}}(i.e.\,Shear\,rate) = (\nabla V + (\nabla V)^T) \tag{2.5.7}$$

Kukukova *et al*., (2011) suggested that computation of stretching distribution is more mathematically transparent approach compared to the striation methods as the former is directly related to the shear field, which is described in Equations 2.5.7. However, the calculation of striations is made easier, in terms of computation time, if a mathematical relationship between stretching and striation thickness is deduced.

Stretching mechanism is characterized using the deformation gradient tensor, denoted by *F*, from which strain could be easily computed. The deformation gradient tensor will provide all-compassing measure of deformation of material element for both 2D and 3D shape while offering insights onto the overall material rotation. The graphical representation of this stretching mechanism is illustrated in Figure 2.4.
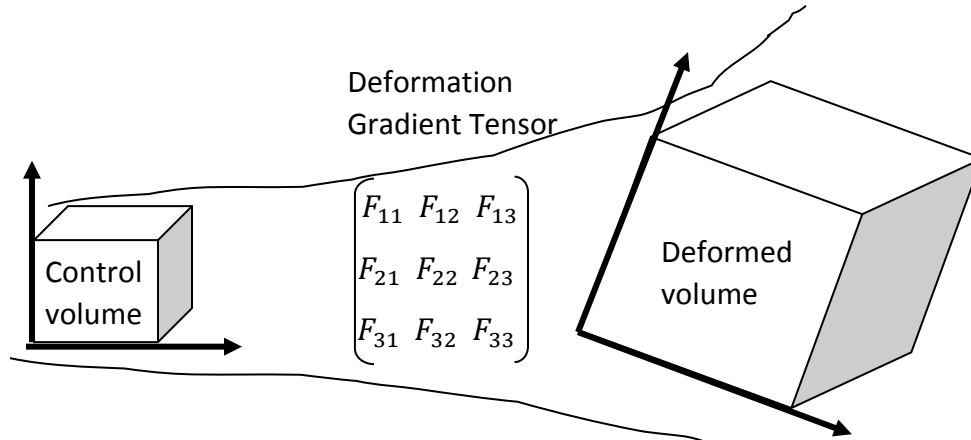
Figure 2.4: Graphical representation of how stretching distributions could be calculated numerically

Considering a control volume as stated in Figure 2.4, the position of any arbitrary fluid particles is marked in black circle. The trajectories of these arbitrary black particles over a period of time is represented in a flow map, ϕ, which is a function of initial position of fluid particles, X, and time span ,Δt. The gradient of the flow map will yield information on stretching mechanism of fluid particles (Chella and Ottino, 1985; Voth *et al*., 2002):

36

$$Deformation\ gradient\ ,\boldsymbol{F}, = \frac{\partial x}{\partial X} \tag{2.5.8}$$

$$Initial\ position\ of\ particle, X = \phi(X,0); \tag{2.5.9}$$

$$Position\ of\ particle\ at\ varying\ time, x = \phi(X,t) \tag{2.6.0}$$

$$Velocity\ gradient,\ \nabla\boldsymbol{v} = \frac{\partial(\frac{x}{t})}{\partial x} \tag{2.6.1}$$

Rearrangement of equation 2.5.8 leads to equation 2.6.2:

$$\partial x = \boldsymbol{F}.\partial X \tag{2.6.2}$$

Unit vector denoting the direction of particle, $X:\ \widehat{\mathbf{M}} = dX/|dX|$

Right Cauchy-Green strain tensor, $\mathbf{C} = \mathbf{F}^{T}.\mathbf{F}$ where superscript, T, denotes transpose of deformation gradient, $\mathbf{F}$.

$$\pi = (\boldsymbol{C}:\widehat{\boldsymbol{M}}\,\widehat{\boldsymbol{M}})^{1/2}, \text{ where } \pi \text{ stands for stretching.} \tag{2.6.3}$$

Alternatively, the stretching could also be expressed as follows:

$$\pi = \lim_{\|dX\|\to 0} \frac{\|dx\|}{\|dX\|} \tag{2.6.4}$$

Computation of Lyapunov exponents' spectrum is considered to be the most resourceful characterization tool for chaotic system, which is often unpredictable and very sensitive to the initial conditions. Lyapunov exponent measures the average rate of divergence or convergence of nearby orbits in phase space. The signs of Lyapunov exponents reveal the dynamic behavior of the fluid particles in a phase space. The positive exponent signifies divergence and chaos. Negative exponent denotes periodicity and convergence. When the Lyapunov exponent is equal to zero, it represents a marginally stable orbit (Wolf, 1985). The maximal Lyapunov exponent is the common diagnostic tool as it is easier to be calculated. Other measurement tools are the short time and local Lyapunov exponents evaluating the rate of divergence or convergence over a finite time interval and when time interval approaches zero, respectively.

The concept of Lyapunov exponents explains the existence of instable region in the phase space and hence marking the necessity for further mixing analysis (McCue, 2011). The importance of

stretching to measure the quality of fluid mixing was emphasized. As the magnitude of stretching increases, the exposure of interfacial area for diffusion increases. Thus, the mixing quality is improved significantly. In order to understand the fluid dynamics of fluorescence dye under chaotic flow, the lamellar structure is analyzed and it is composed of wide distribution of striation thickness attributing to different values of Lyapunov exponents or different rates of stretching at different spatial location (Muzzio, 1991). In 2010, Guegan and Leroux proposed a novel methodology to use local Lyapunov exponent over a finite time interval to predict projection of particles' trajectories in the chaotic system.

For a chaotic system, it is postulated that the nearby trajectories of particles expand exponentially and, as a result, Equation 2.6.4 could also be written as below:

$$\|dX(t=0)\|e^{\lambda t} = \|dx(t)\| \tag{2.6.5}$$

Equations 2.6.4 and 2.6.5 are very much the same except that stretching value,π, is replaced by exponential term, $e^{\lambda t}$, where λ is the Lyapunov exponent- the average rate of separation of trajectories of fluid particles.

In the limit of infinite time, the Lyapunov exponents will yield a maximum value representing the global measure of the rate at which the particles' trajectories diverge. With a postulate that the fluid particles follow an exponential trajectories, Equation 2.6.6 could be rearranged to yield an expression for λ, Lyapunov exponent:

$$\pi = e^{\lambda t} = \lim_{\|dX\| \to 0} \frac{\|dx\|}{\|dX\|} \tag{2.6.6}$$

$$\lambda = \frac{1}{t} ln(\lim_{\|dX\| \to 0} \frac{\|dx\|}{\|dX\|}) \tag{2.6.7}$$

At an infinite time series, the stretching will also become an infinite value as the fluid particles' trajectories is exponential. Accordingly, Equation 2.6.7 will converge asymptotically to zero through the application of L'Hopital's rule:

$$\lambda = \lim_{t \to \infty} \frac{1}{t} ln \left(\lim_{\|dX\| \to 0} \frac{\|dx\|}{\|dX\|} \right) = \frac{\infty}{\infty} \tag{2.6.8}$$

After applying L'Hopital's rule, Equation 2.6.8 becomes:

$$\lambda = \frac{1/\pi}{1} = 0 \ (With\ postulate\ \pi \rightarrow \infty\ as\ t \rightarrow \infty\ for\ exponential\ trajectories) \qquad (2.6.9)$$

Similarly, local Lyapunov exponent is computed by taking the limit as time approaches zero and again, by applying L'Hopital's rule, Equation 2.6.7 will converge asymptotically towards a unity.

$$\lambda = \lim_{t \rightarrow 0} \frac{1}{t} ln \left(\lim_{\|dX\| \rightarrow 0} \frac{\|dx\|}{\|dX\|} \right) = \frac{0}{0} \qquad (2.7.0)$$

As time $t \rightarrow 0$, π is equal to one and $ln\ \pi$ is thus zero. By applying the L'Hopital's rule, Equation 2.7.0 converges to unity.

$$\lambda = \frac{1/\pi}{1} = 1 \qquad (\pi \rightarrow 1\ as\ t \rightarrow 0) \qquad (2.7.1)$$

As described earlier, local Lyapunov exponent method are proposed to predict the trajectories of fluid particles of minimum error size. Short time Lyapunov exponent is similar to the local Lyapunov exponent except that the former is calculated over a finite time interval rather than taking a limit of time approaching zero. To understand the quality of mixing, one could relate how stretching mechanism could greatly enhance the mixing process due to the presence of chaos. However, to infer insightfully on the mixing efficiency, either local or short time Lyapunov exponent could be assessed numerically over the time interval during which the fluid particles reside inside the static mixer. Accordingly, the concept of residence time distribution could be incorporated into short time Lyapunov exponent to evaluate the mixing efficiency over the time interval during which the fluid particles reside inside the static mixer.

In 1952, Danckwerts first proposed the concept of residence time distribution (RTD) for continuous streams of flow in a pipe. Certain assumptions were made for the simplification of calculations such as (1) complete mixing and (2) piston flow meaning that fluids enter the pipe with constant and equal velocity and leave the pipe at the same moment (Danckwerts, 1953; Wittrup, 2007). RTD is experimentally determined by injecting tracers and detecting them at the exit stream of the pipe. It is preferable to use tracer fluid whose density is similar to the flowing fluid to avoid any interference from convective currents from the density difference. RTD analysis is more accurately depicted if measurement of tracer concentration is taken at lower flow rates where significant changes in radial velocity can be noticeable. Correspondingly, the effect of molecular diffusion could also be significant at lower flow rates. Nigam and Vasudeva

(1980) recommended the aforementioned aspects to be considered carefully for experimental RTD analysis.

The injection of tracer fluid could be a step change or a pulse response. Accordingly, RTD profile is expressed as the time record of tracer concentration at the pipe exit normalized by the average concentration for step change and by the total area under the curve for pulse.

If a fluid goes from one steady value to another, for instance, from white to red, the fraction of red material recorded in the exit stream after time ϑ is represented by exit age distribution function $E(\vartheta)$ from which cumulative curve $F(\vartheta)$ could be deduced. Considering the volumetric flow rate as $\dot{V}$ and the volume of pipe as V, the plot of $F(\vartheta)$ versus $\frac{\dot{V}\vartheta}{V}$ yield the F-diagram (Danckwerts, 1953; Torres and Oliveira, 1998).

The probability that fluid element exits before time ϑ is expressed in terms of $E(\vartheta)$ which denotes the fraction of ages per unit time. The function $E(\vartheta)$ is also called as the RTD function:

$$E(\vartheta) = \frac{C(\vartheta)}{\int_0^\infty C(\vartheta)d\vartheta} = \frac{dF(\vartheta)}{d\vartheta} \tag{2.7.2}$$

where C is the concentration of tracer at any time, ϑ.

$$F(\vartheta) = \int_0^\vartheta E(\vartheta)d\vartheta \tag{2.7.3}$$

Similarly, the probability that fluid element exits after time ϑ are expressed using Equation 2.7.2 with different integral limits as shown below:

$$F(\vartheta) = \int_\vartheta^\infty E(\vartheta)d\vartheta \tag{2.7.4}$$

$$\text{Mean time} = \int_0^\infty \vartheta\, E(\vartheta)d\vartheta = \tau \tag{2.7.5}$$

Experimental RTD analysis is very susceptible to measurement errors both in injection and detection of tracer in the main fluid. Similar to Nauman's suggestions (1981), Pustelnik (1985) added few more recommendations to minimize measurement errors such as keeping the volumetric flow rate constant during measurement, recording tracer signal at the inlet and the outlet of the pipe, and recording the concentration of the tracer in the flux of main stream. Using the concentration data of tracer at the inlet and outlet of the pipe, a numerical algorithm was

developed to calculate the exit age distribution function, $E(\vartheta)$, which was then approximated using the log-normal distribution model as described below:

$$E(\vartheta) = \frac{1}{\sigma_R\sqrt{2\pi}}\exp[-\frac{(\log\vartheta - \mu_R)^2}{2(\sigma_R)^2}]$$ (2.7.6)

where μ_R is the mean value while σ_R denotes the standard deviation of the distribution.
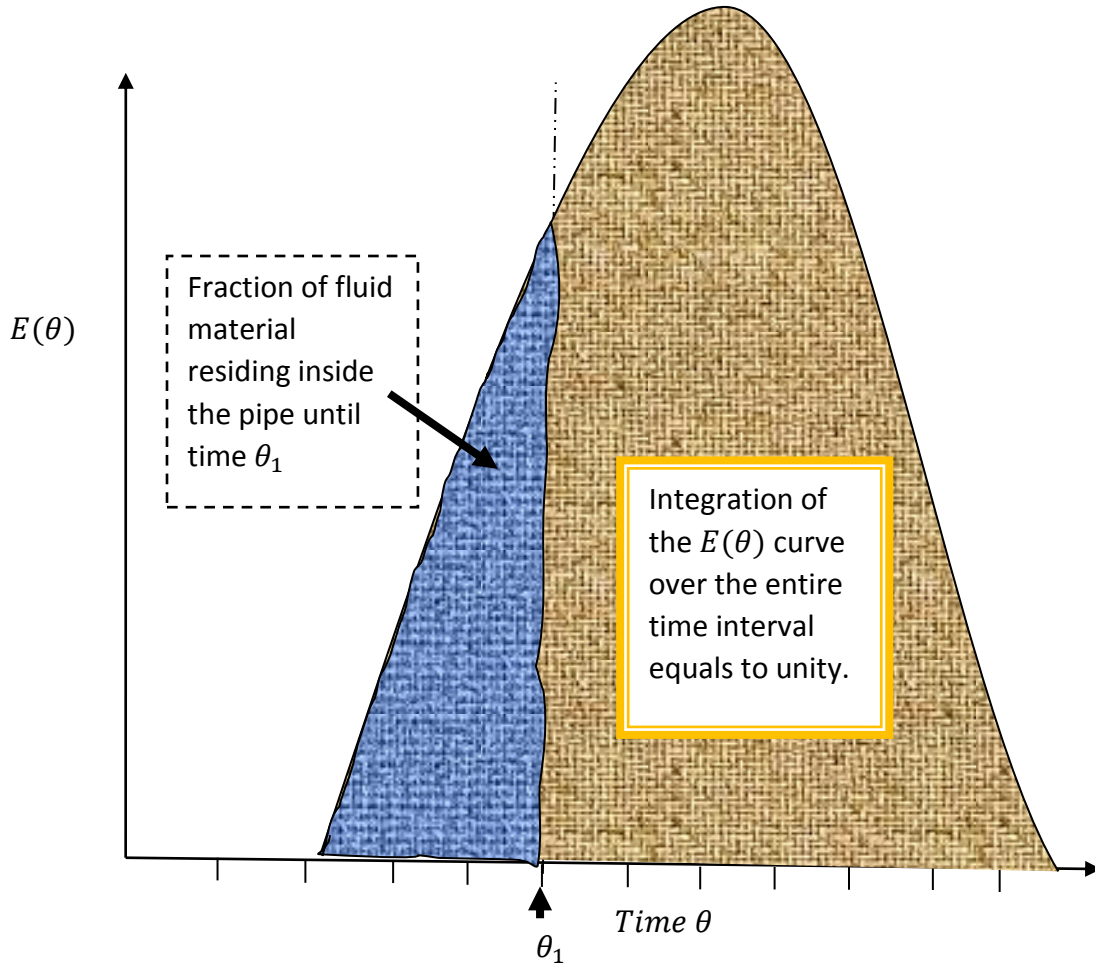
Figure 2.5: Residence time distribution

Fig.2.5 illustrates a typical residence time distribution plot showing the fraction of fluid material residing inside the pipe until time θ_1. Pustelnik (1985) postulated that μ_R and σ_R were both a function of Reynolds number and number of static elements. Later, in 1988, Kemblowski updated the residence time distribution function by taking into consideration of longitudinal dispersion and the flattening of velocity distribution after every Kenics element (Kemblowski

and Pustelnik, 1988). In 1998, Li *et al.,* introduced the transfer function in the Laplace domain to describe the tracer stimulus-response profile. The transfer function was then numerically resolved through inverse Fourier transform to obtain the exit age distribution function, $E(\vartheta)$, which was then plotted with respective to time,ϑ, to obtain the *F*-curve. The above RTD studies highlight the significance of rheological properties of the main fluid stream and thus incorporating the concept of generalized Reynolds number for generalized Newtonian fluids, excluding the ones with yield stress, in the experimental RTD analysis (Kemblowski and Pustelnik,1988; Pustelnik, 1985; Li *et al.,* 1998*;* Ottino, 1983; Hobbs *et al.,* 1998; Braun *et al.,* 1998; Hsu *et al.,* 1975).

2.6 APPLICATIONS OF CFD IN STATIC MIXERS

Computational fluid dynamics (CFD) employs powerful computers and applied mathematics to simulate complex problems and to understand the obscure phenomena which cannot be unveiled from the data gathered in laboratory settings alone. Thus, CFD is widely used in engineering designs as it could predict the performance of new design or processes before actually implementing them (Xia and Sun, 2002). CFD work has been employed extensively to simulate striation thickness, coefficient of variance and stretching histories and these simulated data are used to validate the CFD model by comparing them with the experimental results (Hobbs and Muzzio, 1998a; Hobbs and Muzzio, 1998b; Hobbs and Muzzio, 1997; Hobbs *et al.*1998; Liu *et al.,* 2006; Fourcade *et al.,* 2001).

Distinctive challenges of computational rheology were addressed by Walter and Webster in 2003 for non-Newtonian and viscoelastic fluids. Numerical codes used to predict the behavior of non-Newtonian fluids often leads to inevitable discrepancies with experimental results attributing to the underlying inaccurate assumptions that would only be applicable and hold true for Newtonian fluids. As a result, attempts taken by computational scientist leads to frustration and failures (Walters and Webster, 2003). Munch and Klein (2012) highlighted the important limitations of computational fluid dynamics. For instance, it is difficult to incorporate all details of a flow field and users are not always knowledgeable about the limitations of CFD code which may results in inaccurate results, if applied outside the defined boundaries.

For non-Newtonian fluids, incompressible Navier-Stokes equations is typically used while incorporating the dependence of viscosity on strain-rate tensor. Liu *et al.* (2006) conducted a CFD work to study the mixing of power law fluids in the SMX static mixer. A fully developed flow velocity profile was assumed with no slip boundary condition applied on the tube walls and mixer element surfaces. It was reported that the use of apparent viscosities at the wall creates larger discrepancies for Reynolds number greater than 10 (Hobbs *et al.,* 1998).

Another major challenge with CFD simulations is that tracer particles are sometimes trapped in regions close to the walls and are often lost during the simulation. This violates the law of conservation of mass leading to inevitable errors. To resolve such problem, the mesh was refined to a smaller size closer to these regions to improve the accuracy of calculations. However, due to

the impracticability of the smaller grid refinement, another approach to displace particles perpendicular to the wall is employed (Regner *et al.,* 2006; Hobbs and Muzzio, 1997).

Particularly, for non-Newtonian fluids, the rheology is complex and the viscosity is a function of shear rate and could be time dependent as well. Development of CFD flow model for more complex rheological fluids is quite complicated due to the non-ideal behavior of the non-Newtonian fluids (Patel *et al*., 2013). The non-ideal behaviors can be categorized as 1) channeling; 2) recirculation; 3) dead zones. Thus, it requires more attention on the quality of mesh, and the grid refinement for simulating the CFD flow model for more complex rheological fluids.

2.7 RESEARCH OBJECTIVES

A thorough literature review suggests that a very little information is available in the mixing of yield-psuedoplastic fluids especially in the SMX static mixer. In this research study, the electrical resistance tomography (ERT) and computational fluid dynamics (CFD) tools were employed to understand the mechanisms involved during the mixing of the secondary fluid in the yield-pseudo plastic primary fluid in the SMX static mixer.

To elucidate the mixing mechanism, the research study is conducted as follows:

- To understand the effect of the primary fluid rheology and the primary fluid flow rates on the mixing of miscible fluids in the SMX static mixer using ERT technique.

- To develop and to validate a CFD model and then conducting the following numerical research study using the validated CFD model:

  - To understand the effect of the primary/secondary flow ratio on the mixing of miscible fluids in the SMX static mixer.

  - To understand the effect of the secondary fluid viscosity on the mixing of miscible fluids in the SMX static mixer.

3. EXPERIMENTAL SETUP AND PROCEDURE

3.1 EXPERIMENTAL SETUP

The experimental set-up depicted in Fig.3.1 was utilized for this research study. A transparent PVC pipe with an internal diameter (ID) of 0.1016 m and a length of 2.02 m was used. The pipe was inserted with 5 SMX static mixers (L/D =3) equally spaced inside the pipe. The first SMX static mixer (Sulzer, Switzerland) was located 0.15 m from the pipe inlet. The xanthan gum solutions of three different mass concentrations (0.5 wt%, 1.0 wt%, and 1.5 wt%) were used in this study. The desired amount of xanthan gum powder was added gradually in the feed tank under agitation. The solution was agitated for 4 hours to attain a homogeneous solution and left to stay overnight to remove any air bubbles. The xanthan gum solution was fed into the static mixer by using a progressive cavity pump (Model: BN1-6L, SEEPEX, USA) operated by a variable frequency drive (Model: M1220B, AC Tech, USA). A peristaltic metering pump (Model: A3V24-MNJ, Blue-White, USA) was used to inject a measured volume of the secondary fluid from the tracer tank at a constant flow rate at the center of the pipe. A pressure transmitter (Model: PX409-005DWU5V, Omega, Canada) was used to measure the differential pressure between the pipe inlet (P1) and the pipe exit (P2).
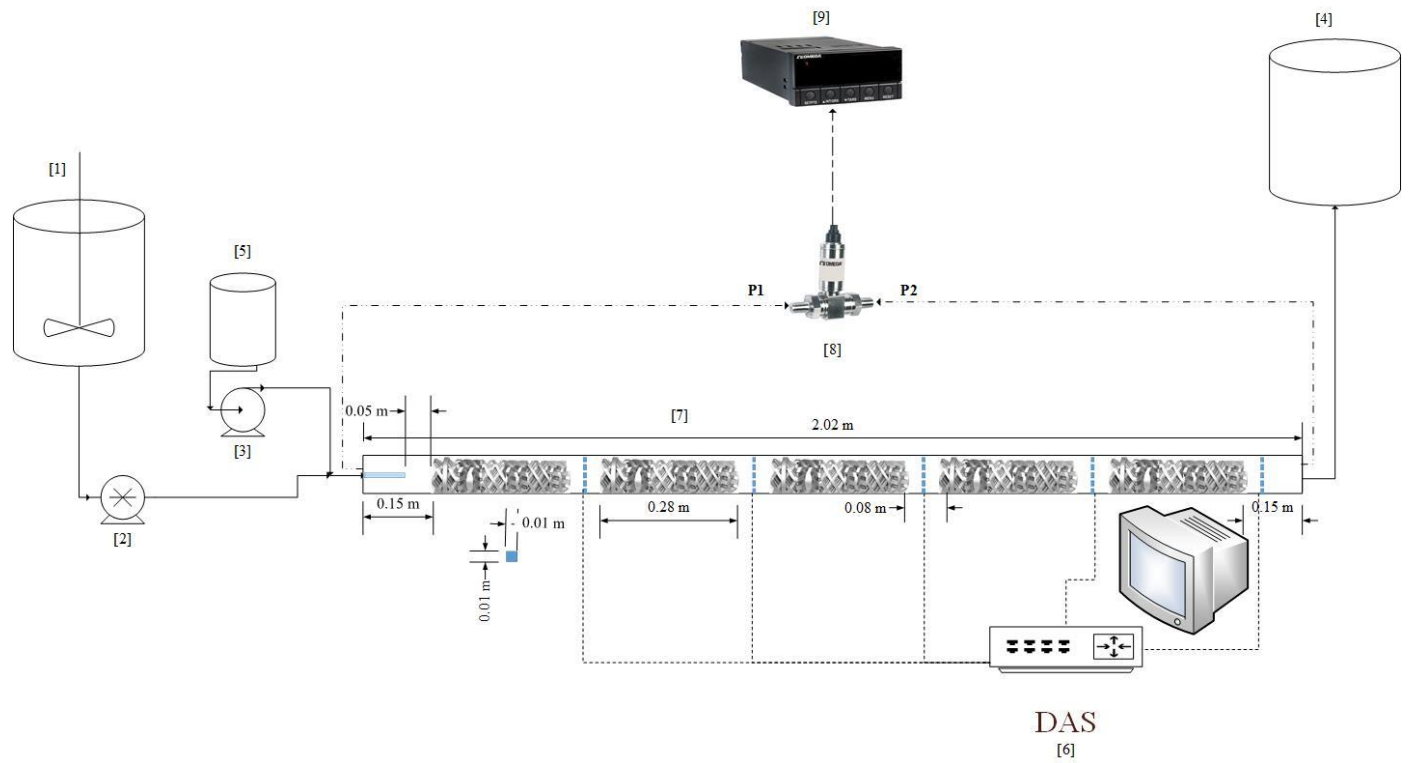
Figure 3.1:Experimental setup of the continuous-flow mixing: (1) feed tank, (2) progressing cavity pump, (3) rotary pump, (4) discharge tank, (5) tracer tank, (6) data acquisition system, (7) in-line pipe mixing, (8) pressure transducer, and (9) digital display

3.2 ELECTRICAL RESISTANCE TOMOGRAPHY (ERT) SYSTEM

The ERT system comprises of three components: the sensor electrodes, the data acquisition system (DAS), and the image reconstruction system. There are 5 ERT planes installed in the pipe setup and each ERT plane consisted of 16 stainless steel electrodes equally spaced out around the pipe periphery. The 1st and 5th ERT planes were located 0.5 m from the pipe inlet and pipe exit, respectively. The height, width and thickness of electrodes were 0.01 m, 0.01 m, and 0.001 m, respectively. Each electrode was in direct contact with the flowing fluid without causing any external disturbances to the fluid flow. All electrodes were connected to the electrical resistance tomography (ERT) system which then connected to the computer for ERT image reconstruction.

The ITS 2000 p2+ ERT system applied a constant AC current of 15mA using adjacent measurement protocol to a pair of electrodes and measured the voltage difference across other electrode pairs to map conductivity distribution across the pipe cross-sectional area (Barber *et al*., 1983). For the 8 pairs of electrodes located around the pipe periphery, the AC current was injected at one pair of electrodes and the voltage differences at the other 7 electrode pairs were measured. The AC current was injected until all possible voltage measurements were taken across the pipe cross sectional area. The ERT system provided 104 individual voltage measurements, using the adjacent measurement protocol according to N (N-3)/2, where N is the number of electrodes per plane (i.e. 16). All tests were conducted with an excitation frequency of 9.6 kHz and 15 mA current. The sampling time interval was 55 ms and 8 measurement sets were taken to be averaged. The ERT system maps the conductivity distribution around the pipe cross-sectional area to a spatial resolution around 5% of the pipe diameter. A reference measurement was taken prior to the injection of the secondary stream to eliminate the effect of all internals (i.e. working fluid, SMX static mixer) inside the pipe on the ERT measurement.

3.3 IMAGE RECONSTRUCTION SYSTEM

A non-iterative image reconstruction algorithm (Linear Back Projection- LBP) was applied to convert raw voltage measurements into a 2D conductivity map. There are 316 pixels that fit the pipe cross-sectional area. The Poisson's equation was used to find the conductivity across the pipe cross-sectional. A numerical method is required to solve Poisson's equation which is given by (Kleinermann *et al.*, 1999):

$$\nabla^2 \varphi = -J(r_0) \tag{3.3.1}$$

where φ is the electrical potential, $J(r_0)$ is the current source at an internal point (r_0).

Equation 3.3.1 is solved by the application of the Green's function and the same equation can be rewritten as below:

$$\nabla^2 G(r|r_0) = -Ci_i(r - r_0) \tag{3.3.2}$$

where $G(r|r_0)$ is the Green's function, r_0 is the actual position of the current source, r is the location of the solution to be calculated, and Ci_i is the conductivity.

The total solution of the electrical potential (φ) at position (r) is calculated using the below equation:

$$\varphi(r) = -\sum_{i=1}^{number\ of\ electrodes} \iint_A G(r|r_0)J_i(r_0)dr_0 \tag{3.3.3}$$

where J_i is the current density applied on the ith electrode, A is the surface area of the ith electrode.

Equation 3.3.3 was substituted in Equation 3.3.1 and non-iterative linear back projection algorithm was employed to reach the approximate solution. This non-iterative method was chosen since it consumes lower computational time to perform the numerical calculation of the 2D conductivity map (Madupu *et al.*, 2005).

3.4 FLUID RHEOLOGY

The working fluids were xanthan gum solution (CP Kelco, USA) with mass concentration of 0.5 wt%, 1.0 wt% and 1.5 wt%. The rheological properties of the xanthan solution are listed in Table 3.1 (Saeed *et al.*, 2008):

Table 3.1: Rheological properties of xanthan gum solution

Xanthan gum Concentration (wt%)	Density (ρ) $(Kg\ m^{-3})$	Yield stress (τ_y) (Pa)	Consistency index (K) $(Pa\ s^n)$	Power law index (n)
0.5	997.36	1.79	3	0.11
1.0	991.80	5.25	8	0.12
1.5	989.76	7.46	14	0.14

Xanthan gum solution is a shear thinning fluid with yield stress and obeys the Herschel-Bulkley model (Herschel and Bulkley, 1926).

$$\tau_{rz} = \tau_y + K(\frac{\partial v_z}{\partial r})^n \qquad (3.4.1)$$

where τ_{rz} is the shear stress, τ_y is the yield stress, $\frac{\partial v_z}{\partial r}$ is the shear rate, and *K* and *n* are the shear rate independent constants. This follows the flow curve of a typical yield-pseudoplastic fluid depicted in Fig. 3.2. To create fluid flow, the shear stress has to exceed the yield stress of the fluid. As the shear rate increases, the applied shear stress increases as well and thus the slope of the flow curve declines signifying the weakening of the solution viscosity as the shear rate increases. That is why, this type of fluid is known as shear thinning since the solution viscosity alleviates with an increasing shear rate. The apparent viscosity of the xanthan gum solution can be expressed as below:

$$\eta = K \left(\frac{\partial v_z}{\partial r}\right)^{n-1} + \frac{\tau_y}{\left(\frac{\partial v_z}{\partial r}\right)} \qquad (3.4.2)$$

Shear
stress

Yield stress

Shear rate
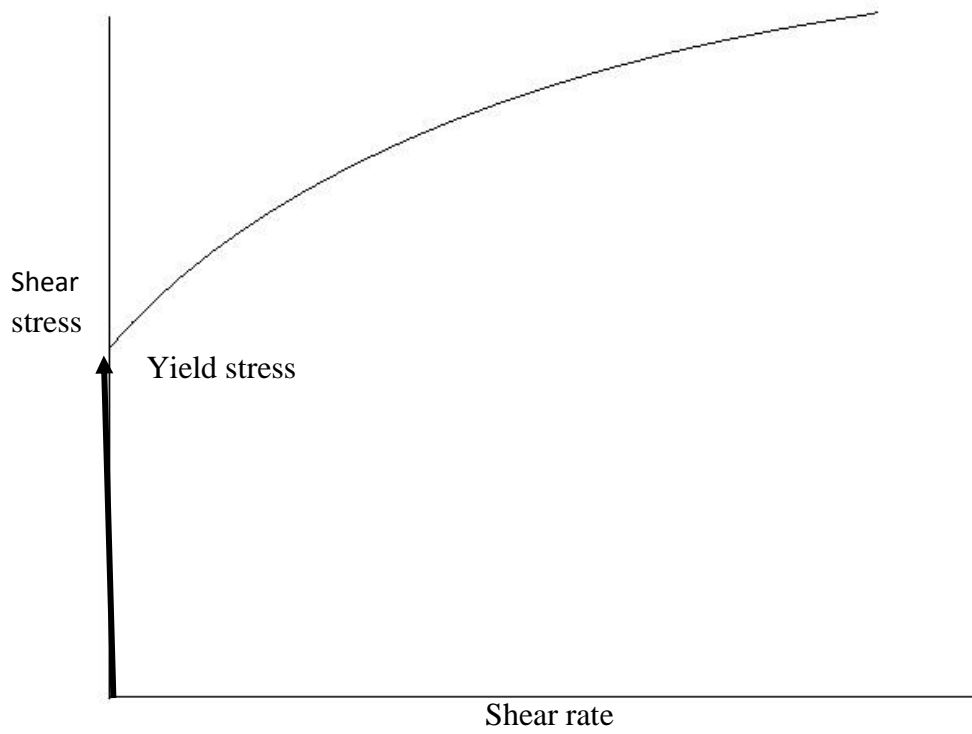
Fig. 3.2. Flow curve of a typical yield-pseudoplastic fluid

3.5 EXPERIMENTAL PROCEDURE

3.5.1 MIXING INDEX MEASUREMENTS

The distributive mixing of the secondary fluid in the xanthan gum solution (primary fluid) was analyzed using the tomography data. The conductivity of the secondary fluid was higher than that of the primary fluid due to the addition of 5 wt% table salt to the secondary fluid. The distribution of the secondary fluid in the xanthan gum solution was monitored by keep tracking of the changes in the conductivities in all 5 different ERT tomography planes after the injection of secondary fluid. It was ensured that the salt concentration in the xanthan gum solution did not exceed 0.17 wt%. Previous studies showed that the salt concentration below this threshold level of 0.17 wt% did not affect the rheological properties of the xanthan gum solutions significantly (Saeed *et al.*, 2008). To measure the mixing index, the secondary fluid was fed to the system with a fixed flow rate at $t = 0$ s. A step change in conductivity was prominently observed for all xanthan gum concentrations (0.5 wt%, 1.0 wt%, and 1.5 wt %) and a sample result is shown in Fig. 3.3. However, the conductivity measurement in tomography plane 1 for 1.0 wt% xanthan gum solution mostly fluctuated compared to that of other tomography planes since Plane 1 was very close to the injection point.
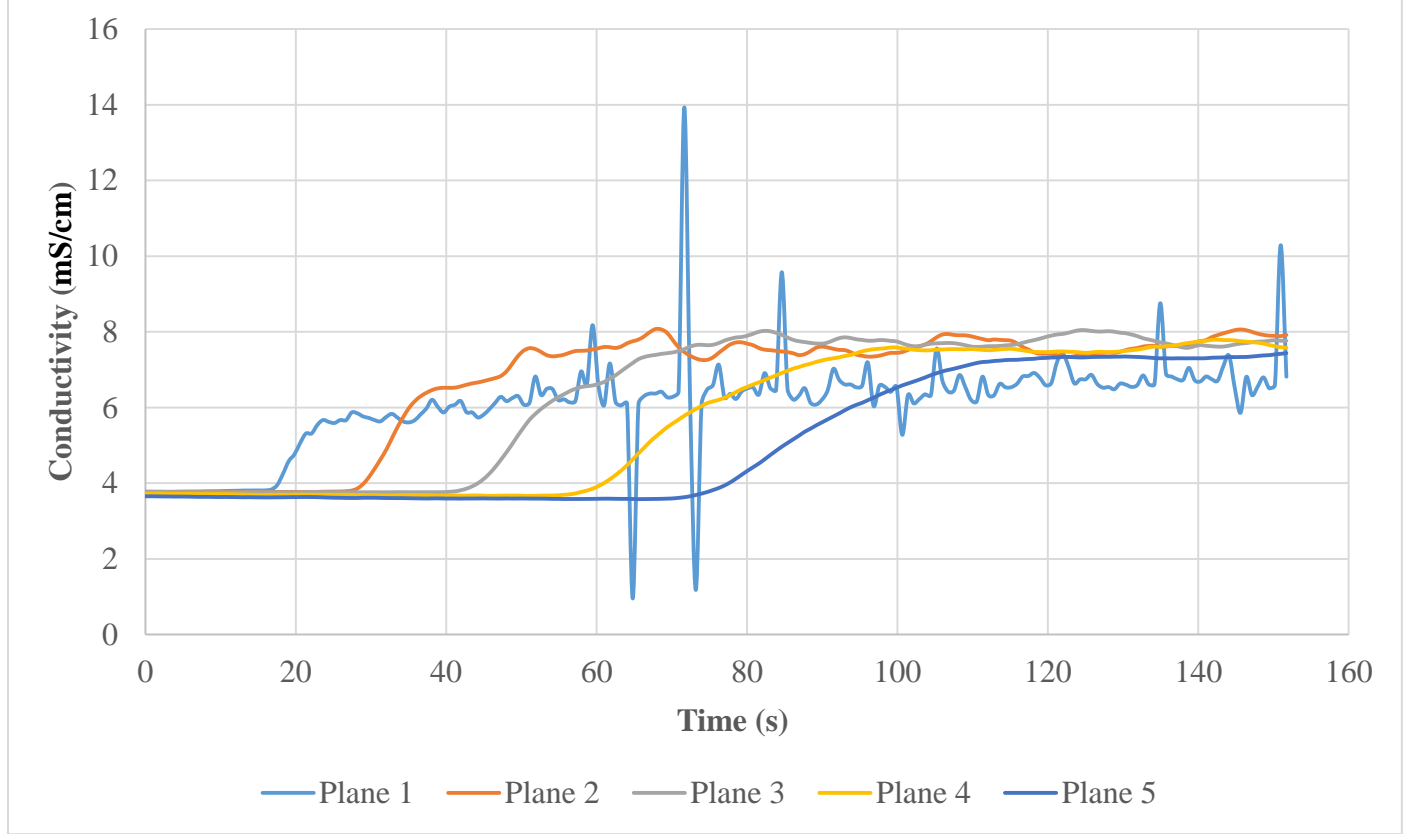
Fig 3.3: Step change in the conductivity of 1.0 wt % xanthan gum solution after the injection of the saline solution as the secondary fluid

Once the step change in conductivity reached to the steady-state conductivity value, the mixing index calculation was performed to study the conductivity distribution in 316 pixels of each tomography planes. The mixing index was calculated using the following equation (Alberini *et al*., 2014; Kukukova *et al*., 2008; Diggle, 2003; Reardon and O'Sullivan, 2004; Yenjaichon *et al*., 2012; Yenjaichon *et al*., 2014):

$$\text{Mixing index} = \frac{\sqrt{\sum_{i=1}^{np} \frac{(Ci_i - \overline{Ci})^2}{(np-1)}}}{\overline{Ci}} \tag{3.5.1}$$

where Ci_i is local conductivity measurement, $\overline{Ci}$ is the average conductivity, and *np* is the total number of pixels for each tomography plane, which is 316. Experimental conditions are listed in Table 3.2. Founargiotakis et al., (2008) developed the generalized Reynolds number for the flow of Herschel-Bulkley fluid in an annulus.

53

The generalized Reynolds number for the flow of non-Newtonian fluid in a round pipe was developed earlier and it is shown below (Metzner, 1957; Metzner and Reed, 1955):

$$Re_{MR} = \frac{D^{n'}V^{2-n'}\rho}{K'8^{n'-1}} \qquad \text{(Metzner, 1957; Metzner and Reed, 1955)} \qquad (3.5.2)$$

The slope of the logarithmic τ_w vs $\dot{\gamma}_{Nw}$ yields n', as shown in Equation 3.5.3

$$n' = \frac{d\ln(\tau_w)}{d\ln(\dot{\gamma}_{Nw})} \text{ and } \tau_w = K'(\dot{\gamma}_{Nw})^{n'} \quad \text{(Founargiotakis \textit{et al}., 2008)}$$

$$(3.5.3)$$

The relationship between n' and Herschel-Bulkley rheological parameters can be expressed as below:

$$n' = \frac{n(1-\xi)(n\xi+n+1)}{1+n+2n\xi+2n^2\xi^2} \qquad (3.5.4)$$

where $\xi = \frac{\tau_y}{\tau_w}$ \qquad (3.5.5)

$$\dot{\gamma}_{Nw} = \frac{8V}{D}; \text{ Newtonian shear rate for a round pipe} \qquad (3.5.6)$$

$$\dot{\gamma}_w = \frac{3n+1}{4n}\frac{8V}{D}; \text{ non-Newtonian shear rate for a round pipe} \qquad (3.5.7)$$

τ_y −yield stress (Pa)

τ_w − Wall shear stress (Pa)

n- flow behavior index (i.e. rheological parameter)

When Equation 3.5.3 is equated to the Herschel-Bulkley rheological model, it becomes:

$$\tau_w = K'(\dot{\gamma}_{Nw})^{n'} = \tau_y + K(\dot{\gamma}_w)^n \qquad (3.5.8)$$

Rearrangement of the above Equation 3.5.8 to solve for K':

$$K' = \frac{\tau_y+K(\dot{\gamma}_w)^n}{(\dot{\gamma}_{Nw})^{n'}} \qquad (3.5.9)$$

Since our pipe geometry is round, $\dot{\gamma}_w$, in Equation 3.5.9, is replaced by Equation 3.5.7 to yield the below equation:

$$K' = \frac{\tau_y + K(\frac{3n+1}{4n}\dot{\gamma}_{Nw})^n}{(\dot{\gamma}_{Nw})^{n'}} \qquad (3.6.0)$$

Equation (3.6.0) is very much similar to what already been reported for Herschel-Bulkley fluid in an annulus which is shown below:

$$K' = \frac{\tau_y + K(\frac{2n+1}{3n}\dot{\gamma}_{Nw})^n}{(\dot{\gamma}_{Nw})^{n'}} \quad \text{(Founargiotakis et al., 2008)}$$

(3.6.1)

where $\frac{2n+1}{3n}\dot{\gamma}_{Nw}$ is the non-Newtonian shear rate for an annulus pipe geometry

Using Equation 3.5.2, the generalized Reynolds number for xanthan gum solution was calculated and shown in Table 3.3.

Table 3.2: Experimental conditions

Xanthan gum mass concentration	Xanthan gum flow rate	Secondary fluid flow rate	Secondary fluid type
0.5 wt%	3.5 L/min, 6 L/min, and 12.5 L/min	100 mL/min	Newtonian fluid (Saline solution)
0.5 wt%	3.5 L/min	100 mL/min	non-Newtonian fluid (0.5 wt% xanthan gum solution)
1.0 wt%	3.5 L/min, 6 L/min, and 12.5 L/min	100 mL/min	Newtonian fluid (Saline solution)
1.0 wt%	3.5 L/min	100 mL/min	non-Newtonian fluid (1.0 wt% xanthan gum solution)
1.5 wt%	3.5 L/min, 6 L/min, and 12.5 L/min	100mL/min	Newtonian fluid (Saline solution)

Table 3.3: Generalized Reynolds Number for Herschel-Bulkley fluid (i.e. xanthan gum solution)

Xanthan gum mass concentration	Xanthan gum flow rate	Generalized Reynolds Number
0.5 wt%		$0.1 < Re_{MR} < 1.26$
1.0 wt%	3.5 L/min -12.5 L/min	$0.039 < Re_{MR} < 0.450$
1.5 wt%		$0.025 < Re_{MR} < 0.280$

4. CFD MODEL DEVELOPMENT

4.1 INTRODUCTION

Computational Fluid Dynamics (CFD) is a powerful tool that helps to study the flow of non-Newtonian fluids in mixing vessels. The CFD tool enables us to simulate the complex fluid flow problems and to understand the obscure phenomena, which cannot be unveiled from the data gathered in a laboratory setting alone. Thus, CFD is widely used in engineering designs as it could predict the performance of the new design or processes before actually implementing them (Xia and Sun, 2002). For non-Newtonian fluids, the incompressible Navier-Stokes equations are typically used while incorporating the dependence of viscosity on strain-rate tensor. The CFD software package (ANSYS FLUENT, V.16.2) was used in this study to generate the flow of yield-psuedoplastic fluid (xanthan gum solution) in the SMX static mixer using a finite volume method.

In this chapter, the flow geometry and the meshing are discussed followed by the grid independence test. Afterwards, the CFD model, relevant boundary conditions, Fluent solver settings, and convergence criteria for the CFD calculations are discoursed briefly for the fundamental understanding of the computational fluid dynamics. The CFD data are presented and discussed in Chapter 5 more elaborately.

4.2 CFD FLOW GEOMETRY

 The CFD flow domain consisted of the injection pipe for the secondary fluid, main pipe for the primary fluid, and the SMX static mixer. The ANSYS DesignModeler (Version. 16.2) was used to create the geometry depicted in Fig. 4.1. The injection pipe and the SMX static mixer are considered to be the solid body while keeping the main pipe as the fluid body. The geometry specifications are listed in Table 4.1. Each static mixer is oriented 90º degree to each to other.
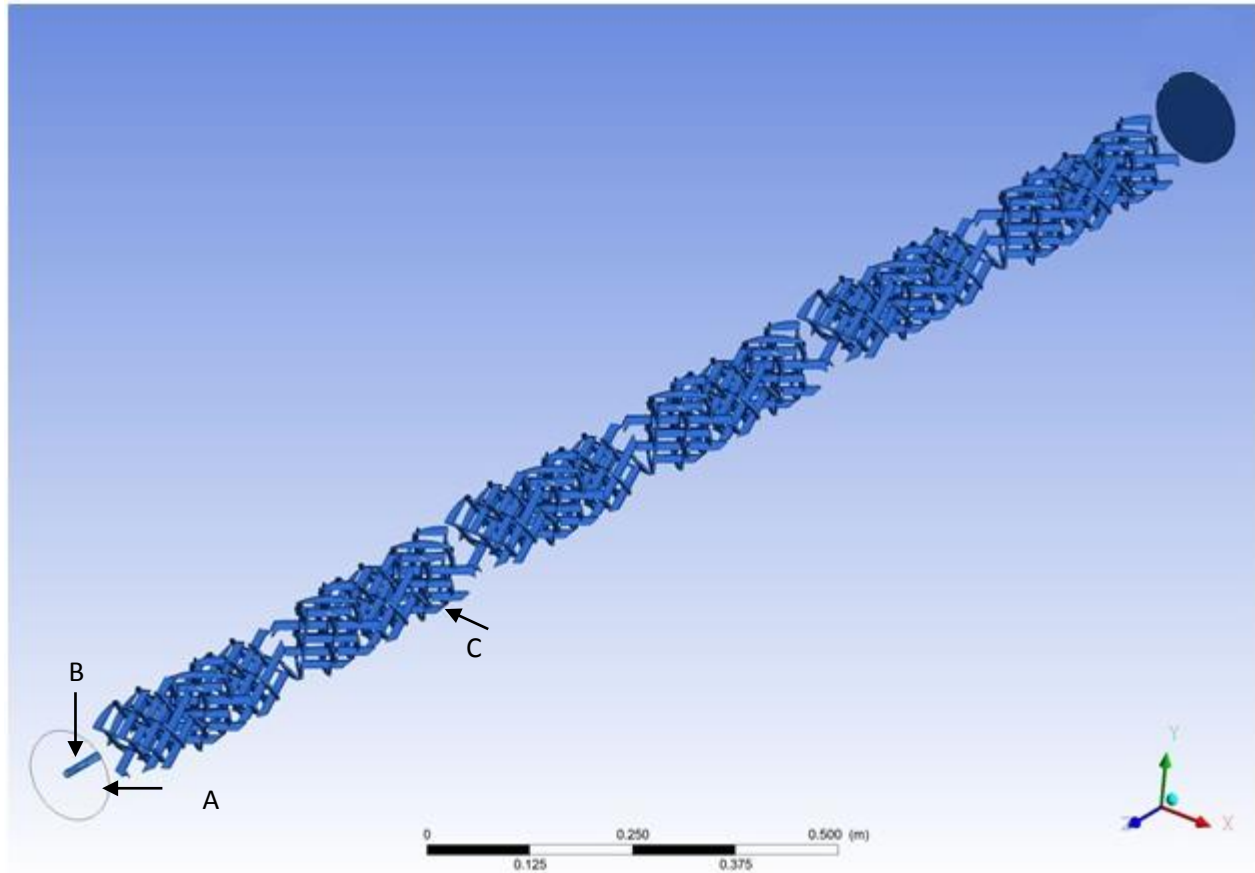
Fig.4.1. CFD flow domain (A: Main pipe; B: Injection pipe; C: SMX static mixer)

Table 4.1: Geometry Specifications

Main Pipe Diameter (m)	0.101
Main Pipe Length (m)	2.43
Injection Pipe Diameter (m)	0.011
Injection Pipe Length (m)	0.10
Static Mixer Length(m)	0.32
Static Mixer Diameter (m)	0.10

4.3 GRID GENERATION

An unstructured tetrahedral mesh was used to discretize the control volume that to be simulated. In the meshing of the fluid domain, the skewed cell above the range of 0.6 was converted to polyhedra. However, due to the complexity of the SMX static mixer geometry, there were a few fractions of the skewed cells above the skewness range of 0.8, which were infeasible to be rectified into polyhedra in ANSYS Fluent.

4.4 GRID INDEPENDENCE TEST

The optimal number of cells employed for the discretization of the fluid domain was determined using the grid independence test. Three different grids were generated for this test: 2,921,003 cells, 7,565,177 cells, and 19,757,603 cells. To examine the grid independence, the pressure drop data between the pipe inlet and the exit were obtained from the CFD flow model for the three different grids. When the number of cells changed from 2,921,003 to 7,565,177 and from 7,565,177 to 19,757,603, the relative errors were 2.52% and 1.63 %, respectively. The relative error decreased as the number of grid size increased. The flow domain discretized with 19,757,603 cells was chosen for further numerical study.

4.5 CFD FLOW MODEL TYPE

Due to the viscous nature of the working fluid (i.e. xanthan gum solution), the CFD flow model is chosen to be laminar since Reynolds number is very small ($Re_{MR} < 0.1$).

For the continuous flow of xanthan gum solution in a pipe, the continuity equation is developed by writing a mass balance over the pipe volume and can be written by using vector notation as follows:

$$\frac{\partial \rho}{\partial t} + \nabla . (\rho v) = 0 \tag{4.5.1}$$

Under steady state condition, the above equation can be simplified for incompressible fluid as below:

$$(\nabla . v) = 0 \tag{4.5.2}$$

The generalized Newtonian model is primarily used for designing flow systems under steady-state shear flow and it incorporates the non-Newtonian viscosity without considering the time-dependent effects (Bird *et al*., 2002). For incompressible Newtonian fluids, the stress tensor is given by:

$$\tau = -\mu(\nabla V + (\nabla V)^T == -\mu \dot{\gamma} \tag{4.5.3}$$

where $\dot{\gamma}$ is the rate of deformation tensor. The generalized Newtonian fluid model is obtained by replacing the constant viscosity μ by the non-Newtonian viscosity η which is a function of the shear rate. Thus, the generalized Newtonian model can be expressed as below:

$$\tau = -\eta \dot{\gamma} \text{ with } \eta = \eta(\dot{\gamma}) \tag{4.5.4}$$

$$\rho \frac{Dv}{Dt} = -\nabla p - [\nabla . \tau] + \rho g \tag{4.5.5}$$

Using generalized Newtonian model, the equation of motion (i.e. momentum equation) can be expressed as below:

$$\rho \frac{Dv}{Dt} = -\nabla p + [\nabla . (\eta \dot{\gamma})] + \rho g \tag{4.5.6}$$

where $\frac{Dv}{Dt} = \frac{\partial v}{\partial t} + v . \nabla v$ (4.5.7)

$(v.\nabla v)$ represents the convective terms

In order to study the mixing of secondary fluid (Newtonian fluid) in primary fluid (xanthan gum solution), the species model was activated. The species transport equation can be expressed as below:

$$\frac{\partial}{\partial t}(\rho w) + \nabla.(\rho \bar{v} w) = -\nabla.(\rho D_m \nabla w) \tag{4.5.8}$$

where w is the local mass fraction of the secondary fluid, $\bar{v}$ is the mean velocity vector, ρ is the fluid density, D_m is the molecular diffusivity of the secondary fluid in the mixture, which was assumed to be $10^{-9} \frac{m^2}{s}$ as a typical value for liquids (Montante et al., 2005).

The boundary conditions should be properly specified in order to solve the transport equations. At the pipe inlet, the velocity of the primary fluid was specified (i.e. the primary flow rate was divided by the pipe cross sectional area). At the injection pipe, the velocity of the secondary fluid was specified (i.e. the secondary flow rate was divided by the cross sectional area of the injection pipe). No-slip boundary condition was used at the pipe wall and at the surface of the SMX static mixer. At the pipe outlet, the outflow boundary condition was chosen since the pressure at the pipe outlet was unknown.

4.6 SOLVER SETTING

4.6.1 PRESSURE-VELOCITY COUPLING ALGORITHM IN STEADY FLOW

The SIMPLE (Semi-Implicit Method for Pressure-Linked Equation) algorithm is a guess-and-correct method for the calculation of pressure and velocity field until the continuity equation is satisfied (Patankar and Spalding, 1972). A pressure field is estimated initially and the corresponding velocity field is solved using the momentum equation. Until the velocity fields satisfy the continuity equation, the pressure field is solved using a guess-and-correct method.

4.6.2 PRESSURE INTERPOLATION SCHEME

The PRESTO (PREssure STaggering Option) interpolation scheme was used to solve the pressure gradient term in the momentum equation. If the linear interpolation scheme was used, the pressure gradients would appear to be uniform at all nodal points even though pressure field exhibits spatial fluctuations in nodal points. In order to rectify this issue, a staggered grid for velocity component is employed (Harlow and Welch, 1965) such that the pressure gradient terms in the discretized momentum equation is significantly non-zero and thus it incorporates the realistic fluctuations in pressure field terms across the nodal points. The PRESTO interpolation scheme also calculates the velocities at exact nodal points where they are required for species transport (convection-diffusion) computations and no interpolation is required. As a result, the PRESTO interpolation scheme provides an accurate evaluation of the pressure field. Since the SMX static mixer geometry is complex and the flow dynamics around the static mixer is complicated to simulate, the PRESTO interpolation scheme would be the best option to solve for the pressure gradient in discretized momentum equation (Versteeg and Malalasekera, 2007).

4.6.3 DISCRETIZATION SCHEME FOR CONVECTIVE TERMS

The Second-order upwind scheme was chosen to solve the discretized momentum equation. This scheme is more accurate than the first order upwind and power law scheme. The accuracy of this scheme is second-order from the point of Taylor series truncation error.

4.6.4 SOLUTION CONVERGENCE

The convergence limit for the continuity equation, x-velocity, y-velocity, z-velocity and the transport species model were set to 10^{-5} and the corresponding convergence history of the residual plot is shown in Fig. 4.2. The residual measures the changes in the continuity equation, x-velocity, y-velocity, z-velocity, and the transport species equation between every iteration. The CFD flow model was run for 6000 iterations to meet the convergence criteria. The facilities of High Performance Computing Virtual Laboratory (HPCVL) were accessed for the simulation of the CFD flow model. Twelve computer nodes were used to simulate the CFD flow model and it took about 40 hours to converge.
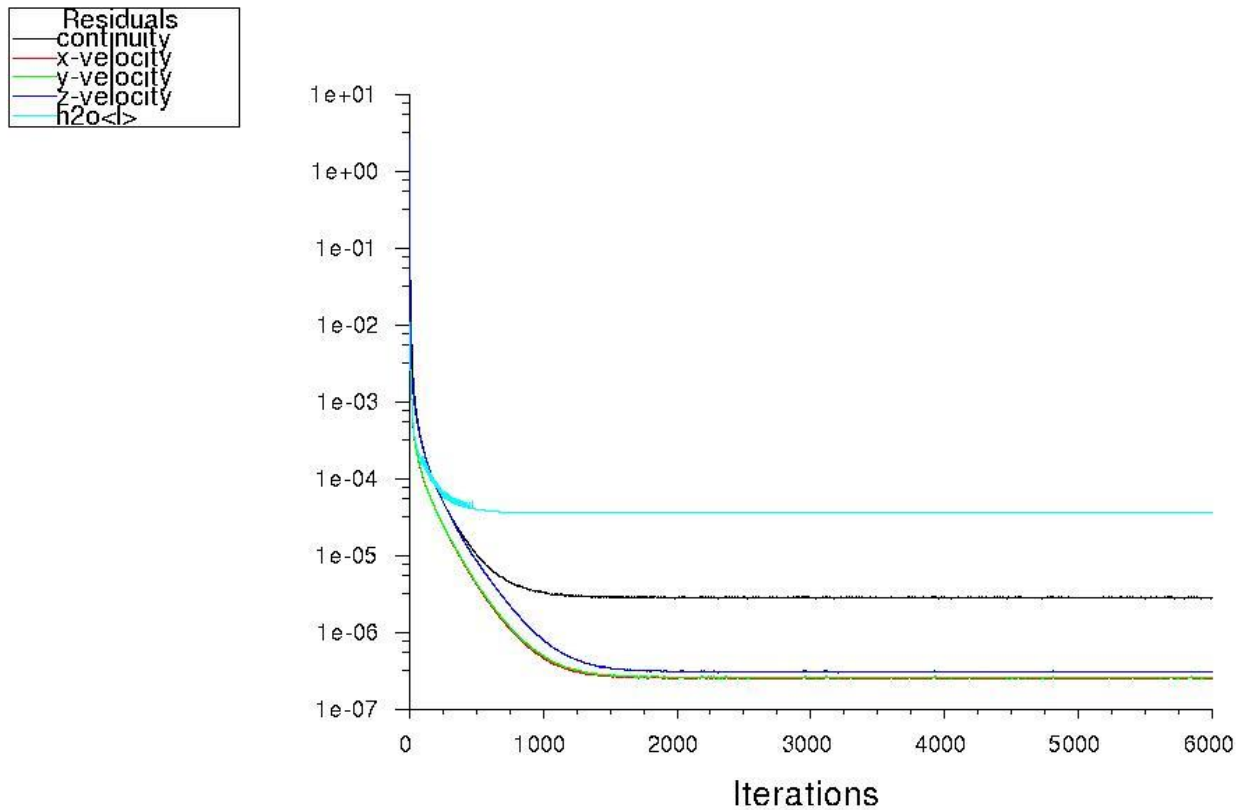
Fig. 4.2. Convergence history of the scaled residuals

4.7 CFD RESEARCH OBJECTIVES

Experimentally, the effect of primary fluid flow rates was studied between 3.5 L/min and 12.5 L/min while keeping the secondary flow rate constant at 100 mL/min. Thus, a numerical work was conducted for different secondary fluid flow rates (i.e. 100- 1000 mL/min). Numerically, the effect of primary fluid flow rates was studied below 3.5 L/min. In the literature, lower primary fluid flow rates have been recommended for the effective mixing of viscous fluids in the SMX mixer taken into the consideration of both the mixing quality and the energy requirement (Zalc *et al.,* 2002). The effect of secondary fluid viscosity was also explored. The variables investigated through CFD are shown in Table 4.2.

Table 4.2: Variables investigated through CFD

Xanthan gum mass concentration	Xanthan gum velocity (m/s)	Xanthan gum flow rate (L/min)	Secondary fluid velocity (m/s)	Secondary fluid flow rate (L/min)	Secondary fluid type and viscosity range
0.5 wt%	0.007260	3.5	0.00438	0.025	Newtonian fluid $\mu = 0.001$ kg/ms
	0.001020	0.5	0.00438	0.025	
	0.007260	3.5	0.08760	0.500	
	0.000514	0.25	0.01750	0.100	
	0.000257	0.125	0.01750	0.100	
	0.001020	0.5	0.17500	1.000	
	0.001020	0.5	0.17500	1.000	Newtonian fluid $\mu =0.01$, 1, and 10 kg/ms

5. RESULT AND DISCUSSION

5.1 INTRODUCTION

In this study, ERT was used to characterize the mixing of the secondary fluid in the yield pseudo plastic primary fluid (xanthan gum solution) in the SMX static mixer. The effect of primary fluid flow rate was studied between the range of 3.5 L/min and 12.5 L/min experimentally. A CFD model was developed for the primary fluid of 0.5 wt% xanthan gum solution in the SMX static mixer and validated using the experimental pressure drop and ERT mixing index measurements. This CFD flow model was then extensively used to study the effect of secondary fluid viscosity (i.e. 0.01-10 kg/m-s), and the primary/secondary flow ratio (i.e. 0.5- 140) on the mixing performance of the SMX static mixer.

In the following section, the effect of the primary fluid rheology, the primary fluid flow rate, the primary/secondary flow ratio, and the secondary fluid viscosity will be addressed in sequence using both the ERT and CFD tools.

5.2 EFFECT OF THE PRIMARY FLUID (XANTHAN GUM SOLUTION) RHEOLOGY ON THE MIXING PERFORMANCE OF THE STATIC MIXER USING ELECTRICAL RESISTANCE TOMOGRAPHY

The effect of the xanthan gum mass concentration on the mixing quality was explored in this experimental work. Since the rheological properties of xanthan gum solution is dependent on the mass concentration, it is crucial to investigate how the rheology of xanthan gum solution can influence the distributive mixing of the secondary stream in the primary fluid. Two sets of experiments were conducted where, in the first case, the secondary fluid was Newtonian and, in the second case, the secondary fluid was non-Newtonian.

Since the secondary fluid had a higher conductivity than the primary fluid, the distribution of the secondary stream inside the non-Newtonian primary fluid was monitored by tracking the changes in conductivity at the tomography planes. From the cross-sectional images and the volume rendering images, the appearance of the red region can be used to study the distributive mixing of the secondary stream inside the primary stream. In the tomography images, the highest conductivity region is denoted in red colour while the blue region signifies the lowest conductivity.

For the injection of 100 mL/min of the Newtonian secondary fluid (saline solution) into the primary fluid (0.5 wt% xanthan gum solution) flowing at 3.5 L/min, a red region was recorded closer to the pipe inlet at $t = 3$ s relative to the onset of the secondary fluid injection, according to Fig. 5.1. From the volume rendering images depicted in Fig 5.1, it was observed that the Newtonian secondary fluid was directed away from the pipe center to the pipe wall after $t = 7$ s. It was the static mixer that directed the Newtonian secondary fluid radially towards the pipe wall. Since Newtonian fluid (i.e. Saline solution) had constant viscosity and had no rheological complications, it flowed rapidly through the primary fluid (0.5 wt% xanthan gum solution) and this was why tomography was able to record the penetration of secondary fluid within 3 s of the injection. Since the red region denotes high conductivity, the appearance of red region was due to the penetration of secondary fluid in the primary fluid.

66

As the secondary fluid disperse into the primary fluid, the conductivity of the primary stream increases and hence the colour changes from blue (lowest conductivity) to green (average conductivity). Upon the injection of secondary fluid, the SMX static mixer was able to distribute the secondary fluid both axially and radially. The Newtonian secondary fluid was dispersed entirely in the primary fluid at $t = 23$ s relative to the point of injection. From the cross-sectional ERT images captured at 5 different axial locations in Fig. 5.2, the penetration of secondary fluid in 2nd and 4th ERT planes were noticeable in about 3 s and 7 s respectively, by tracking the presence of red colour. At $t = 23$ s, the Newtonian secondary stream reached the 5th ERT plane and was radially distributed across the entire cross-sectional area of the tomography planes.

$t = 3$ s

$t = 7$ s

$t = 10.5$ s

$t = 23$ s

Fig.5.1: 3D tomograms obtained after the injection of the Newtonian secondary stream (saline solution) into the non-Newtonian primary stream (0.5 wt% xanthan gum concentration) for the secondary flow rate of 100 mL/min and the primary flow rate of 3.5L/min.

Fig. 5.2: 2D tomograms obtained after the injection of the Newtonian secondary stream (saline solution) into the non-Newtonian Primary stream (0.5 wt% xanthan gum concentration) for the secondary flow rate of 100 mL/min and the primary flow rate of 3.5L/min.

With the secondary fluid flowing at 100 mL/min and the primary fluid flowing at 3.5 L/min, the xanthan gum mass concentration of the primary fluid was increased from 0.5 wt% to 1wt%. With increasing mass concentration, the xanthan gum rheology became more complex than 0.5 wt%. According to Fig. 5.3 and Fig. 5.4, for 1 wt% xanthan gum solution, the Newtonian secondary fluid was only able to reach the 2nd ERT plane in about 28 s while for 0.5 wt% xanthan gum solution, the secondary fluid was mixed and reached upto the 5th ERT plane around the same elapsed time. It is clearly seen that for 1 wt% xanthan gum solution, the Newtonian secondary fluid reached the 3rd ERT plane in about 45 s and the 4th plane in about 83 s. At $t = 108$ s, the Newtonian secondary fluid was completely dispersed across the entire cross-sectional area of the 5th tomography plane.

$t = 28$ s

$t = 45$ s

$t = 83$ s

$t = 108$ s

Fig.5.3: 3D tomograms obtained after the injection of the Newtonian secondary stream (saline solution) into the non-Newtonian primary stream (1.0 wt% xanthan gum concentration) for the secondary flow rate of 100 mL/min and the primary flow rate of 3.5 L/min.

Fig. 5.4: 2D tomograms obtained after the injection of the Newtonian secondary stream (saline solution) into the non-Newtonian primary stream (1.0 wt% xanthan gum concentration) for the secondary flow rate of 100 mL/min and the primary flow rate of 3.5L/min.

Similarly, while injecting the secondary fluid with the flow rate of 100 mL/min into the primary fluid flowing at 3.5 L/min, the xanthan gum mass concentration of the primary fluid was then increased from 1.0 wt% to 1.5 wt%. The elapsed time for the Newtonian secondary fluid to penetrate through the 1.5 wt% xanthan gum solution and to reach the 2nd and the 4th ERT planes were roughly the same around 28 s and 83 s, respectively, according to Fig. 5.5 and Fig. 5.6. However, around 28 s , the radial distribution of the secondary fluid across the 1st ERT plane was more effective for 1.5 wt% xanthan gum solution than for 1.0 wt% xanthan gum solution according to Fig. 5.4 and 5.6. The 2D and 3D ERT images illustrated in Fig.5.1-5.6 show that the presence of the red region was suppressed as the xanthan gum concentration increased from 0.5 wt% to 1.5 wt% resulting in a more pronounced distributive mixing. In fact, the radial dispersion of the Newtonian secondary fluid in the 1.5% xanthan gum solution was more effective compared to those for the 0.5 and 1.0 wt%.

As the xanthan gum mass concentration increased, the time for the Newtonian secondary fluid to reach upto the 5th ERT plane became longer, owing to a higher apparent viscosity of the primary fluid. In fact, the higher viscosity of the primary fluid hindered the penetration of the secondary fluid . As a result, the time taken to sense the changes in conductivity in the 5th ERT plane was longer for 1.0 wt% and 1.5 wt% compared to 0.5wt% xanthan gum solution.

$t = 28$ s

$t = 56$ s
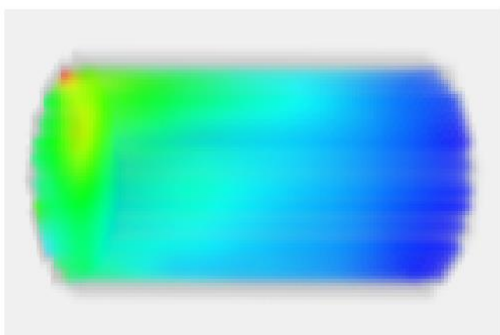
$t = 83$ s
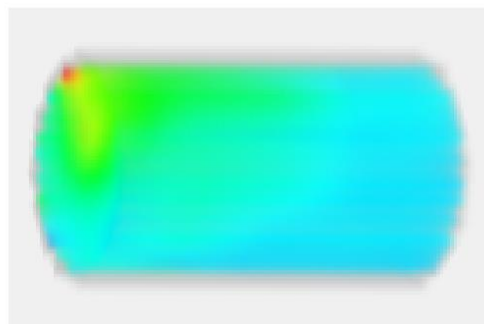
$t = 183$ s

Fig. 5.5: 3D tomograms obtained after the injection of the Newtonian secondary stream (saline solution) into the non-Newtonian primary stream (1.5 wt% xanthan gum concentration) for the secondary flow rate of 100 mL/min and the primary flow rate of 3.5 L/min.
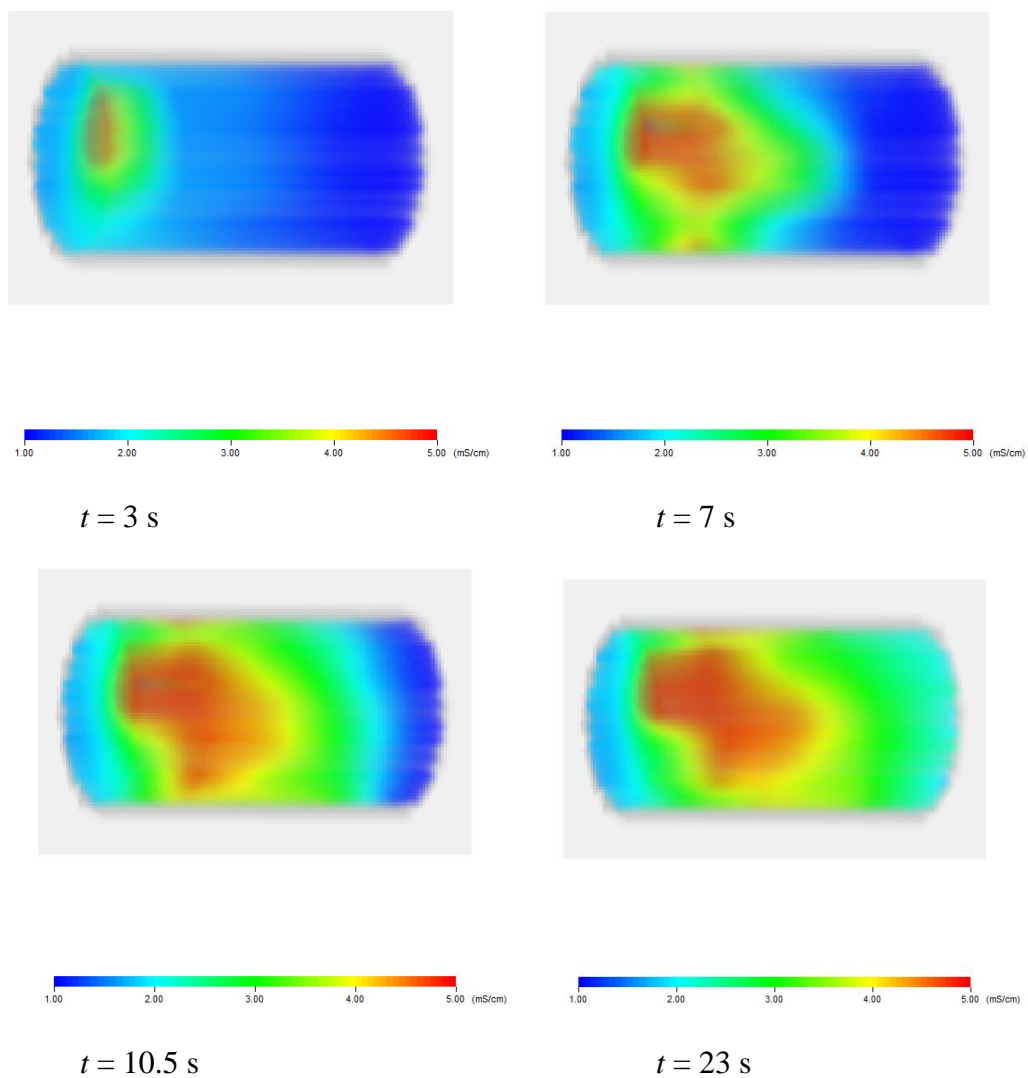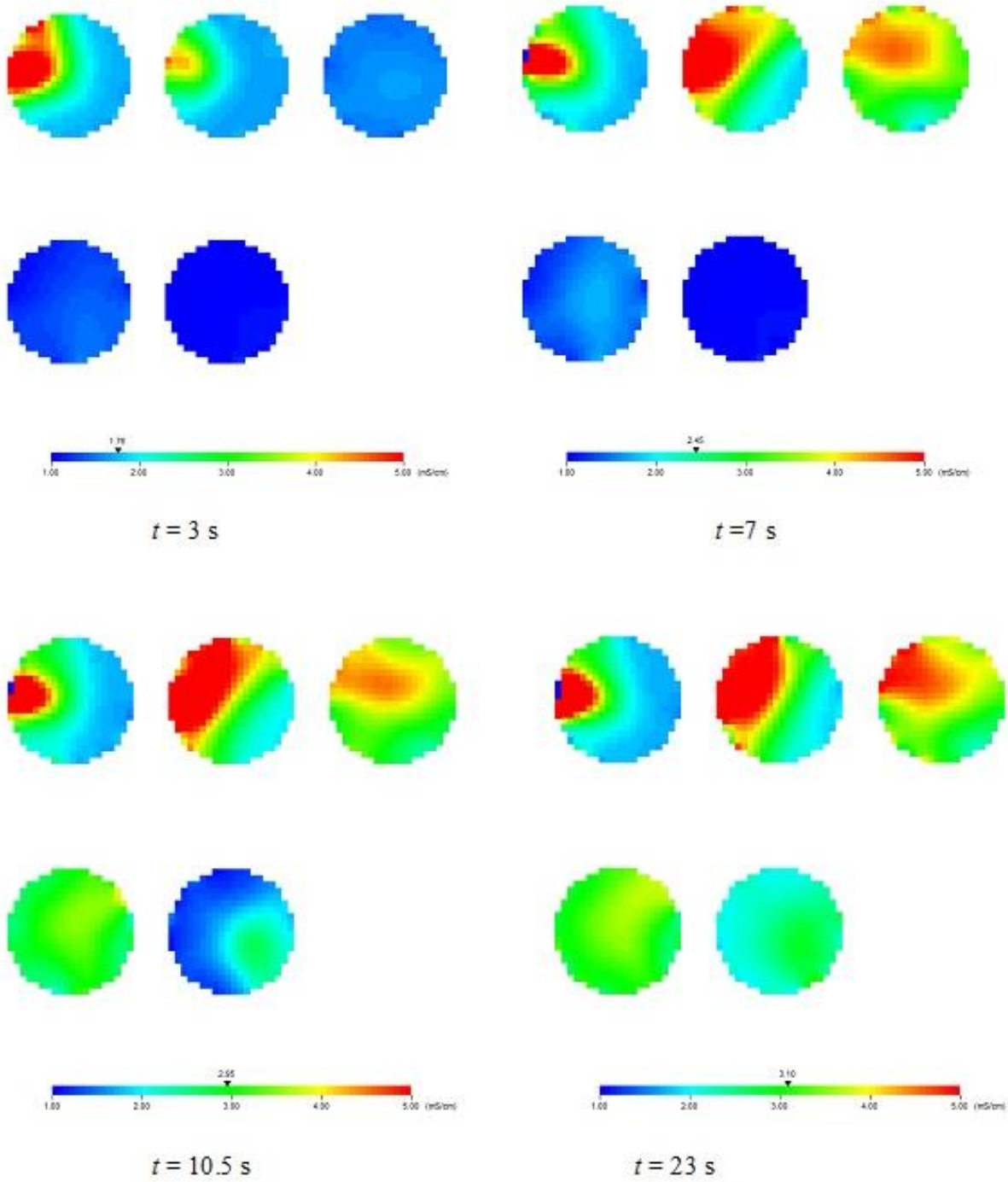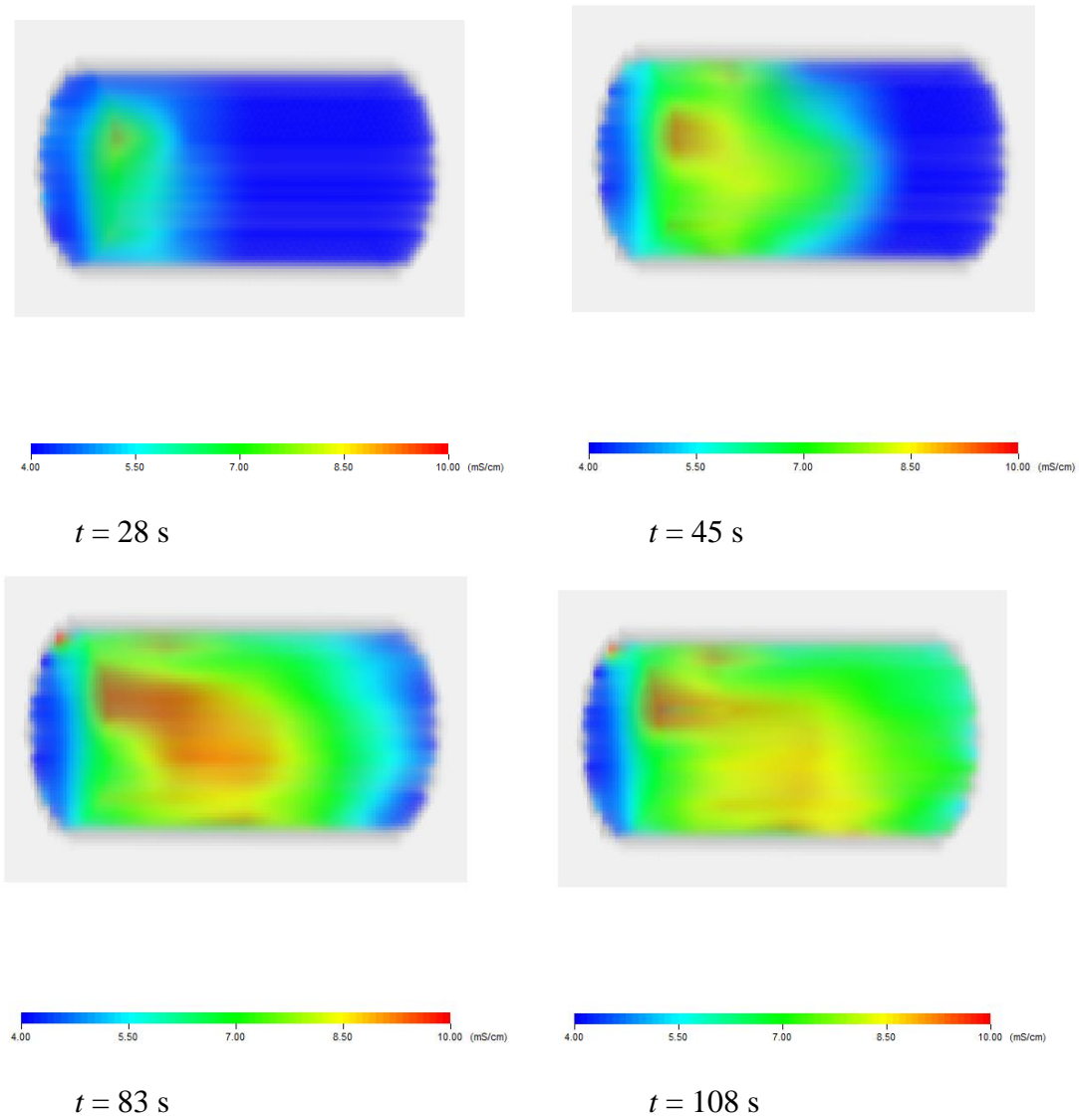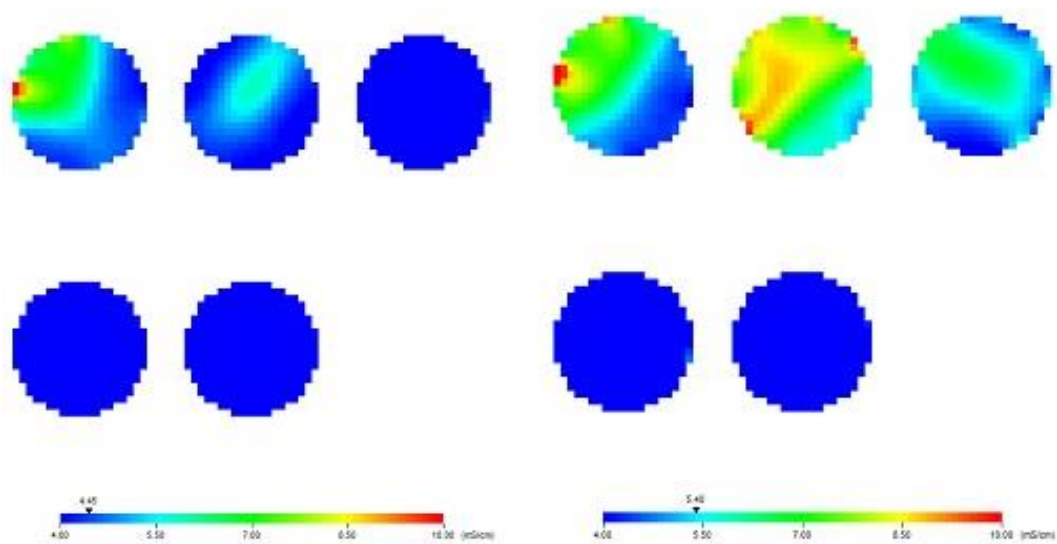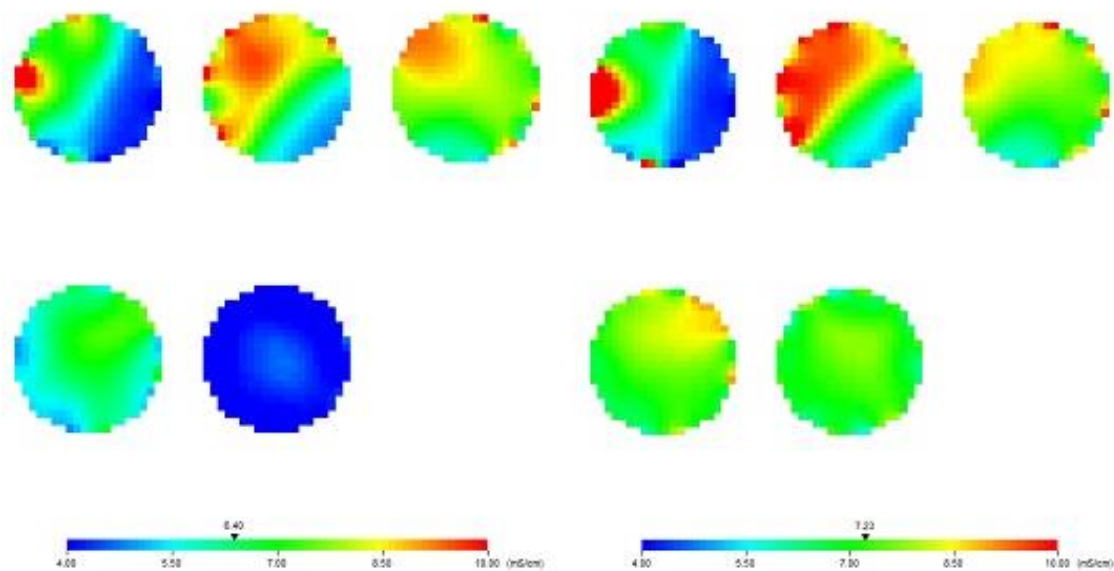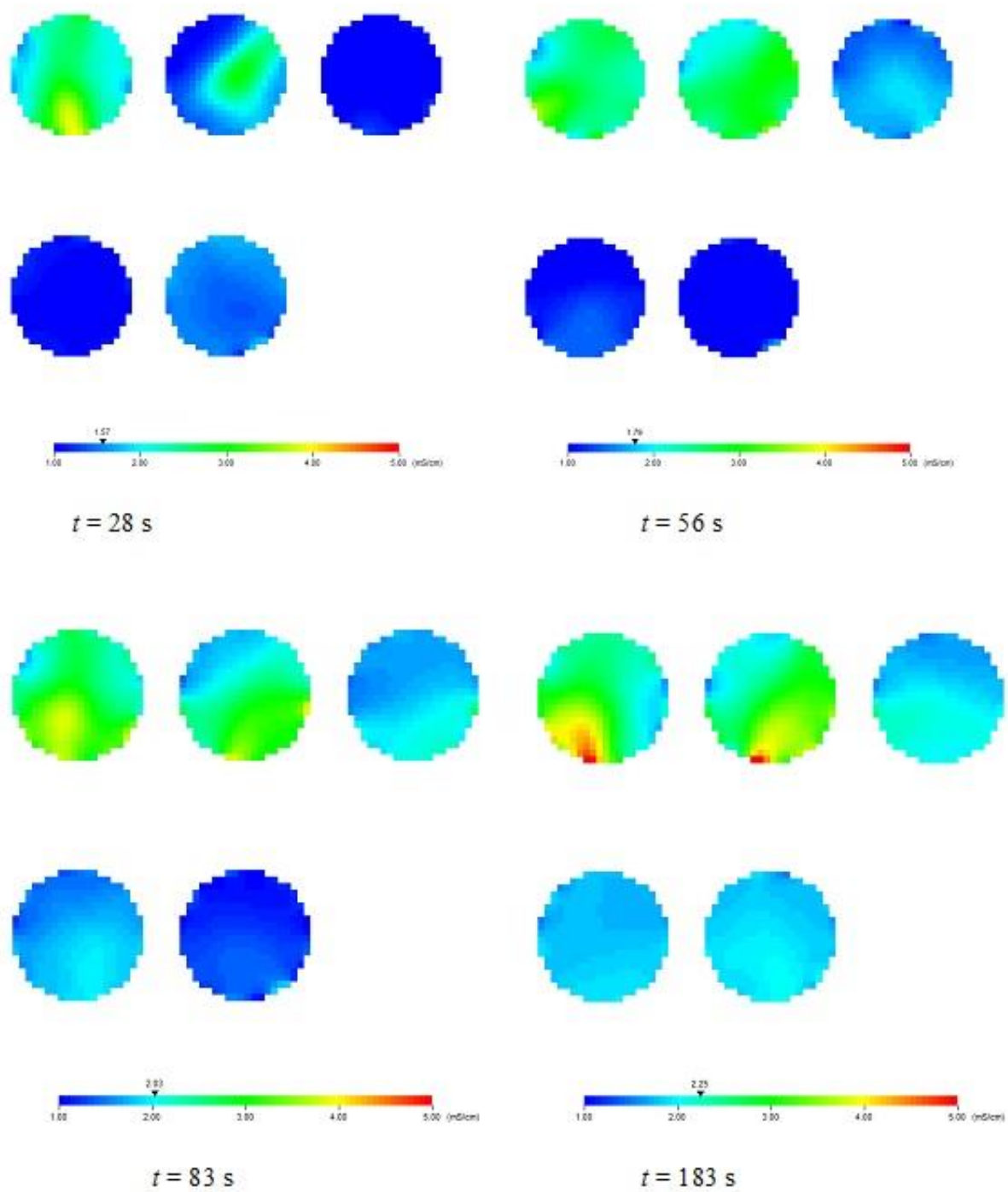
Fig. 5.6: 2D tomograms obtained after the injection of the Newtonian secondary stream (saline solution) into the non-Newtonian primary stream (1.5 wt% xanthan gum concentration) for the secondary flow rate of 100 mL/min and the primary flow rate of 3.5 L/min.

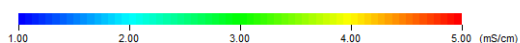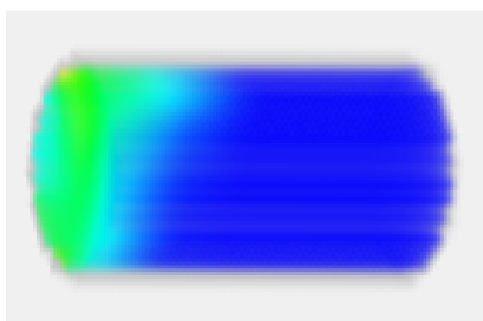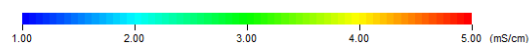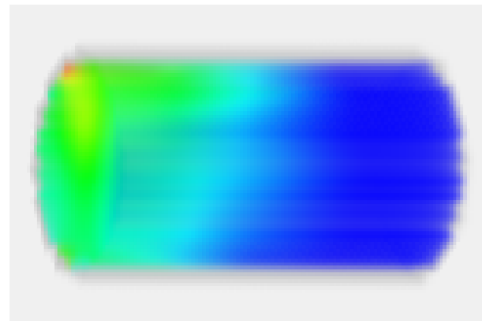Fig. 5.7 and Fig. 5.8 illustrate the volume rendering and cross-sectional ERT images for the distributive mixing of the non-Newtonian secondary fluid (0.5 wt% xanthan gum solution) in the primary fluid of 0.5 wt% xanthan gum solution. The flow rate of the secondary fluid was fixed at 100 mL/min whilst the primary flow rate was still remaining at 3.5 L/min. In this test, it took about 28 s, 56 s, and 83 s for the secondary fluid to reach the 1st, 3rd and 4th ERT planes, respectively. However, for the injection of the Newtonian secondary fluid in the primary fluid of 0.5 wt% xanthan gum solution, the elapsed times for the Newtonian secondary fluid to reach the corresponding ERT planes were drastically different, according to Fig.5.1 and Fig.5.2. The Newtonian fluid with a much lower viscocity traveled faster through the primary fluid. However, for the non-Newtonian secondary stream, the energy dissipation was faster and hence, it took a longer time to reach the corresponding ERT planes than for the Newtonian secondary fluid.

For the mixing of the non-Newtonian secondary stream (1.0 wt% xanthan gum solution) in the primary stream of 1.0 wt% xanthan gum solution, as depicted in Fig. 5.9 and Fig.5.10, it took roughly the same time to reach the corresponding ERT planes as to what observed for 0.5 wt% xanthan gum secondary fluid in Fig. 5.7 and Fig. 5.8. However, interestingly, the radial dispersion of 1 wt% xanthan gum secondary fluid in the primary fluid of 1 wt% xanthan gum solution across the cross-sectional area of the static mixer was more effective than that of 0.5 wt% xanthan secondary stream in the primary fluid of 0.5 wt% xanthan gum solution. Consistent with our experimental findings about the distributive mixing of the Newtonian fluid in the xanthan gum solution, a higher mass concentration of the xanthan gum always resulted in a more pronounced distributive mixing irrespective of the type of secondary fluid and disparate secondary/primary viscocity ratios. Similar to our previous observations for the distributive mixing of the Newtonian fluid in the xanthan gum solution, the presence of the red region (i.e. higher concentration of the secondary fluid) was suppresed as the xanthan gum mass concentration increased from 0.5 wt% to 1.0 wt% according to volume rendering images depicted in Fig. 5.7 and Fig. 5.9. As the xanthan gum mass concentration increased, the viscosity of the solution increased. The 1.5 wt% xanthan gum solution remained in contact with the SMX static mixer longer than 0.5 wt% xanthan gum solution. Hence, the static mixer was able to stretch the 1.5 wt% xanthan gum solution more effectively than the 0.5 wt% xanthan gum solution. Due to the higher degree of stretching, the interfacial area increased and enhanced the diffusion across the interface (Muzzio *et al*., 1991). Thus, the higher mass concentration of

xanthan gum solution exhibited a more effective radial mixing due to the enhanced diffusion across the interfacial area.
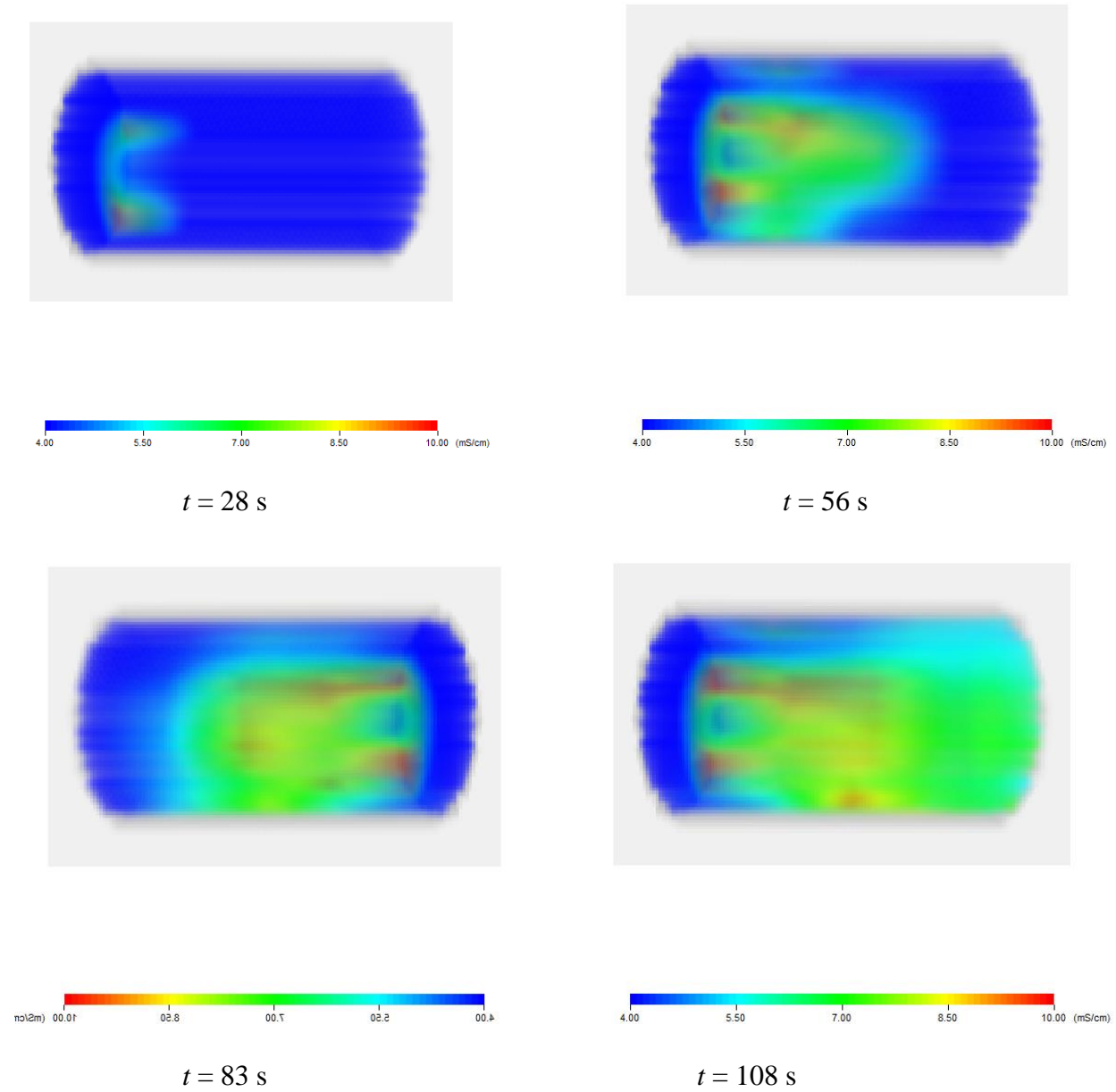
Fig. 5.7: 3D tomograms obtained after the injection of the non-Newtonian secondary stream (0.5 wt% xanthan gum) into the non-Newtonian primary stream (0.5 wt% xanthan gum) for the secondary flow rate of 100 ml/min and primary flow rate of 3.5L/min.
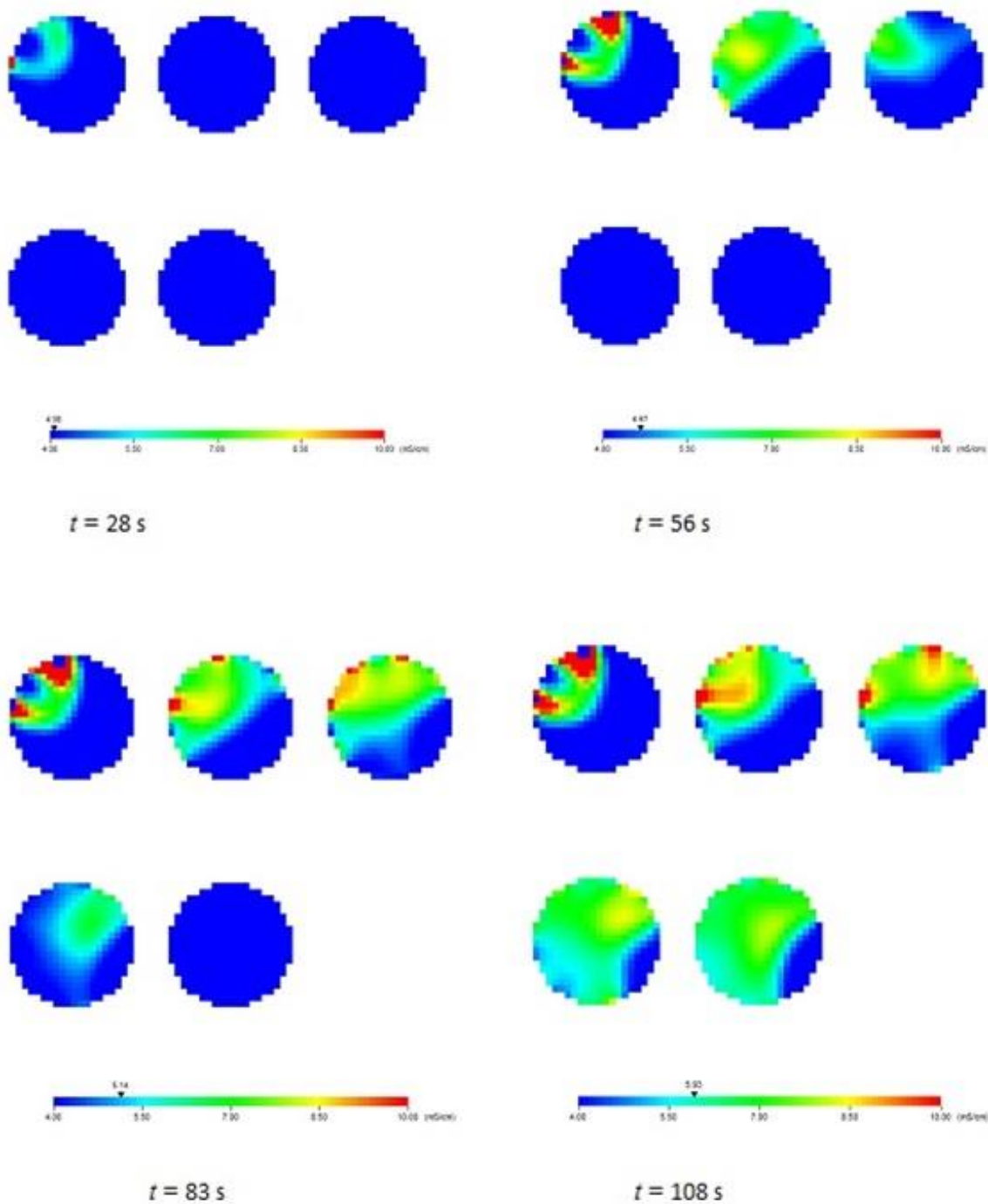
Fig. 5.8: 2D tomograms obtained after the injection of the non-Newtonian secondary stream (0.5 wt% xanthan gum) into the non-Newtonian primary stream (0.5 wt% xanthan gum) for the secondary flow rate of 100 mL/min and the primary flow rate of 3.5 L/min.

$t = 28$ s

$t = 56$ s

$t = 83$ s

$t = 108$ s
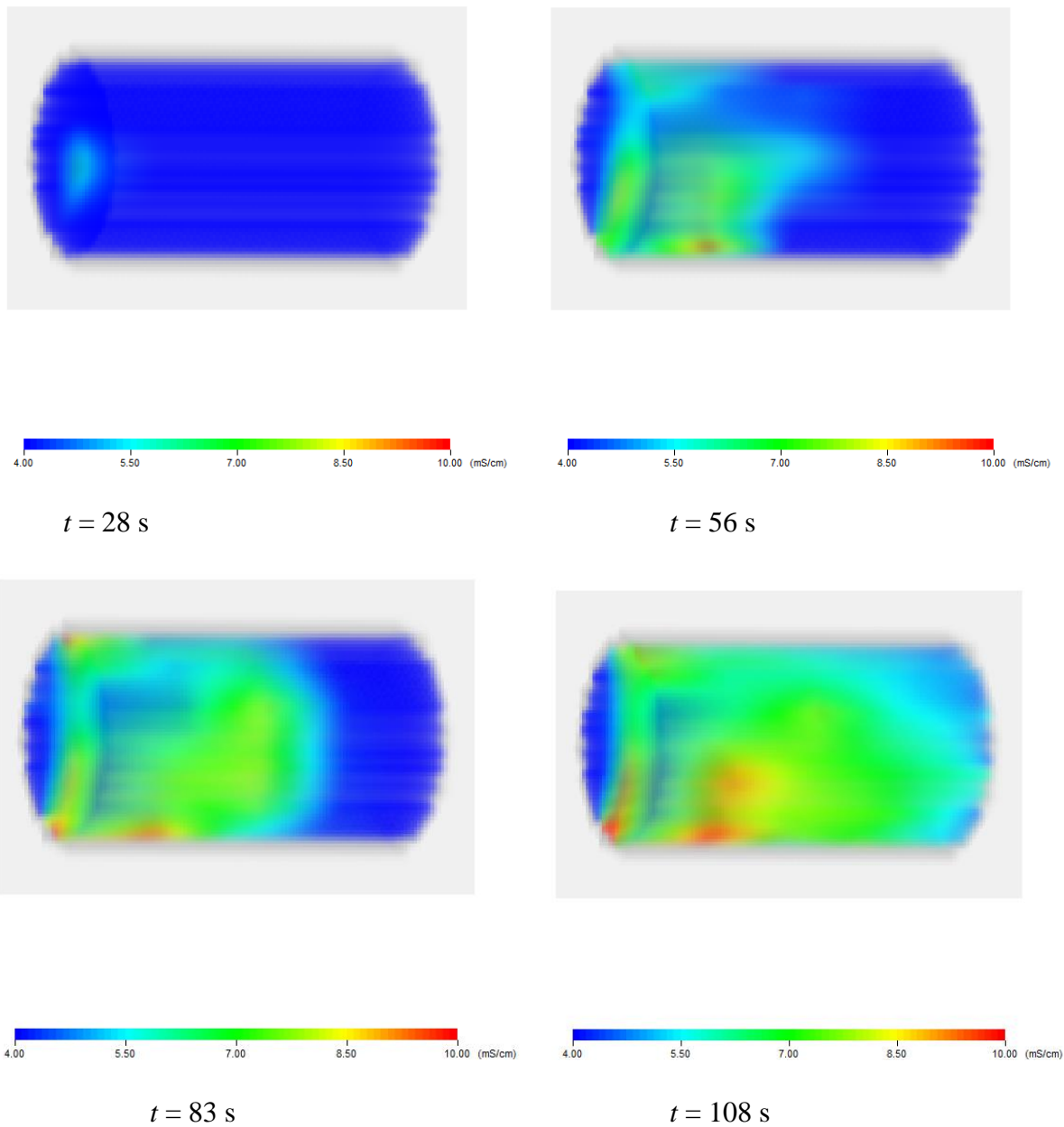
Fig. 5.9: 3D tomograms obtained after the injection of the non-Newtonian secondary stream (1.0 wt% xanthan gum) into the non-Newtonian primary stream (1.0 wt% xanthan gum) for the secondary flow rate of 100 ml/min and primary flow rate of 3.5 L/min.
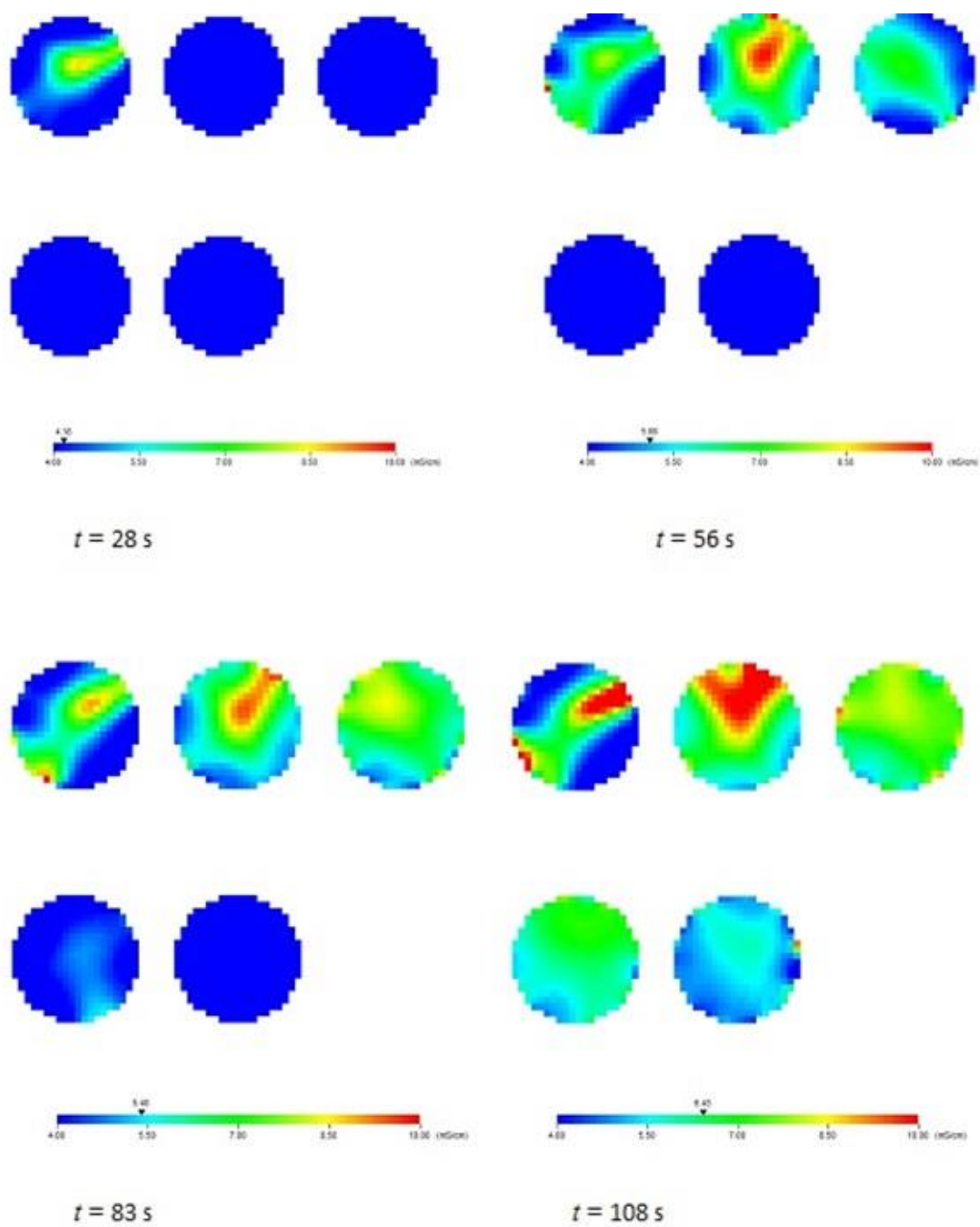
Fig. 5.10: 2D tomograms obtained after the injection of the non-Newtonian secondary stream (1.0 wt% xanthan gum) into the non-Newtonian primary stream (1.0 wt% xanthan gum) for the secondary flow rate of 100 mL/min and the primary flow rate of 3.5 L/min.

From the qualitiative point of view, it was observed that the primary fluid with a higher xanthan gum mass concentration resulted in a more pronounced mixing quality despite the complex fluid rheology at higher mass concentration. Quantitatively, the distributive mixing quality was determined using the coefficient of variation (CoV) of the conductivity values in each ERT image, which is also known as the mixing index. The mixing index can be calculated using the below expression (Alberini *et al*., 2014; Kukukova *et al*., 2008; Diggle, 2003; Reardon and O'Sullivan, 2004; Yenjaichon *et al*., 2012; Yenjaichon *et al*., 2014):

$$\text{Mixing index} = \frac{\sqrt{\sum_{i=1}^{np}\frac{(Ci_i - \overline{Ci})^2}{(np-1)}}}{\overline{Ci}} \tag{5.2.1}$$

where Ci_i is local conductivity measurement, $\overline{Ci}$ is the average conductivity, and *np* is the total number of pixels for each tomography plane, which is 316. For lower xanthan gum concentration (0.5 wt%), the mixing index calculated for tomography plane 1 was around 2.0. However, for higher xanthan gum concentration (1.0 wt% and 1.5 wt %), the mixing index attained for ERT plane 1 was around 0.5. The electrical noises were observed in plane 1 due to the direct contact of salt ions with the ERT electrodes since the plane 1 was very close to the injection point. However, the 0.5 wt% xanthan gum solution exhibited higher electrical noises than 1 wt% and 1.5 wt% xanthan gum solutions. This was observed because the viscosity of 0.5 wt% xanthan gum solution was relatively lower than those of 1.0 wt% and 1.5 wt% xanthan gum solutions. As a result, the chaotic nature of the SMX static mixer was significantly experienced by the lower xanthan gum concentration leading to more pronounced conductivity fluctuations. That was why, the normalized mixing index of 0.5 wt% xanthan gum solution was significantly higher than other xanthan gum solutions at the first tomography plane. The mixing index is the same as the standard deviation but normalized to the average conductivity of each tomography image. If the distribution of the secondary fluid in the primary fluid is more uniform across the cross-sectional area of tomography plane, the standard deviation will be lower and hence the mixing index value will be lower as well. Hence, a lower mixing index value means a better mixing quality. From the point of mixing index analysis shown in Fig. 5.11 and Fig.5.12, the higher xanthan gum mass concentration produced a more effective distributive mixing. It is observed that the change in the mixing index value of all xanthan gum concentration became insignificant after tomography plane 3. Most signicant changes in the mixing index value was noticeable for tomography planes

1 and 2. The secondary fluid and the primary fluid were miscible and the chaotic nature of the SMX static mixer was sufficient enough for effective distributive mixing such that the two static mixer elements were adequate to effectively disperse the secondary fluid in the primary fluid. The standard deviation table for normalized mixing index is depicted in Table 5.1. The standard deviation of the 1st tomography plane was relatively higher compared to other tomography planes due to the fluctuations in conductivity measurement.
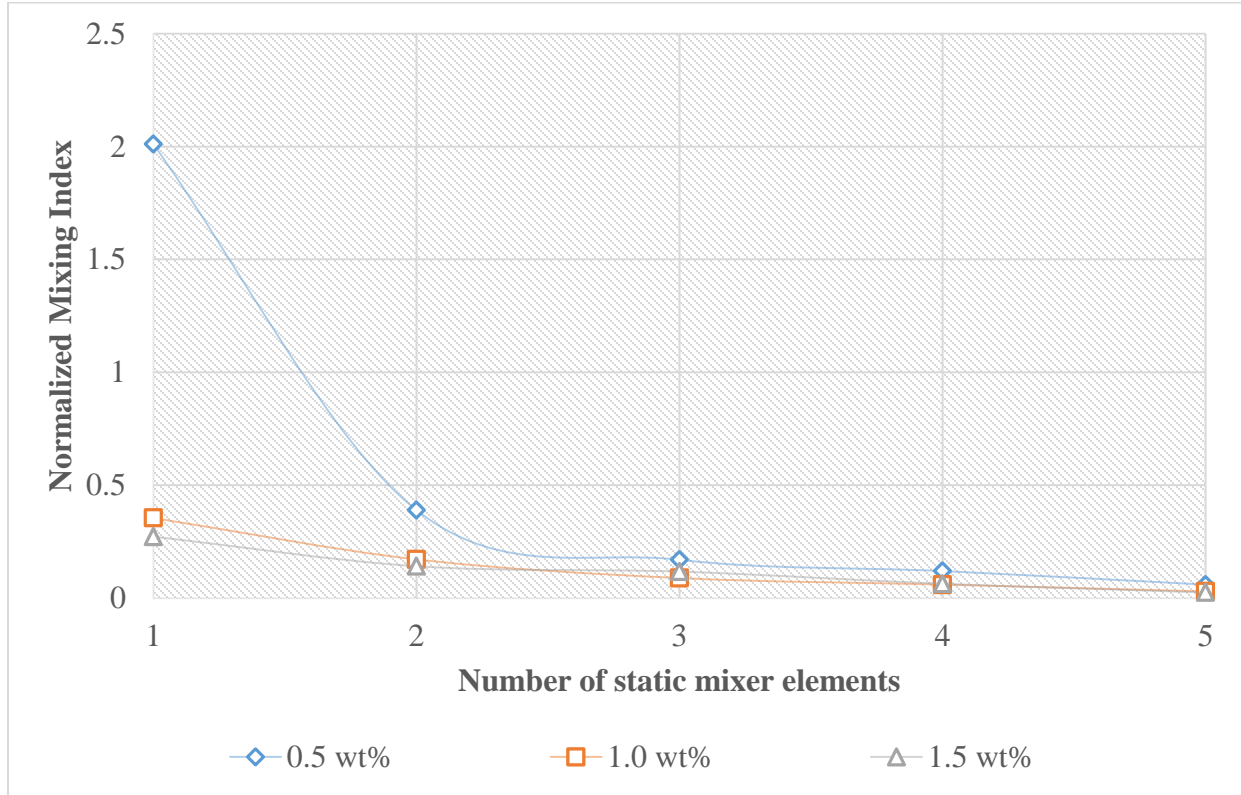
Fig. 5.11: Normalized mixing index graph for the distributive mixing of the Newtonian secondary stream (saline solution) into the non-Newtonian primary stream (0.5-1.5 wt% xanthan gum solution) for the secondary flow rate of 100 mL/min and the primary flow rate of 3.5 L/min. The maximum standard deviation observed for the normalized mixing index in 5th ERT plane was ±0.010.

Table 5.1: Standard deviation data for the normalized mixing index (Primary flow rate of 3.5 L/min and secondary flow rate of 100 mL/min)

| Xanthan gum mass concentration	1st element	2nd element	3rd element	4th element	5th element
0.5	0.493	0.010	0.010	0.010	0.010
1.0	0.642	0.016	0.018	0.015	0.008
1.5	0.031	0.020	0.026	0.019	0.002
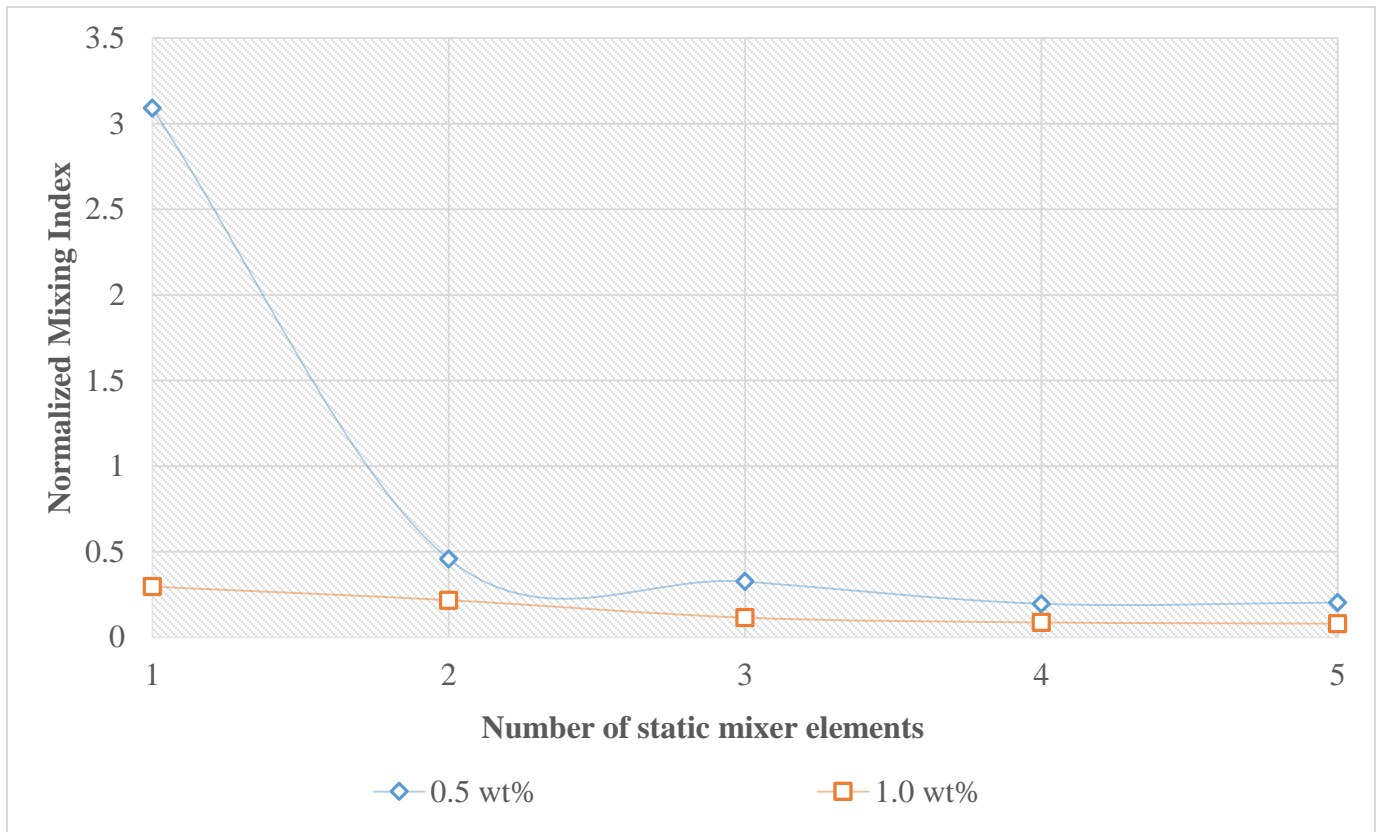
Fig. 5.12: Normalized mixing index graph for the distributive mixing of the non-Newtonian secondary stream into the non-Newtonian primary stream (i.e. 0.5 wt% xanthan gum secondary stream into 0.5 wt% primary stream and 1.0 wt% xanthan gum secondary stream into 1.0 wt% primary stream) for the secondary flow rate of 100 mL/min and the primary flow rate of 3.5 L/min. The maximum standard deviation observed for the normalized mixing index in 5th ERT plane was ±0.051.

5.3 EFFECT OF THE PRIMARY FLUID FLOW RATE ON THE MIXING QUALITY USING ELECTRICAL RESISTANCE TOMOGRAPHY

For the sake of simplicity, the tests described in previous sections were conducted at one experimental condition (primary flow rate: 3.5 L/min and secondary flow rate: 100 mL/min) to study the effect of the xanthan mass concentration (0.5 wt%, 1.0 wt%, and 1.5 wt%) on the mixing quality. In this section, other primary flow rates (6 L/min and 12.5 L/min) were studied while keeping the secondary flow rate constant at 100 mL/min for three different xanthan mass concentrations (0.5 wt%, 1.0 wt%, and 1.5 wt%). The 2D ERT images for the distributive mixing of the secondary fluid (saline solution with the flow rate of 100 mL/min) into the primary fluid (0.5-1.5wt% xanthan gum solution with the flow rate of 6 L/min) are depicted in Fig. 5.13, Fig. 5.14, and Fig. 5.15. Similarly, for a different primary flow rate at 12.5 L/min, the 2D ERT images are shown in Fig. 5.16, Fig.5.17, and Fig.5.18 for the distributive mixing of the secondary fluid (saline solution with the flow rate of 100 mL/min) into the primary fluid (0.5-1.5wt% xanthan gum solution with the flow rate of 12.5 L/min). Similar to our previous observations for the primary flow rate of 3.5 L/min depicted in Fig. 5.2, Fig. 5.4, and Fig. 5.6, a more pronounced radial mixing was observed for the other primary flow rates such as 6 L/min and 12.5 L/min when the xanthan gum mass concentration increased.

According to the data presented in Fig. 5.2, Fig.5.13, and Fig. 5.16 for 0.5 wt% xanthan gum solution flowing at 3.5 L/min, 6 L/min, and 12.5 L/min, the appearance of red region (i.e. higher concentration of the secondary fluid) shrinked as the flow rate increased from 3.5 L/min to 12.5 L/min. This is due to the magnitude of advection created by the bulk flow as the primary flow rate increased. However, the time taken to reach the corresponding tomography planes were the same for the 0.5 wt% xanthan gum solution flowing at 3.5 L/min, 6 L/min, and 12.5 L/min. This is because the secondary fluid was able to penetrate through the primary fluid without any hindrance. As a result, the axial transport of the secondary fluid was not fully dependent on the advection of the primary fluid (0.5wt% xanthan gum solution).

For the other xanthan gum concentrations (1.0 wt% and 1.5 wt%), the time taken to reach the 1st tomography plane was dependent on the advection created by the primary flow. To reach the 1st

84

tomography plane, it took about $t = 28$ s when the primary flow rate was 3.5 L/min and $t = 14$ s when the primary flow rate was 6 L/min. Upon increasing the primary flow rate from 6 L/min to 12.5 L/min, the elapsed time to reach the tomography planes became even shorter. For instance, the elapsed time to reach the 5th tomography plane for 1 wt% xanthan gum solution flowing at 3.5 L/min , 6 L/min and 12.5 L/min were $t = 108$ s, $t = 70$ s, and $t = 43$ s, respectively. Similarly, the elapsed time to reach the 5th tomography plane for 1.5 wt% xanthan gum solution were $t = 183$ s, $t = 85$ s, and $t = 43$ s, respectively. When the viscosity of the xanthan gum solution increases at higher mass concentration (1 wt% and 1.5 wt%), the resistance for the secondary fluid to penetrate through the primary fluid increases. Hence, for higher xanthan gum mass concentration, the secondary fluid depends on the primary fluid advection for the axial transport of the secondary fluid. When the primary flow rate increased from 3.5 L/min to 12.5 L/min, the primary fluid was able to transport the secondary fluid much faster axially and hence, the time required to reach the corresponding tomography planes became shorter.
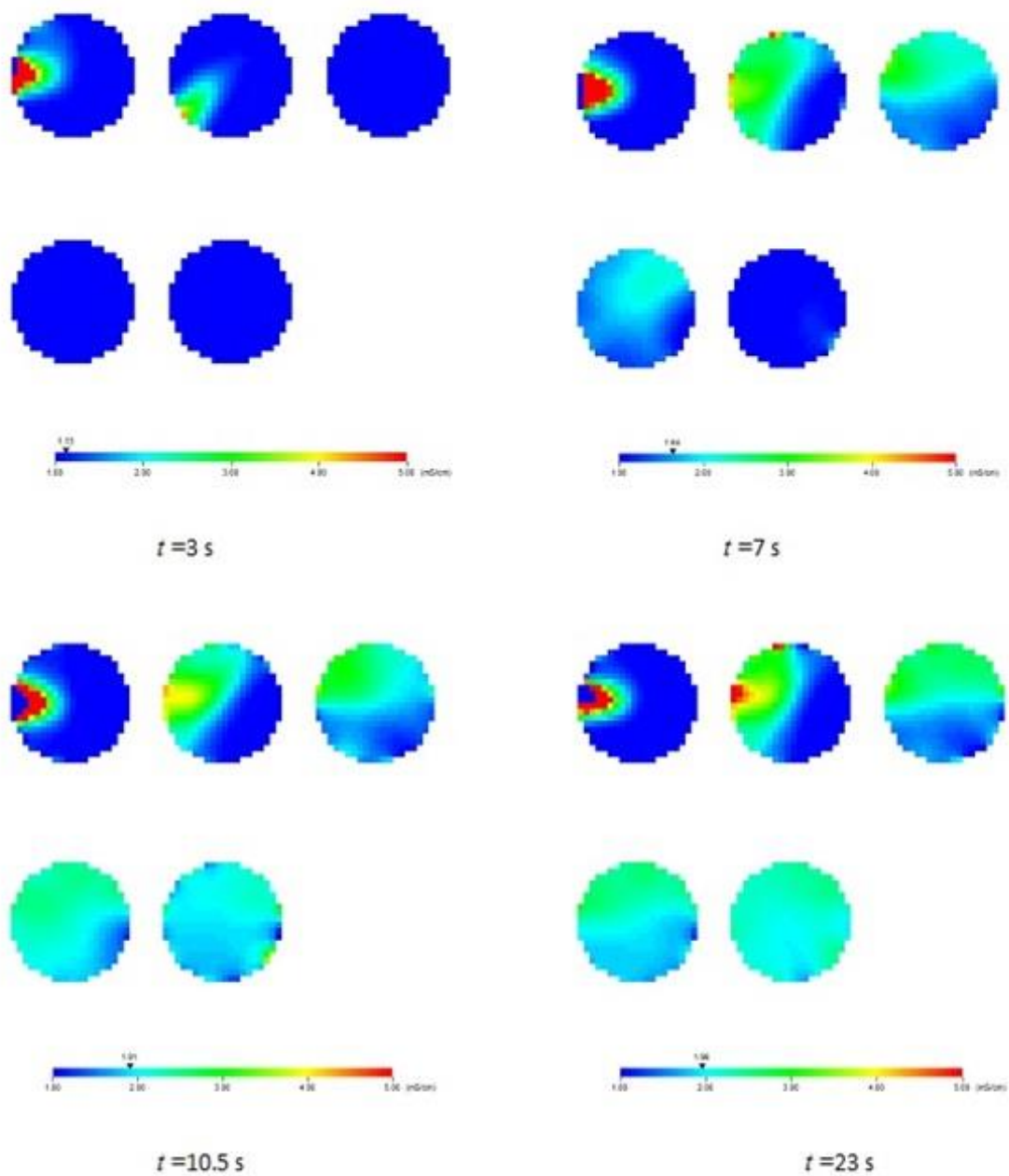
Fig. 5.13: 2D tomograms obtained after the injection of the Newtonian secondary stream (saline solution) into the non-Newtonian primary stream (0.5 wt% xanthan gum) for the secondary flow rate of 100 mL/min and the primary flow rate of 6 L/min.
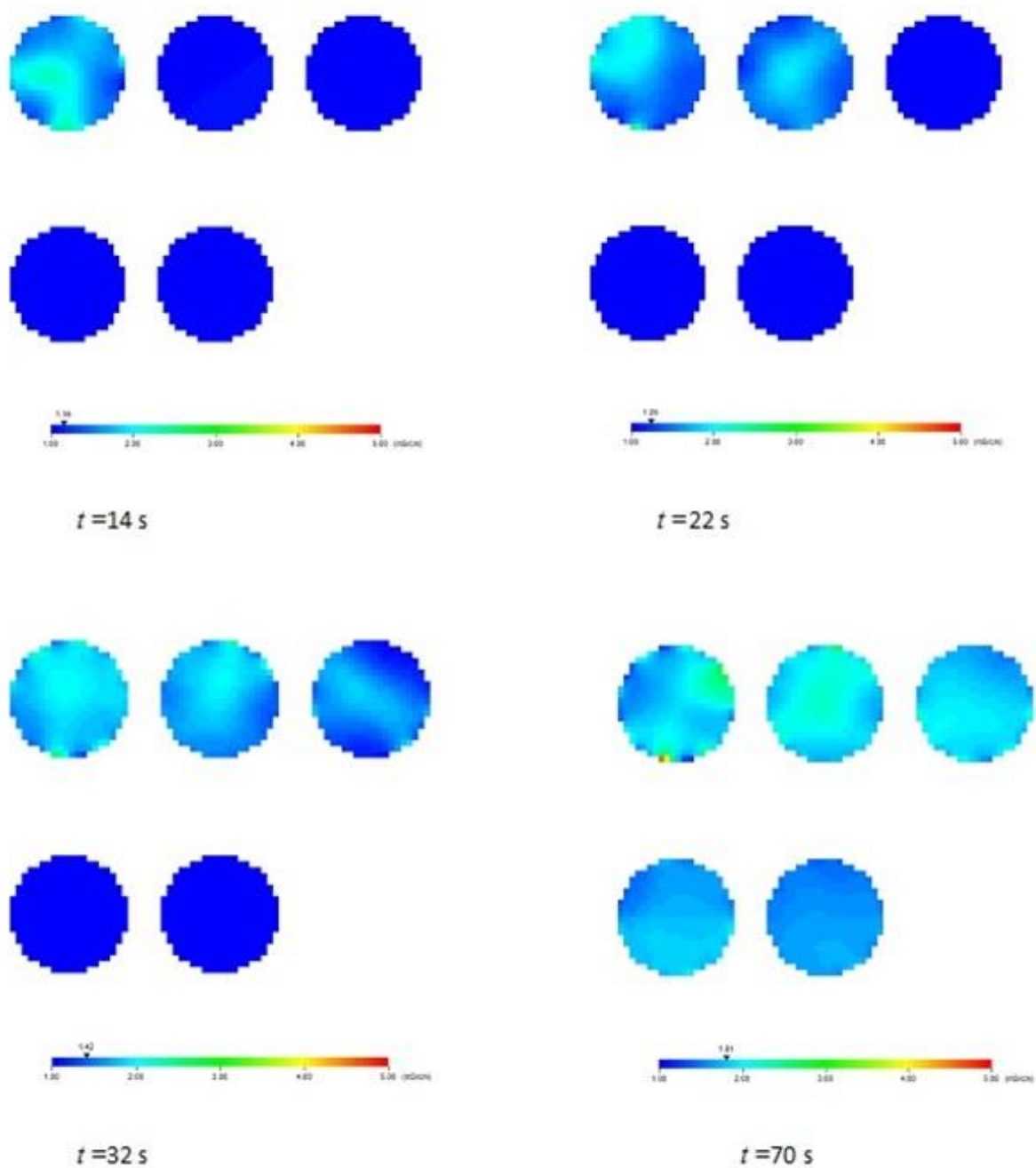
Fig. 5.14: 2D tomograms obtained after the injection of the Newtonian secondary stream (saline solution) into the non-Newtonian primary stream (1.0 wt% xanthan gum) for the secondary flow rate of 100 mL/min and the primary flow rate of 6 L/min.
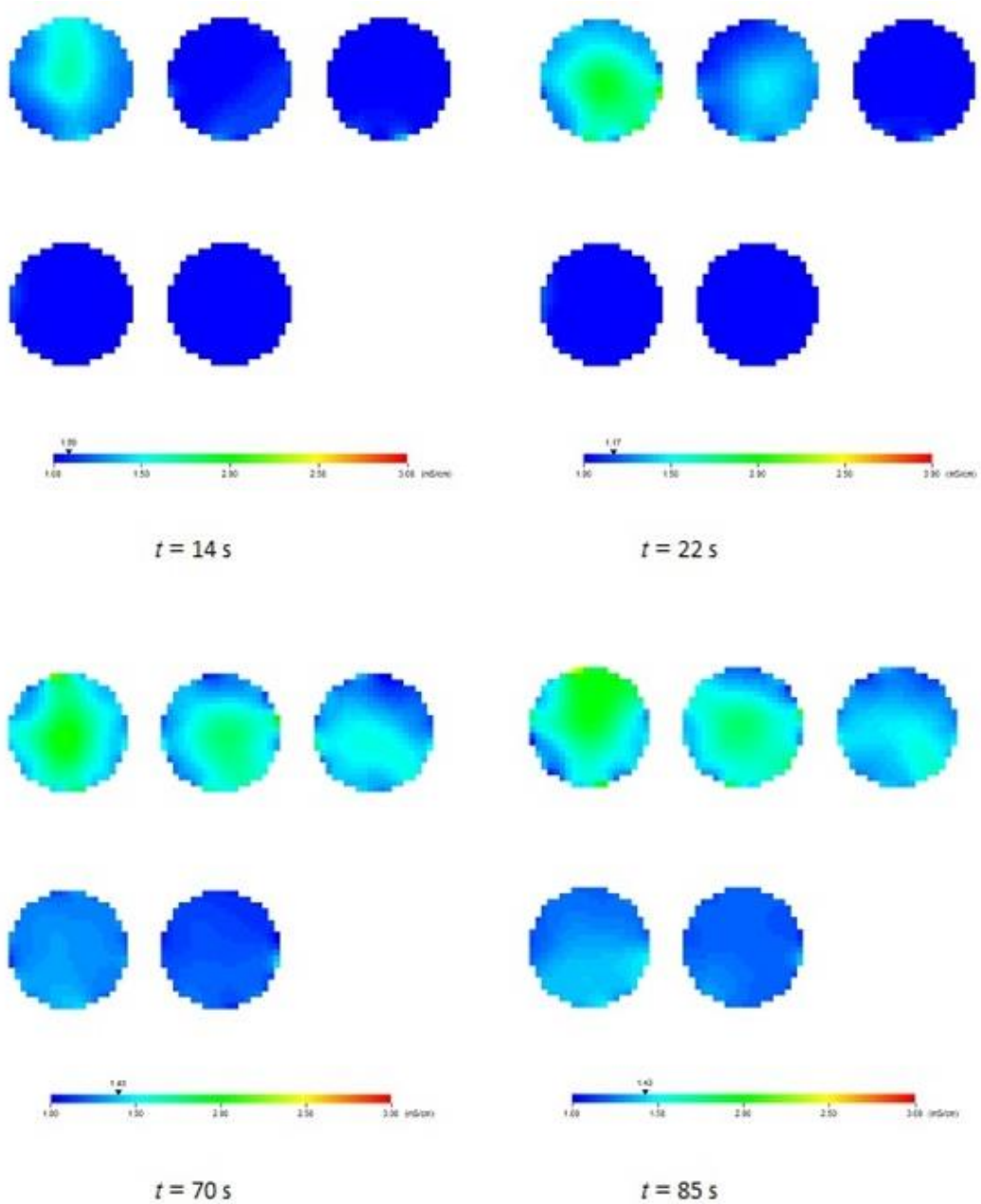
Fig. 5.15: 2D tomograms obtained after the injection of the Newtonian secondary stream (saline solution) into the non-Newtonian primary stream (1.5 wt% xanthan gum) for the secondary flow rate of 100 mL/min and the primary flow rate of 6 L/min.
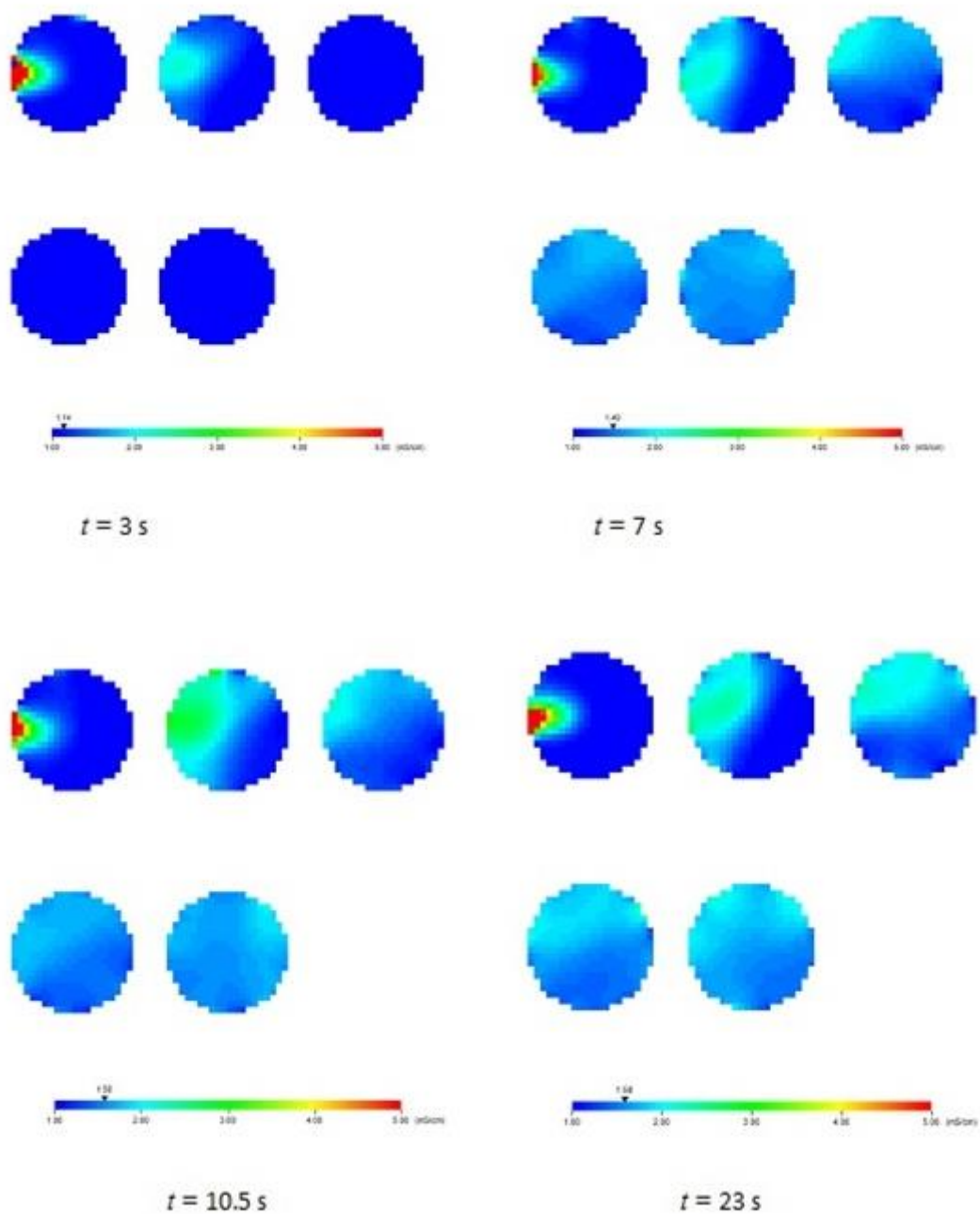
Fig. 5.16: 2D tomograms obtained after the injection of the Newtonian secondary stream (saline solution) into the non-Newtonian primary stream (0.5 wt% xanthan gum) for the secondary flow rate of 100 mL/min and the primary flow rate of 12.5 L/min.
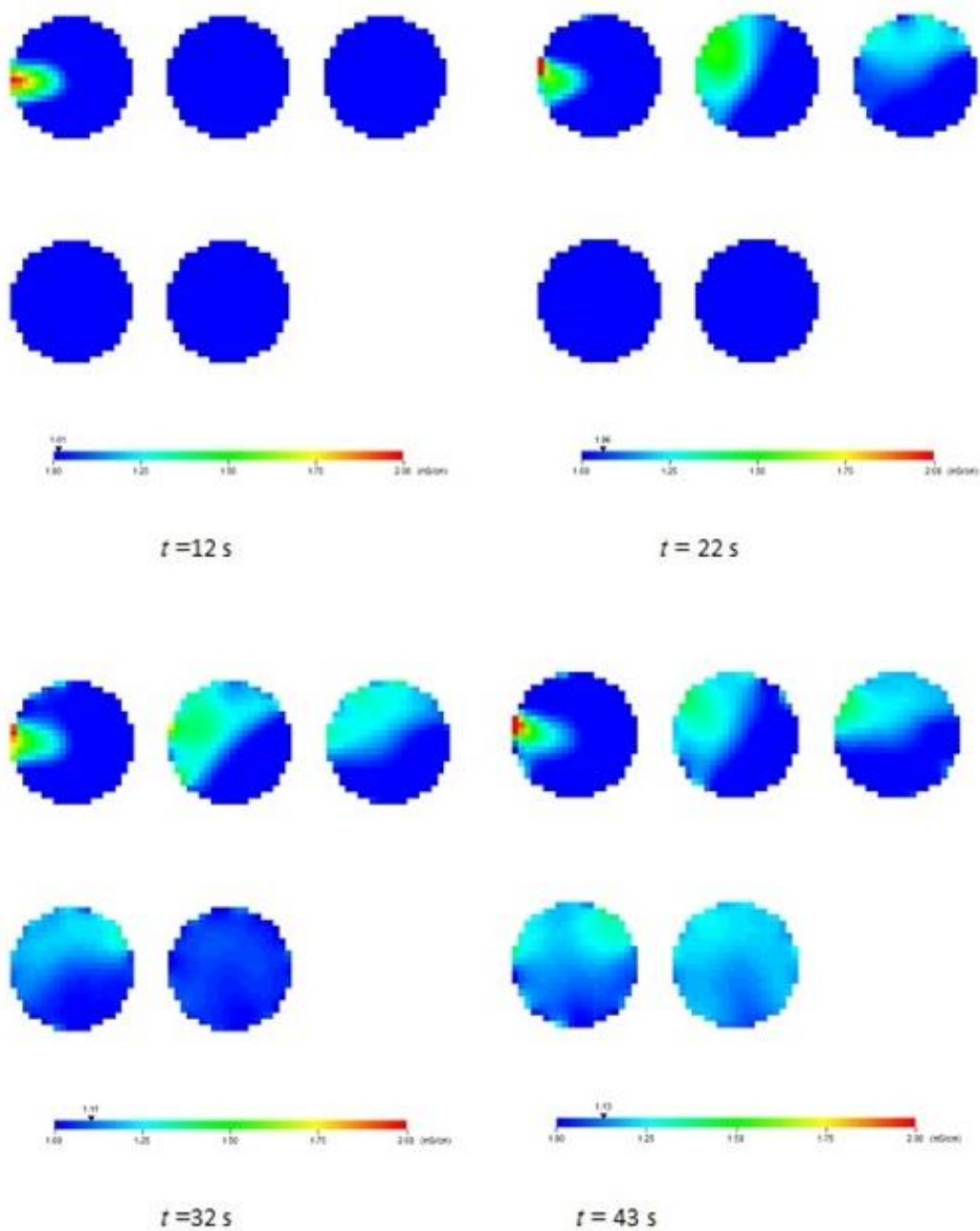
Fig. 5.17: 2D tomograms obtained after the injection of the Newtonian secondary stream (saline solution) into the non-Newtonian primary stream (1.0 wt% xanthan gum) for the secondary flow rate of 100 mL/min and the primary flow rate of 12.5 L/min.
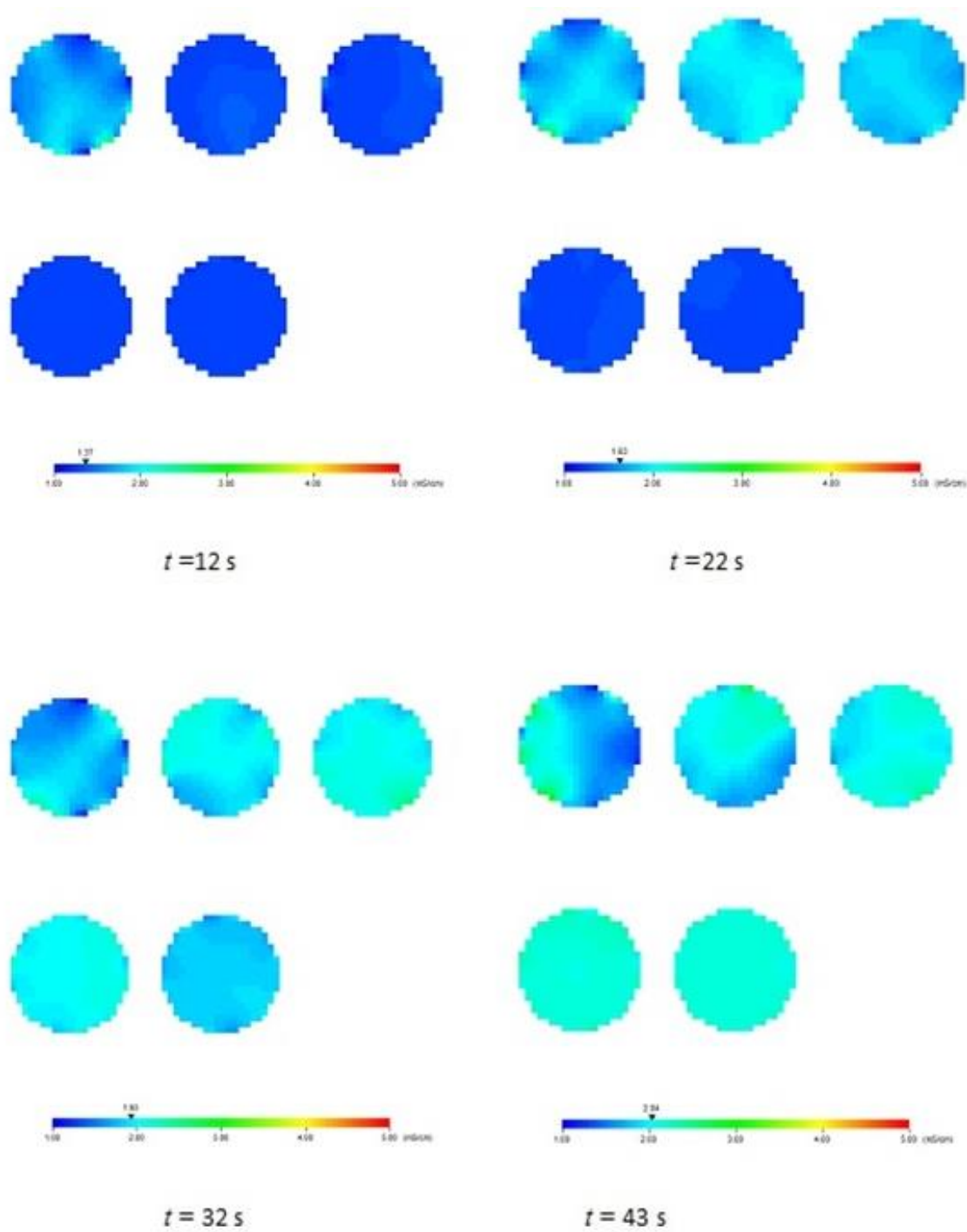
Fig. 5.18: 2D tomograms obtained after the injection of the Newtonian secondary stream (saline solution) into the non-Newtonian primary stream (1.5 wt% xanthan gum) for the secondary flow rate of 100 mL/min and the primary flow rate of 12.5 L/min.

According to the data shown in Fig. 5.11, Fig. 5.19, and Fig. 5.20, it was observed that the mixing quality was independent of the primary flow rates for all xanthan gum concentrations. Since the generalized Reynolds number was very low (Re<1.26; Refer to Table 3.3), the inertial effect was not significant in order to show a drastic change in the mixing quality when the primary flow rates changed from 3.5 L/min to 12.5 L/min. In 2002 and 2003, Zalc *et al*. reported a similar observation for the centerline injection of additive material (with equal viscocity as the polymer melt) into the bulk flow of polymer melt in the SMX static mixer. However, the time taken to attain the desired level of mixing was relatively shorter for higher xanthan gum mass concentration (1wt% and 1.5 wt%) when the primary flow rate increased from 3.5 L/min to 12.5 L/min.
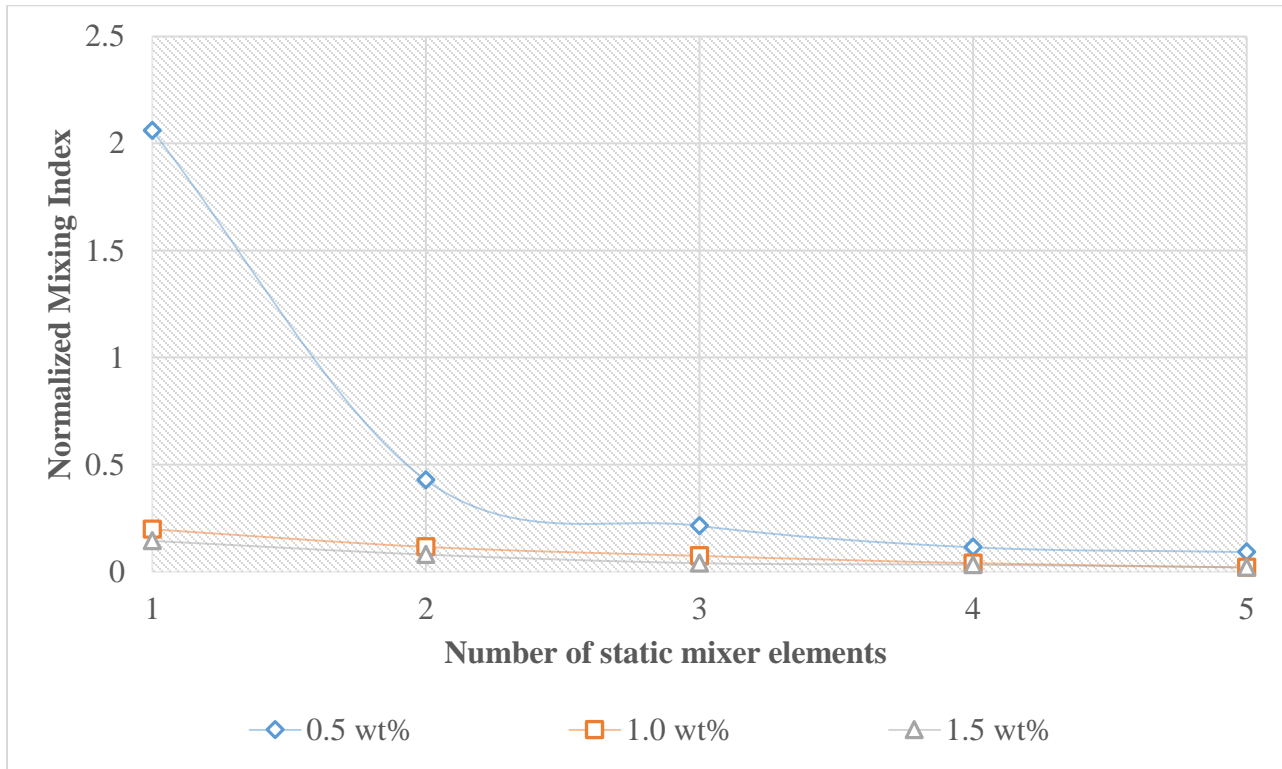
Fig. 5.19: Normalized mixing index graph for the distributive mixing of the Newtonian secondary stream (saline solution) into the non-Newtonian primary stream (0.5-1.5 wt% xanthan gum solution) for the secondary flow rate of 100 mL/min and the primary flow rate of 6 L/min). The maximum standard deviation observed for the normalized mixing index in 5th ERT plane was $\pm$0.027.
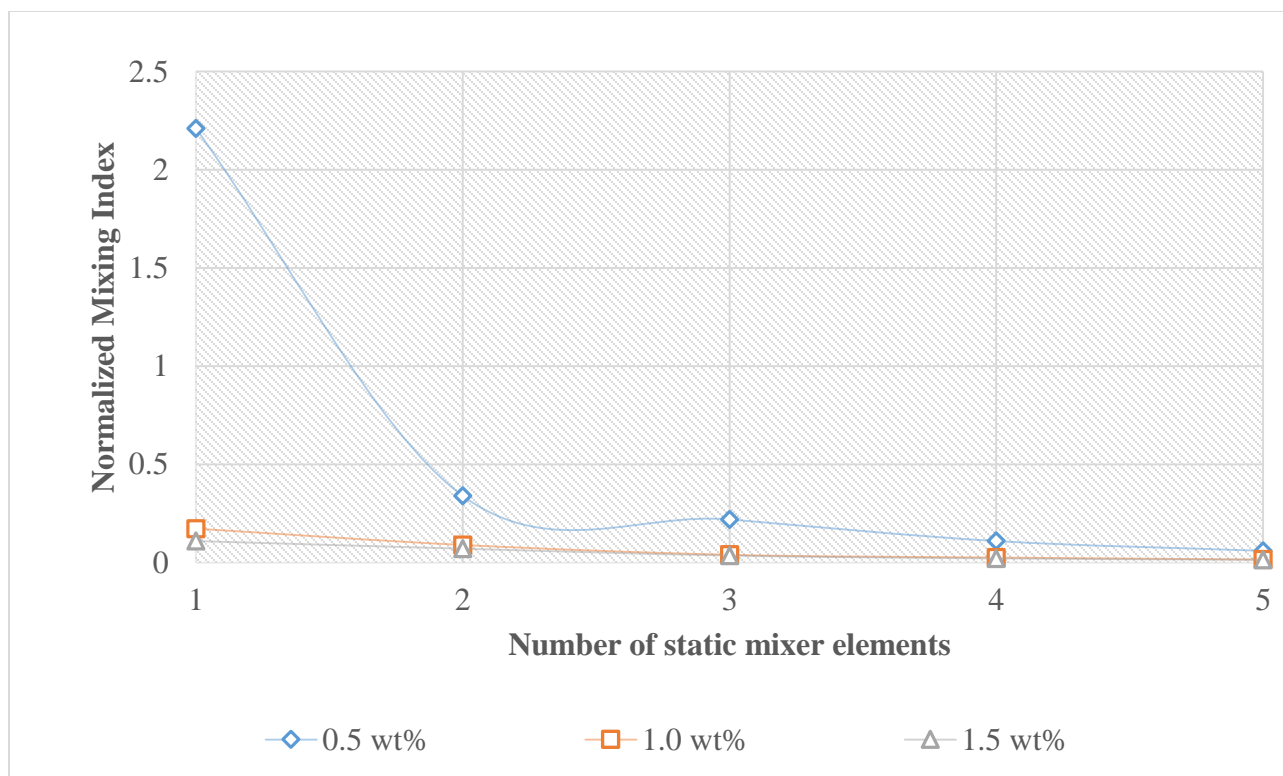
Fig. 5.20: Normalized Mixing index graph for distributive mixing of the Newtonian secondary stream (saline solution) into the non-Newtonian primary stream (0.5-1.5 wt% xanthan gum solution) for the secondary flow rate of 100 mL/min and the primary flow rate of 12.5 L/min. The maximum standard deviation observed for the normalized mixing index in 5th ERT plane was ±0.010.

5.3.1 EXPERIMENTAL PRESSURE DROP DATA

The differential pressure measurement was taken by connecting a tube through a small opening at the pipe inlet and the pipe exit to a pressure transducer. The tube was filled with water and the small opening at the pipe inlet and the pipe exit were able to discharge a small volume of primary fluid through the tube. This can cause the water inside the tube to displace and the force applied by water inside the tube is then converted into pressure drop measurement by the pressure transducer through the digital display. It is important to note that, at lower pumping frequency, the pressure drop measurement was fluctuating. Hence, the CFD flow model was validated using the pressure drop data obtained at higher pumping frequency (i.e. at higher flow rates). The experimental pressure drop data for xanthan gum solution (0.5wt% - 1.0 wt %) are shown in Fig. 5.21. The pressure drop data was nearly constant for 0.5 wt% xanthan gum solution for the primary flow rates studied between 3.5 L/min and 12.5 L/min. Possibly, the pressure transducer was not sensitive enough to accurately record the pressure drop at lower flow rates. The viscous force exerted on the water inside the tube connecting to the pressure transducer might not be significant enough for the pressure transducer to detect. A sharp decline in pressure drop data was observed for 1.5 wt% xanthan gum solution at higher flow rate (12.5 L/min).
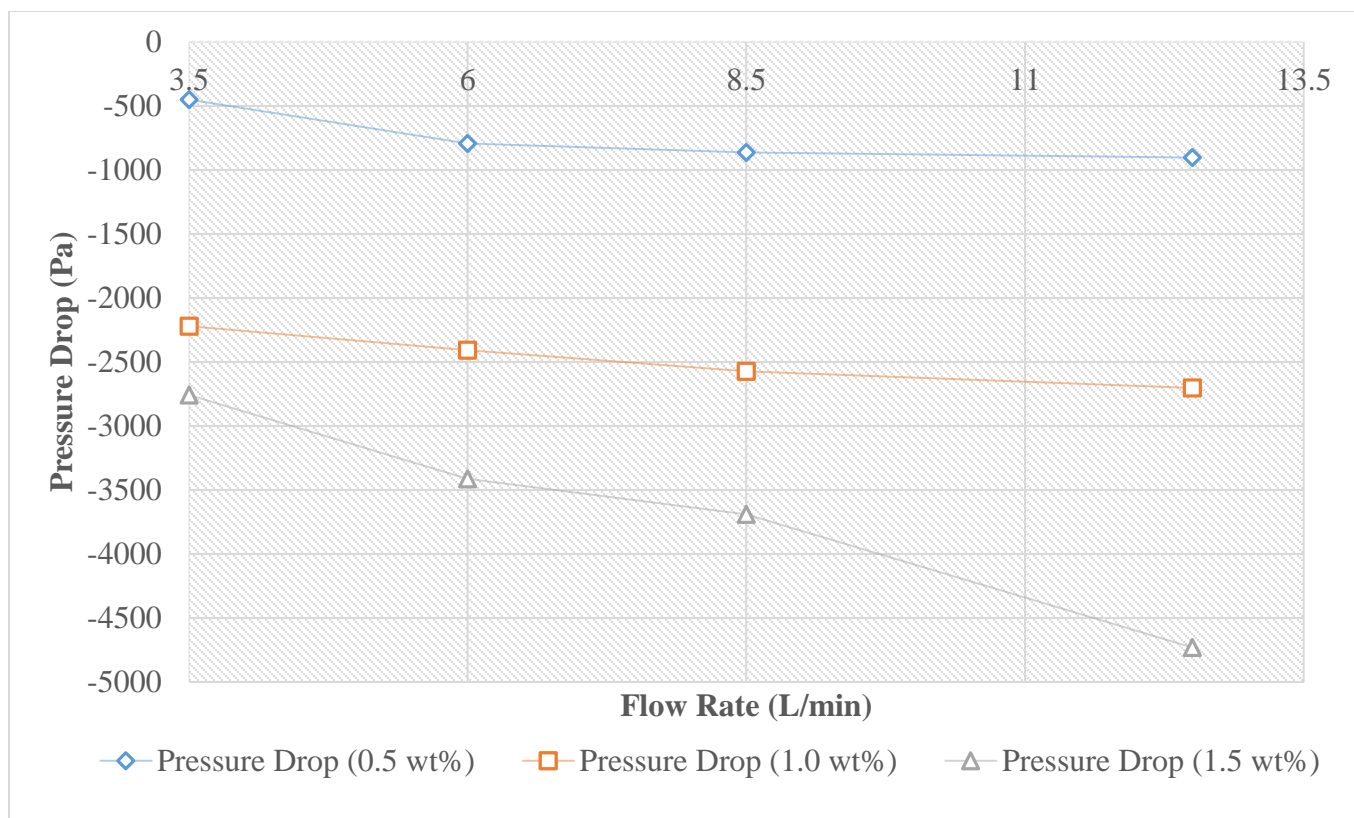
Fig. 5.21: Experimental pressure drop data for the xanthan gum solution (0.5 wt%, 1.0 wt%, and 1.5 wt %) flowing at a volumetric rate ranging from 3.5 L/min to 12.5 L/min.

5.3.2 QUANTITATIVE COMPARISON OF THE EXPERIMENTAL AND CFD DATA

From Table 5.2, it is evident that the pressure drop data calculated using the CFD model for 0.5 wt% xanthan gum solution was in very good agreement with experimental data at higher flow rate. The percent error between CFD and ERT data were 26.44%, 4.18%, and 2.03% for the primary flow rates of 3.5 L/min, 8.5L/min, and 12.5 L/min, respectively. Possibly, the pressure transducer was not sensitive enough to accurately detect the pressure drop at lower flow rates. The comparison of ERT and CFD mixing index value for 0.5 wt% xanthan gum solution flowing at 8.5 L/min and 12.5 L/min are depicted in Fig. 5.22 and Fig. 5.23, respectively. The mixing index values are in good agreement with ERT data for all tomography planes except the very first plane. Significant fluctuations in conductivity measurement were observed experimentally after the 1st static mixer element due to the direct contact of ions with electrodes.

Table 5.2: Comparison of the CFD and the ERT pressure drop data for 0.5 wt% xanthan gum solution

Primary FlowRate (L/min)	CFD Pressure Drop (Pa)	ERT Pressure Drop (Pa)	Percent Error (%)
3.5	-331.7	-450.1	26.44
8.5	-899.386	-861.8	4.18
12.5	-921.918	-903.2	2.03
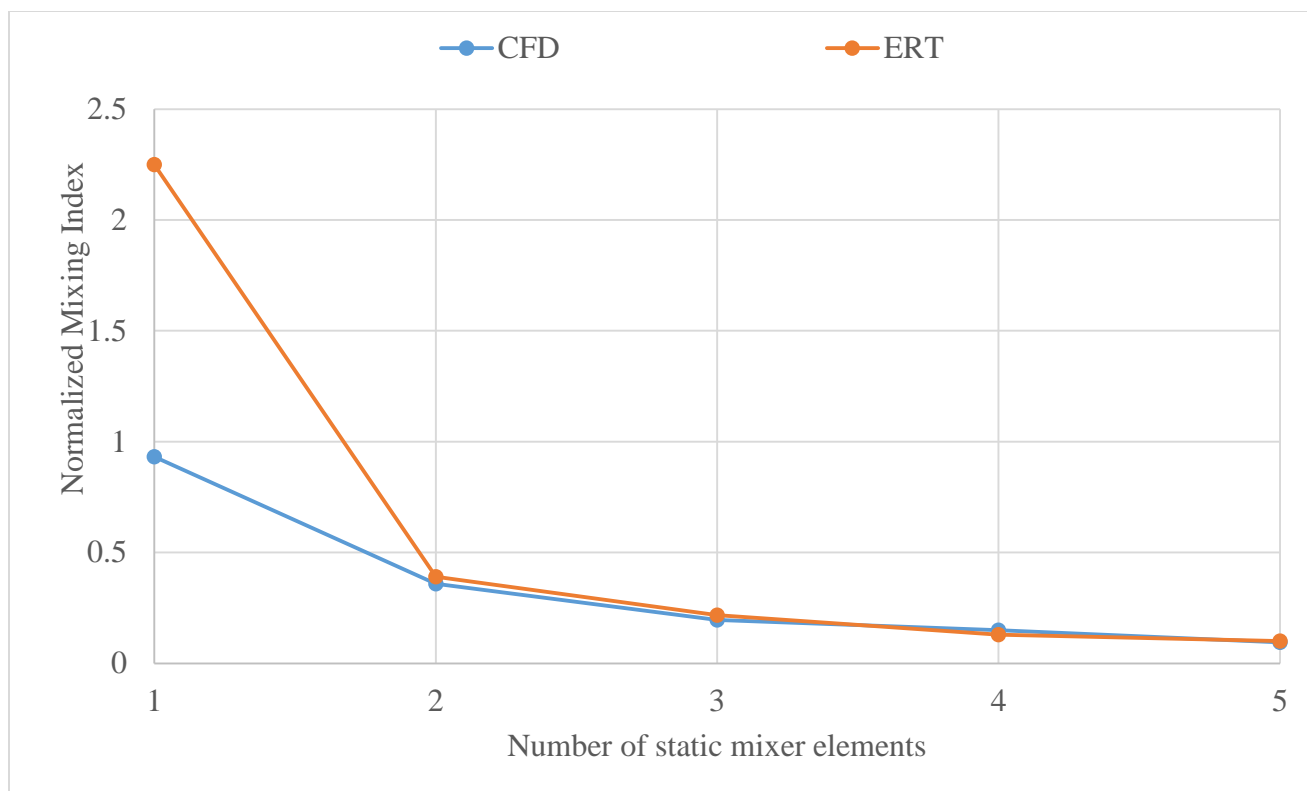
Fig. 5.22: Comparison of ERT and CFD mixing index values for 0.5 wt% xanthan gum solution flowing at 8.5 L/min
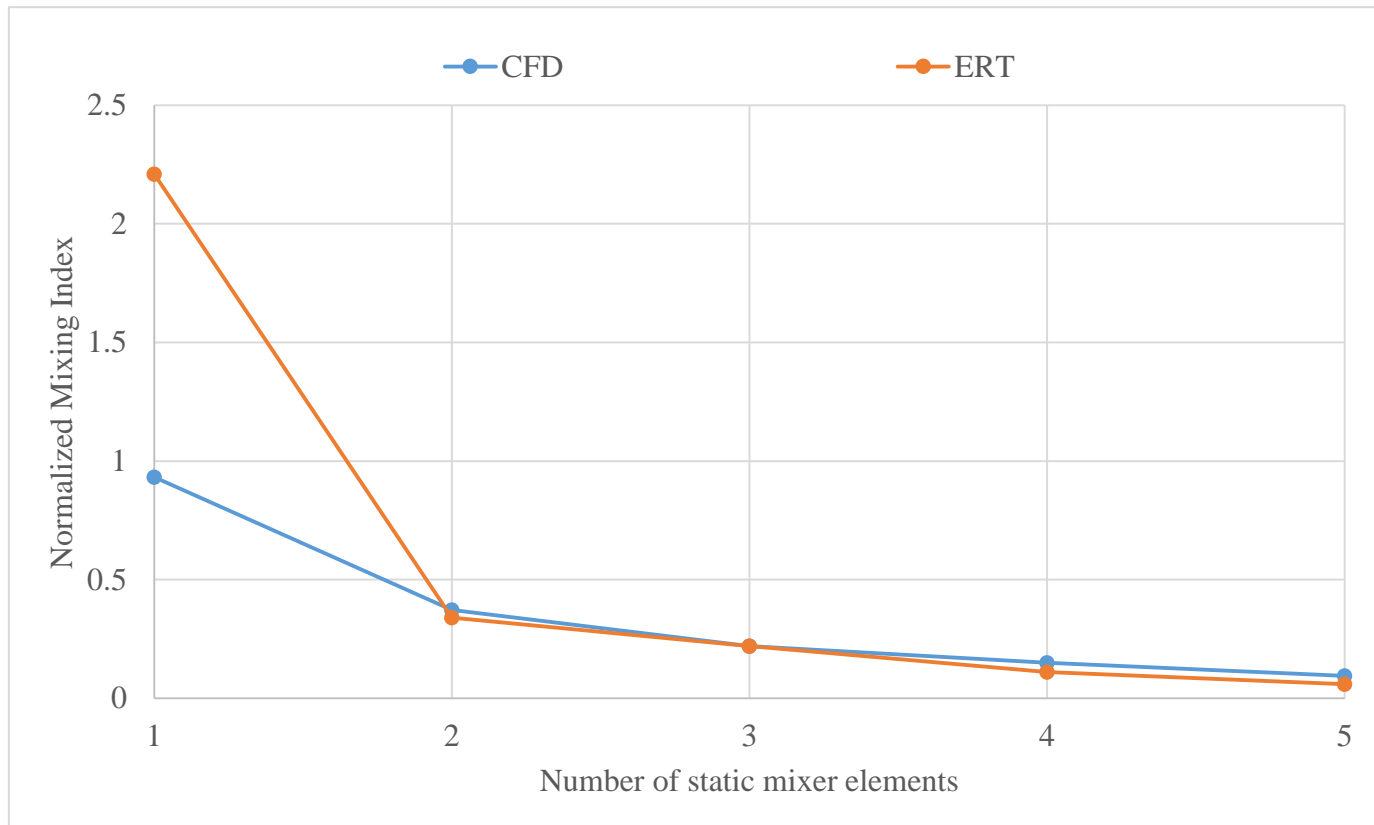
Fig. 5.23: Comparison of ERT and CFD mixing index value for 0.5 wt% xanthan gum solution flowing at 12.5 L/min

Experimentally, it was observed that the mixing quality was independent of the primary flowrates. Even from the numerical point of view, the mixing quality was still independent of primary flow rates. Since the pressure transducer could not be sensitive enough to accurately record the pressure data at lower flow rates, the CFD flow model was only validated at higher flow rates. Thus, the CFD flow model was validated for the 0.5wt% xanthan gum primary solution using both the pressure drop and the mixing index data at higher flow rates. Using the CFD flow model of 0.5 wt% xanthan gum solution, the effect of the primary/secondary fluid flow ratio and the secondary fluid viscosity will be discussed in the next section of the report.

5.4 EFFECT OF THE PRIMARY/SECONDARY FLUID FLOW RATIO ON THE MIXING QUALITY USING COMPUTATIONAL FLUID DYNAMICS (CFD)

The CFD tool was utilized extensively to study the effect of the primary/secondary fluid flow ratio by manipulating the primary fluid flow rate (0.5wt % xanthan gum solution: 0.125 L/min, 0.25 L/min, 0.5 L/min, and 3.5 L/min) and the secondary fluid flow rate (water: 25 mL/min, 100 mL/min, 500 mL/min, and 1000 mL/min). The velocity of the secondary fluid and the primary fluid were calculated by dividing the corresponding fluid flow rates by the cross-sectional area of the injection pipe (I.D. =0.011 m) and the cross-sectional area of the main pipe (I.D. =0.101 m), respectively. Hence, the secondary fluid flow rates, primary fluid flow rates, the secondary fluid velocities, the primary fluid velocities, and the corresponding primary/secondary fluid flow ratios are shown in Table 5.3. The effect of the primary/secondary fluid flow ratio on the mixing of the secondary fluid in 0.5wt% xanthan gum solution is shown in Fig. 5.24.

Table 5.3: Primary flow rates, secondary flow rates and the corresponding Primary/Secondary flow ratios

Primary Flow Rate (L/min)	Primary Fluid Velocity (m/s)	Secondary Flow Rate (L/min)	Secondary Fluid Velocity (m/s)	Primary/Secondary Flow Ratio	Secondary/Primary Velocity Ratio
3.5	0.007260	**0.025**	0.00438	**140.00**	**0.60**
0.5	0.001020	**0.025**	0.00438	**20.00**	**4.30**
3.5	0.007260	**0.500**	0.08760	**7.00**	**12.10**
0.25	0.000514	**0.100**	0.01750	**2.50**	**34.10**
0.125	0.000257	**0.100**	0.01750	**1.25**	**68.10**
0.5	0.001020	**1.000**	0.17500	**0.50**	**171.50**
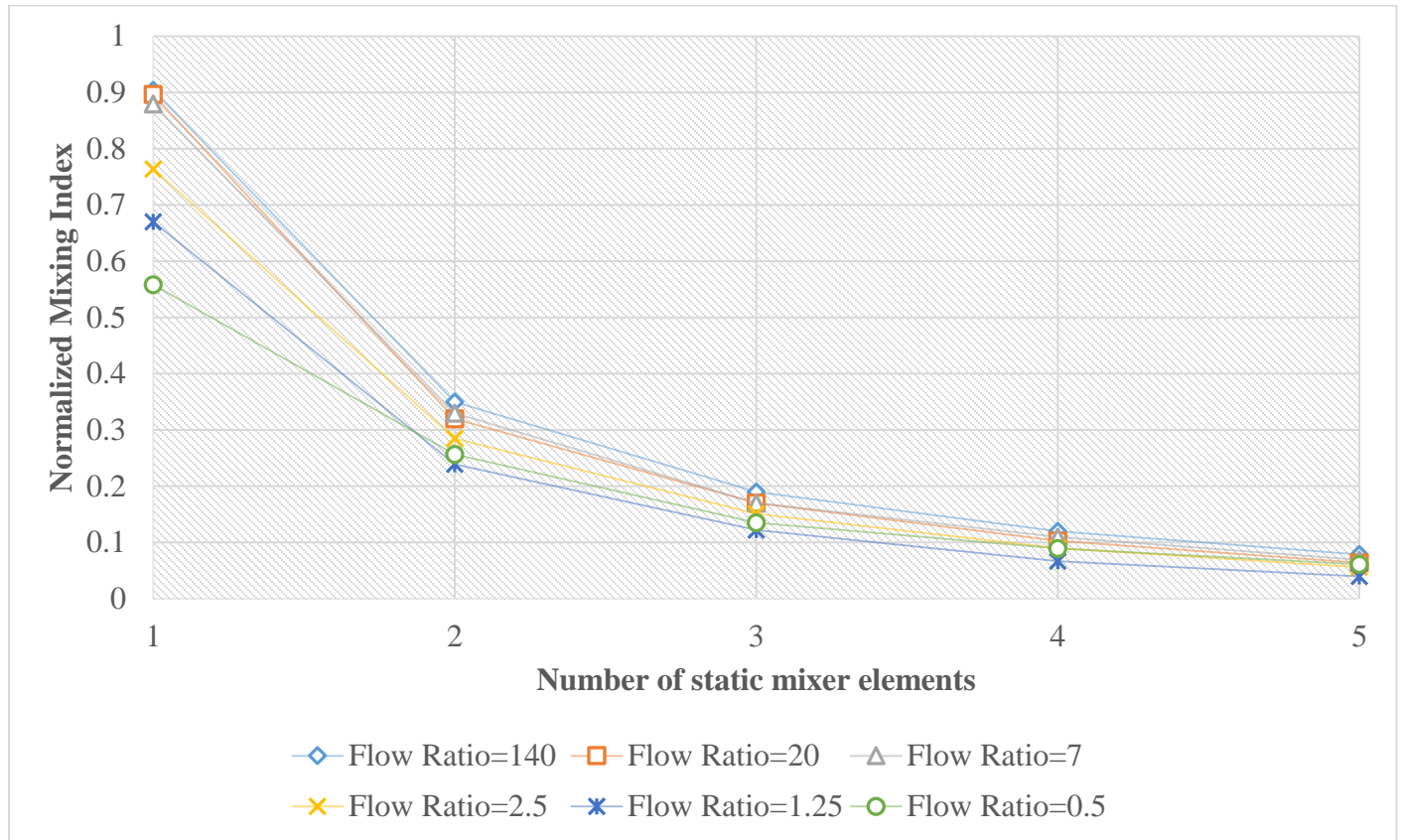
Fig. 5.24: Effect of the primary/secondary flow ratio on the mixing of the secondary fluid in 0.5 wt% xanthan gum solution.

It is clearly noticeable in Fig. 5.24 that the mixing index value recorded after the 1st static mixer element signifcantly dropped as the primary/secondary flow ratio decreased. The mixing index value measured after the 2nd and the 3rd static mixer element also decreased as the primary/secondary flow ratio decreased, but the magnitude of the decline in the mixing index value was not significantly noticeable as what observed after the 1st static mixer. In our numerical research study, the secondary fluid was water which is a Newtonian fluid possessing a constant viscosity unlike the xanthan gum solution, which is a shear thinning fluid. Thus, the viscosity of the xanthan gum solution decreases with an increasing in the shear rate while the viscocity of water remains constant at any applied shear rate. On the contrary, for a different type of static mixer (Kenics KM), it was reported that a primary/secondary flow ratio of 25 was more suitable for enhancing the mixing of two non-Newtonian shear thinning fluids than the flow ratio

of 10 at constant velocity. In their research study, both primary and secondary fluids were non-Newtonian fluids obeying the Herschel-Bulkley rheological model (Alberini *et al*., 2014).

To investigate why the mixing index value dropped significantly as the primary/secondary flow ratio decreased, the viscocity profile of the primary and the secondary fluid were studied on the first two static mixer elements. Each static mixer was cut into four sections and thus, the viscosity profiles were captured at 8 different axial positions (slice of XY plane at $z = 0$ m, $z = -0.1$ m, $z = -0.2$ m, $z = -0.3$ m, $z = -0.383$ m, $z = -0.48$ m, $z = -0.58$ m, $z = -0.68$ m) on the two static mixers placed closer to the injection pipe as shown in Fig. 5.25.
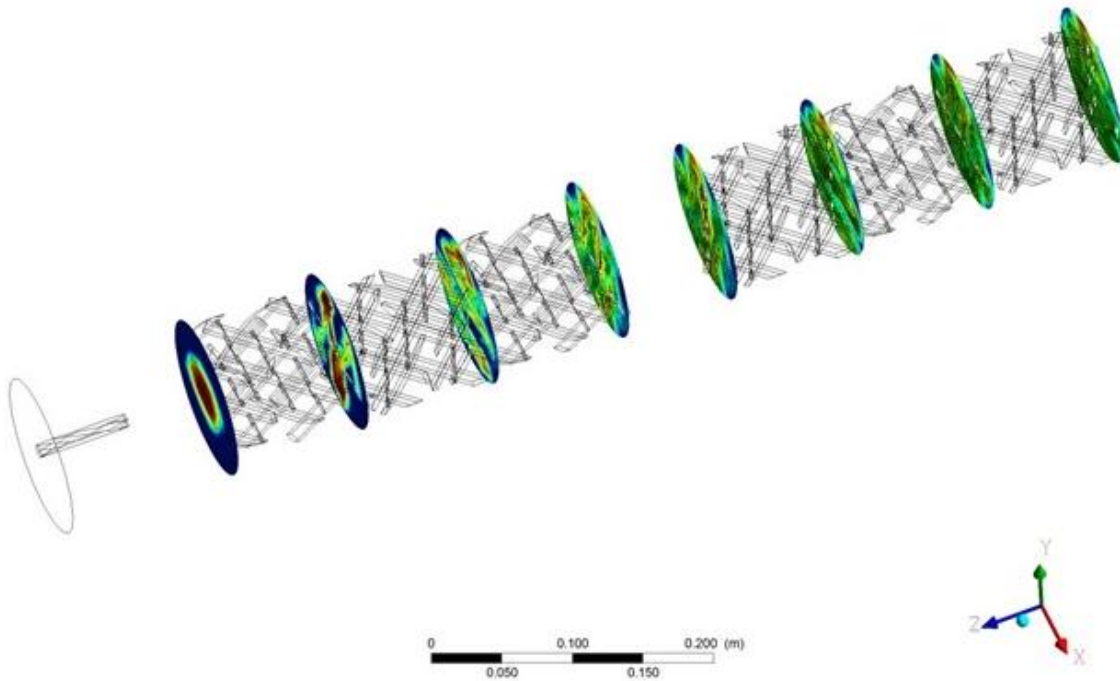
Fig. 5.25: 2D cross sectional view of the pipe showing the 8 different axial positions

Fig. 5.26 depicts the viscocity profile of the primary and the secondary fluids captured at 8 different planes for the primary/secondary flow ratio of 140. Since the secondary fluid was Newtonian and it had a constant viscosity of 0.001 kg/ms, the changes in the viscosity profile was due to the shear thinning xanthan gum solution since its viscocity decreases with an increase in the shear rate. According to Fig. 5.26, the viscosity of all the 8 planes were dominatly red (μ=0.835 kg/ms) with some patches of the regions with lessened viscocity (μ <0.835 kg/ms) signifying that the 0.5wt% xanthan gum solution is shear thinning and its viscosity decreased

slightly at some region of the planes due to the penetration of the secondary fluid through the primary fluid.

Fig.5.26: Viscosity profile for the flow ratio of 140 and the secondary/primary velocity ratio of 0.6 in the mixing of the secondary fluid (water) in 0.5 wt% xanthan gum solution (viscosity in kg/ms).

As the primary/secondary flow ratio was decreased from 140 to 20, a blue spot was observed at plane 1 ($\mu = 0.073$ kg/ms), which is higher than the viscosity of water ($\mu = 0.001$ kg/ms). When the primary flow rate decreased from 3.5 L/min to 0.5 L/min while keeping the secondary flow rate fixed at 25 mL/min, the primary/secondary flow ratio decreased from 140 to 20 and the secondary/primary fluid velocity ratio increased from 0.6 to 4.30. Since the secondary fluid traveled at a relatively higher velocity than the primary fluid when the primary/secondary flow ratio decreased from 140 to 20, the secondary fluid was able to penetrate through the viscous primary fluid intensely. This is why a blue spot (i.e. lower viscosity region) was observed in

plane 1 signifying the shear thinning of the xanthan gum solution due to the penetration of the Newtonian secondary fluid at a higher secondary/primary fluid velocity ratio.

Fig. 5.27: Viscosity profile for the flow ratio of 20 and the secondary/primary velocity ratio of 4.30 in the mixing of the secondary fluid (water) in 0.5 wt% xanthan gum solution (viscosity in kg/ms).

When the secondary flowrate was increased from 25 mL/min to 1000 mL/min while keeping the primary flow rate at 0.5 L/min, the primary/secondary flow ratio was further decreased from 20 to 0.5. At these conditions, the secondary/primary fluid velocity ratio was increased from 4.30 to 171.5. Due to this drastic increase in the secondary/primary fluid velocity ratio, a prominent blue region was observed in plane 1 depicted in Fig. 5.28 compared to what observed in plane 1 illustrated in Fig. 5.26 and Fig. 5.27. Due to the intense penetration of the secondary fluid at a relatively higher velocity, the shearing of this secondary fluid through the primary fluid drastically lessened the viscosity of the primary fluid. In Fig.5.28, the viscosity is represented in bluish-green colour ($\mu = 0.377$ kg/ms) in plane 3 whilst the same plane 3 is mostly red ($\mu = 0.836$ kg/ms) in Fig. 5.26 and Fig. 5.27.

When the high-velocity secondary fluid was pumped into the static mixer, it applied a higher shear rate through the primary fluid. Without the presence of the static mixer, the high-velocity secondary fluid would penetrate at the pipe core and a phenomena called viscous fingering would be resulted (Ventresca *et al*., 2002; Cao *et al*., 2003). However, with the presence of the SMX static mixer, the high-velocity secondary stream is deflected in different directions allowing the secondary fluid to shear through the primary fluid and to alleviate the viscocity of shear thinning primary fluid. This is evidently observed in Fig. 5.26-5.28 as the secondary/primary fluid velocity ratio increased.
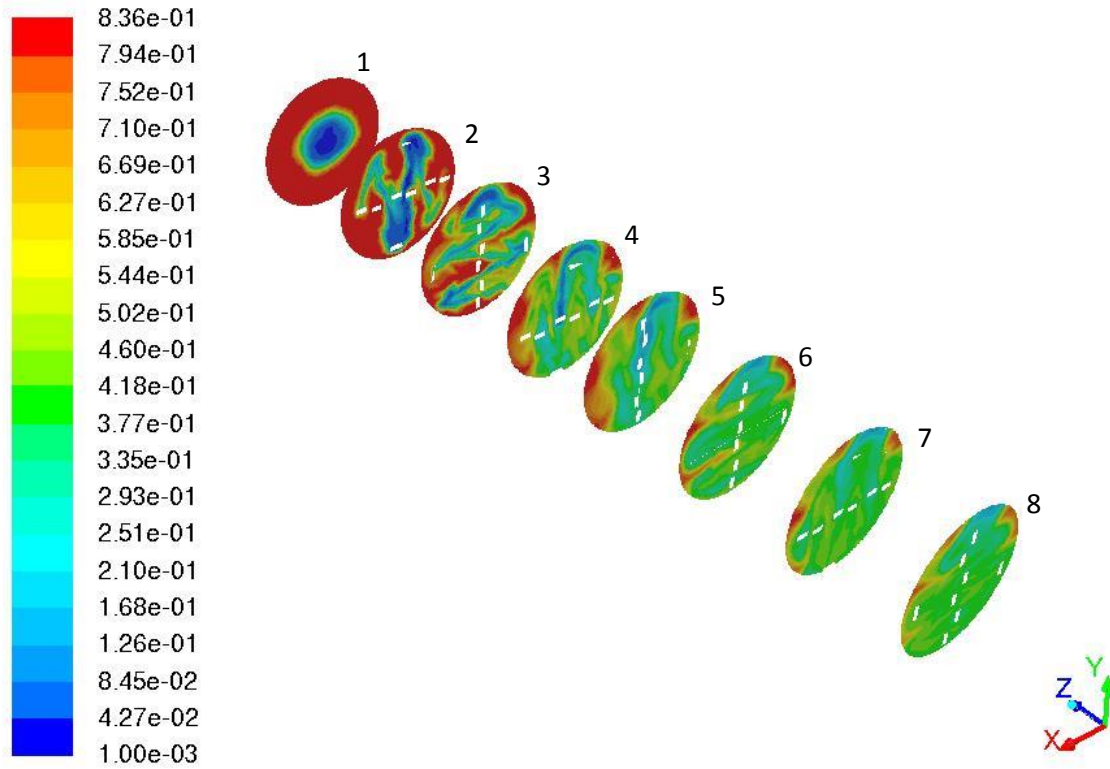
Fig. 5.28: Viscosity profile for the flow ratio of 0.5 and the secondary/primary velocity ratio of 171.5 in the mixing of the secondary fluid (water) in 0.5 wt% xanthan gum solution (viscosity in kg/ms).

The concentration profile of water depicted in Fig. 5.29-5.31 is very much similar to the viscocity profile of the primary fluid shown in Fig. 5.26-5.28. This clearly shows that the water was dispersing into the primary fluid (0.5 % xanthan gum solution), where the viscocity in this primary fluid region was relatively alleviated than the bulk primary fluid. When the viscocity of the primary fluid decreased due to the intensity of shearing by the high velocity secondary fluid, the resistance to flow of the primary fluid become lessened and hence, the SMX static mixer was able to disperse the Newtonian secondary stream (Water) more effectively into the shear thinning primary fluid, where the viscosity was relatively lessened compared to the bulk primary fluid. In parallel to the observation reported for Sulzer SMV static mixer in turbulent flow regime, the SMX static mixer also depends on this secondary/primary velocity ratio to influence the radial mixing even though our flow regime is laminar (Karoui *et al*.,1998).

Mass fraction of water (%)
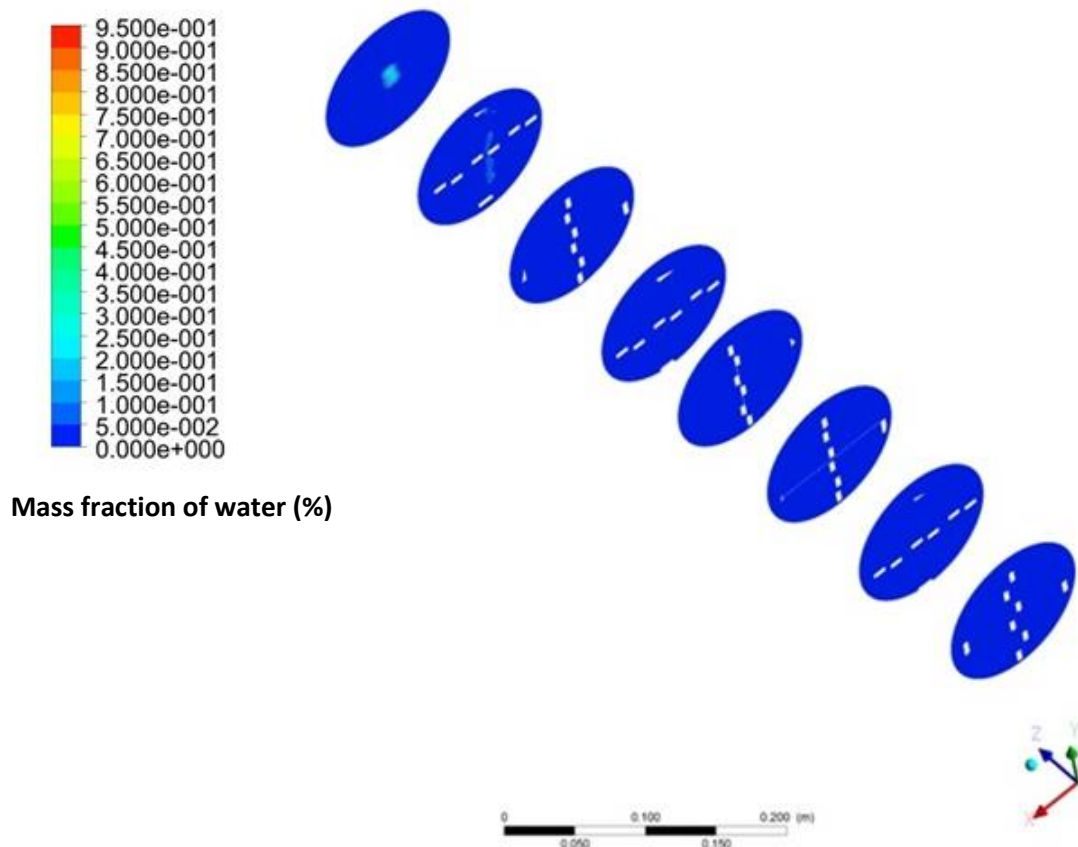
Fig. 5.29: Concentration profile of water for the flow ratio of 140 and the secondary/primary velocity ratio of 0.6 in the mixing of the secondary fluid (water) in 0.5 wt% xanthan gum solution.
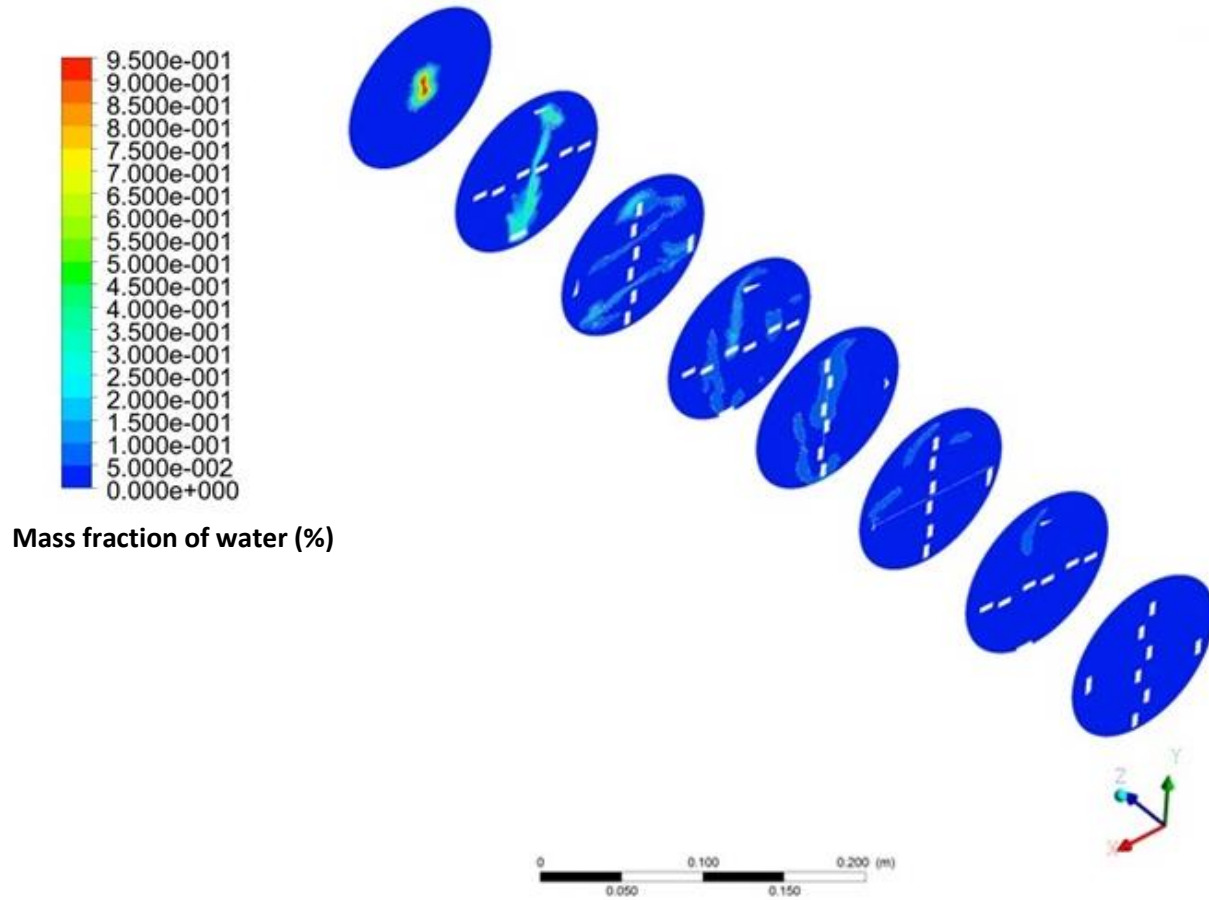
Fig. 5.30: Concentration profile of water for the flow ratio of 20 and the secondary/primary velocity ratio of 4.30 in the mixing of the secondary fluid (water) in 0.5 wt% xanthan gum solution.

Mass fraction of water (%)

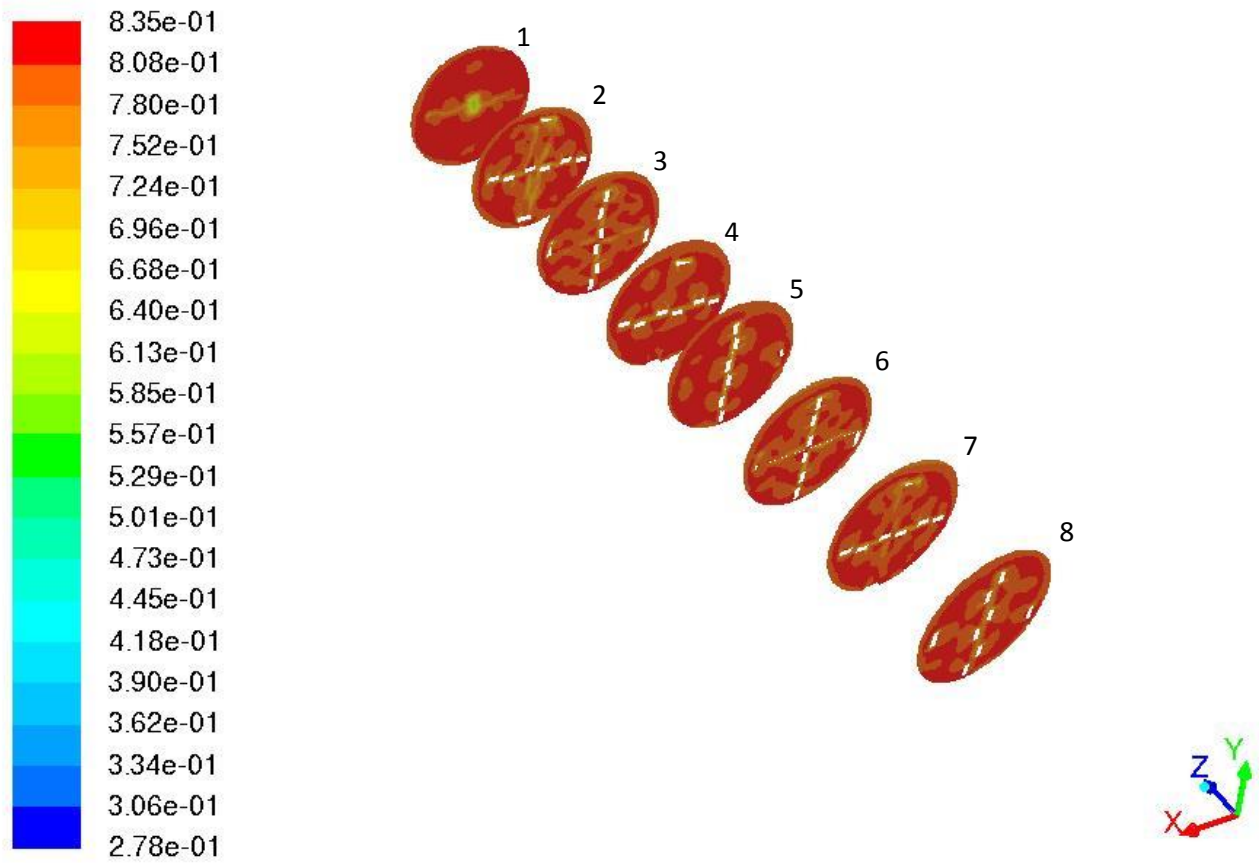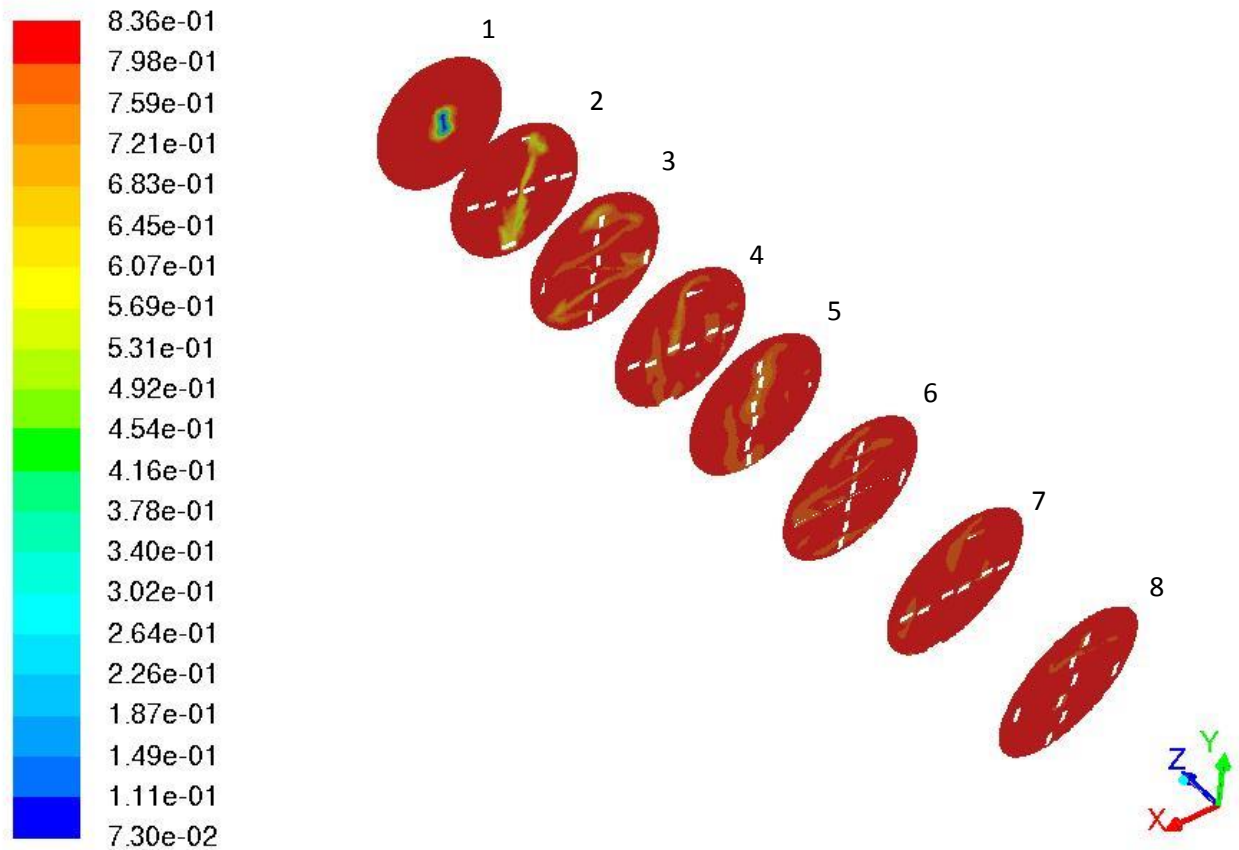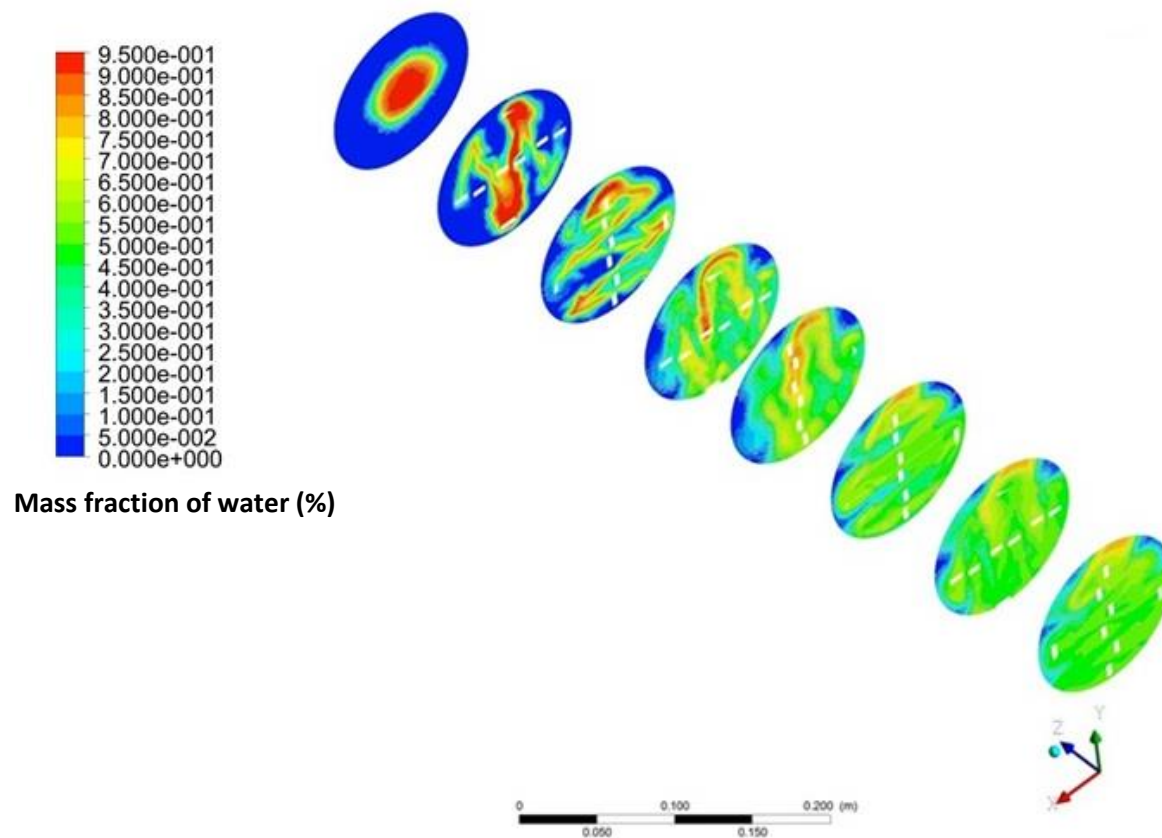Fig.5.31: Concentration profile of water for the flow ratio of 0.5 and the secondary/primary velocity ratio of 171.5 in the mixing of the secondary fluid (water) in 0.5 wt% xanthan gum solution.

5.5 EFFECT OF THE SECONDARY FLUID VISCOSITY ON THE MIXING QUALITY USING COMPUTATIONAL FLUID DYNAMICS (CFD)

The effect of the secondary fluid viscosity (i.e. 0.001-10 kg/ms) on the mixing performance of the SMX static mixer was investigated. From the results graphically depicted in Fig. 5.32, it is clear that the SMX static mixer was more effective when the secondary fluid had a higher viscosity. To investigate this effect, the radial velocity profiles were computed using the CFD model for three different secondary fluid viscosities ($\mu_1 = 0.01$ kg/ms, $\mu_2 = 1$ kg/ms, and $\mu_3 = 10$ kg/ms) as shown in Fig. 5.33. In order to compare these radial velocity profiles, all the numerical studies were conducted for a fixed flow ratio. Since the mixing quality was dependent on the primary/secondary fluid flow ratio, it was very crucial to control the flow ratio in order to solely study the effect of the secondary fluid viscosity on the mixing performance of the SMX static mixer. A primary/secondary flow ratio of 0.5 was chosen for this numerical study in order to capture the prominent features in the radial velocity profiles since the flow of secondary fluid was slighlty greater than the primary fluid flow.

For the secondary fluid with the viscosity of $\mu_1 = 0.01$ kg/ms), two red regions were observed at the centre of plane 1 signifying that the radial velocity was more dominant at the centre due to the penetration of the secondary fluid.

As the viscosity increased from $\mu_1 = 0.01$ kg/ms to $\mu_2 = 1$ kg/ms, the red region became more elongated and displaced from the centre of plane 1. This signifies that the regions of higher radial velocity moved away from the centre of plane 1 upon increasing the secondary fluid viscosity. When the viscosity was increased from $\mu_2 = 1$ kg/ms to $\mu_3 = 10$ kg/ms, the red region became wider and intense. The occurrence of these red regions in plane 1 showed the dominance of the radial velocity away from the centre of plane 1 as the viscosity of the secondary fluid was increased. This was due to the stretching of the viscous fluids by the chaotic nature of the SMX static mixer (Zalc *et al*., 2002 and 2003). As the viscosity of the secondary fluid increased, the static mixer was able to enhance the fluid deformation through fluid stretching. As the magnitude of fluid stretching increased, the exposure of interfacial area for diffusion increased (Muzzio et al., 1991). As a result, a more radial dispersion of the secondary fluid into 0.5 wt% xanthan gum

solution was observed as the secondary fluid viscosity was increased, according to the results presented in Fig. 5.34. This resulted in a decline in the mixing index value when the viscosity of the secondary fluid was increased (Fig. 5.32) due to the effective radial dispersion of the secondary fluid in the primary fluid. Alberini *et al*. (2014) reported that a poor mixing quality was obtained when a higher viscous secondary fluid was injected into a lower viscous primary fluid in the Kenics KM static mixer. However, in their experimental research study, both the primary and the secondary fluids were shear thinning and both were obeying the Herschel-Bulkley rheological model. Our research study, which was conducted on the viscous Newtonian secondary fluid and non-Newtonian primary fluid, revealed that the SMX static mixer was more effective for the mixing of higher viscous secondary fluid in the yield-pseudoplastic primary fluid.
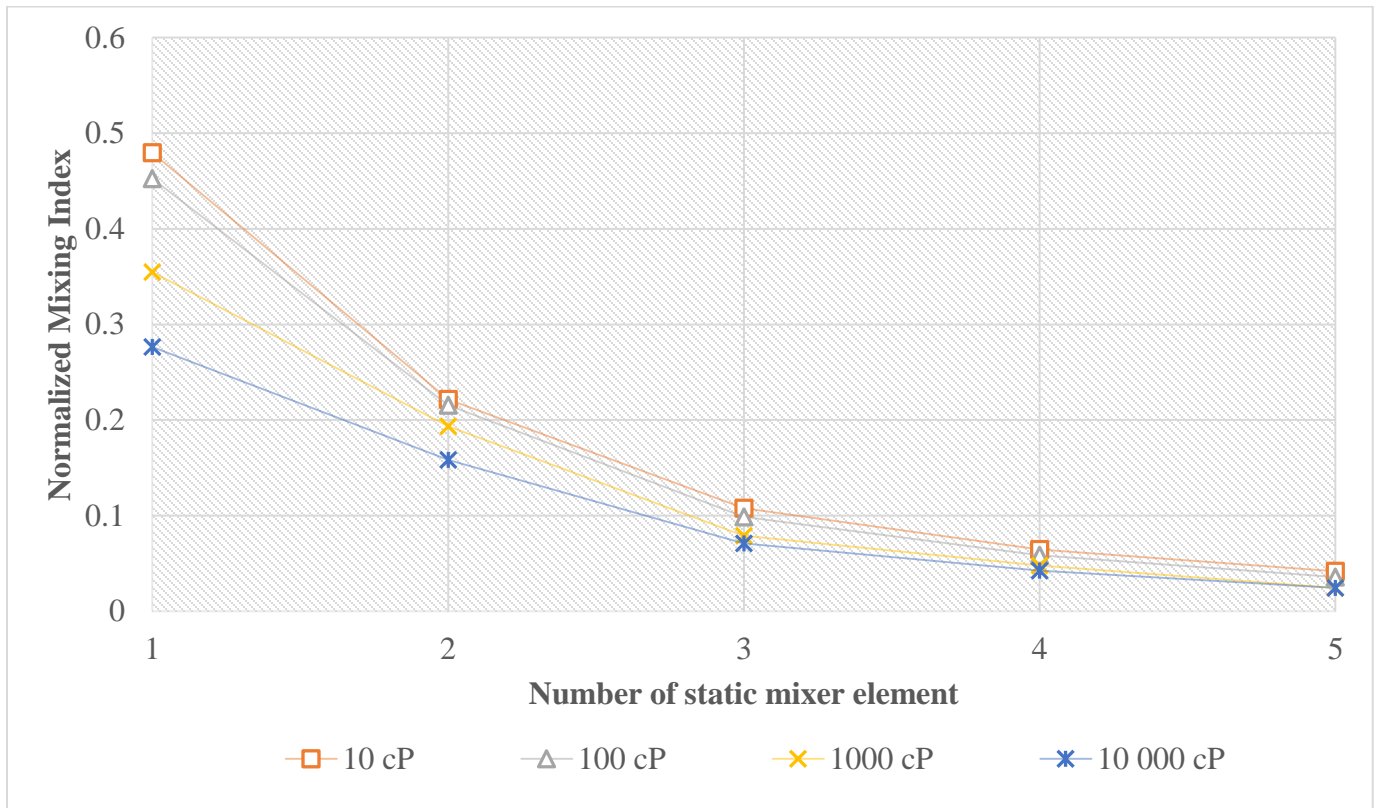
Fig. 5.32 Effect of the secondary fluid viscosity on the mixing performance of the SMX static mixer (flow ratio = 0.5 and secondary/primary velocity ratio = 171.5).
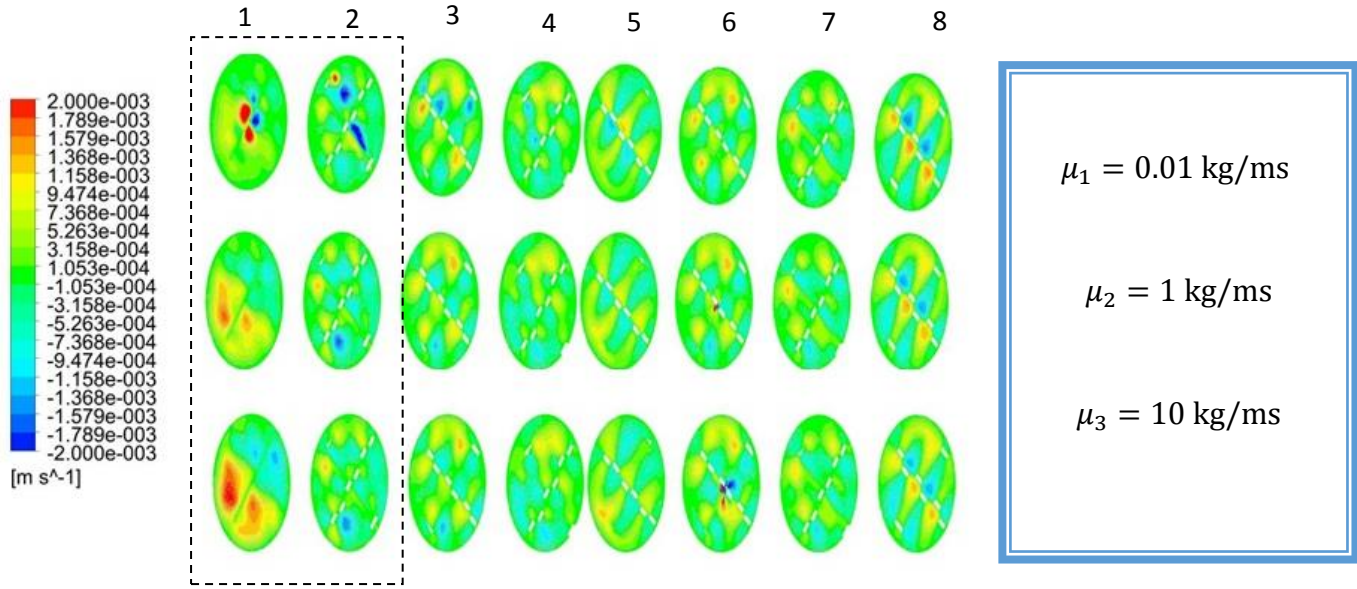
Fig. 5.33: Radial velocity profiles as a function of the secondary fluid viscosity (flow ratio = 0.5 and secondary/primary velocity ratio = 171.5).
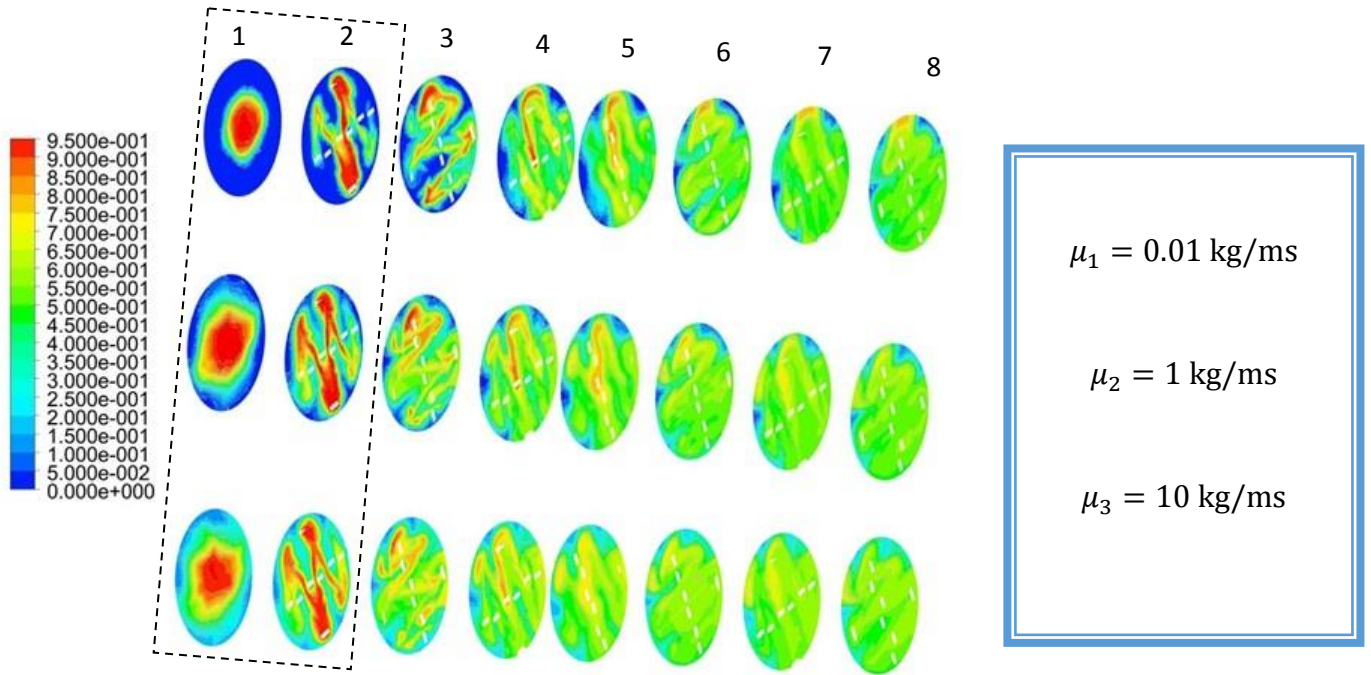
Fig. 5.34: Concentration profile of the secondary fluid as a function of the secondary fluid viscosity (flow ratio = 0.5; secondary/primary velocity ratio = 171.5).

6. CONCLUSION

Using electrical resistance tomography (ERT) and computational fluid dynamics (CFD), a comprehensive research study was conducted to understand the mixing mechanism of two miscible fluids in the SMX static mixer.

From experimental work conducted using ERT technique, the following conclusion could be drawn:

- The Newtonian secondary fluids with a constant viscosity penetrated through the non-Newtonian primary fluids more effectively than the non-Newtonian fluids, which often experienced faster energy dissipation. Hence, the Newtonian secondary fluids promoted effective axial mixing over the non-Newtonian fluids. Especially, for 0.5wt% xanthan gum solution, it was more effective to inject the Newtonian secondary fluid than the non-Newtonian 0.5 wt% xanthan secondary fluid.

- At higher xanthan gum mass concentration (1.0 wt% and 1.5 wt%), the axial penetration times of the Newtonian secondary fluid and the non-Newtonian secondary fluid were relatively the same owing to the hindrance caused by the higher viscous nature of the primary fluid. The advection created at higher primary flow rates led to a more effective axial transport of the secondary fluid in a shorter time span.

  As the xanthan gum mass concentration increased from 0.5 wt% to 1.5 wt%, the radial dispersion of the secondary fluid in the primary fluid was enhanced. These results demonstrated that the SMX static mixer is more effective for the mixing applications of higher viscous fluids.

- Consistent with the existing literature, our research findings also revealed that the radial mixing quality was independent of the primary flow rates for the centerline injection. However, the time taken to reach the 5th tomography plane became shorter at higher primary flow rates. In other words, the axial mixing was improved when the primary flow rate was increased.

From the CFD study, the following conclusion can be drawn:

- Unlike Kenics KM static mixer, a lower primary/secondary flow ratio was suitable for the SMX static mixer applications for the mixing of two miscible fluids. Lowering the primary/secondary flow ratio led to a higher secondary/primary fluid velocity ratio since the injection pipe and the main pipe diameters were kept constant throughout the numerical study. The shearing effect caused by the high-velocity secondary fluid alleviated the viscosity of the shear thinning primary fluid and the SMX static mixer was able to disperse the secondary fluid into the primary fluid more effectively.

- SMX static mixer was found to be effective for the mixing applications of higher viscous secondary fluids. This enhanced the radial dispersion of higher viscous secondary fluid in the primary fluid more effectively. From the radial velocity profiles, it was inferred that the radial velocity was enhanced and moved away from the centre of the static mixer signifying an effective radial dispersion of the secondary fluid in the primary fluid. The primary/secondary fluid flow ratio of 0.5 was chosen for this numerical study in order to capture the prominent features in the radial velocity profile.

6.1 FUTURE RECOMMENDATIONS

The experimental and the numerical work conducted in this study drew attention to the areas for future considerations as follows:

- To extend the experimental and the CFD work for other applications such as solid/liquid, gas/liquid, and immiscible liquid/liquid mixing in the SMX static mixer

- To extend this work on other static mixers and to compare them with respective to the parameters studied in this work (i.e. Primary/secondary flow ratio, Secondary fluid viscosity range, and Primary fluid rheology)

BIBLIOGRAPHY

Amirtharajah, A., & Jones, S.C., (1996). Mixing for coagulation: Organic polymers, static mixers and modelling. *Chemical water and wastewater treatment IV* (pp. 3-15). Berlin: Springer-Verlag.

Al-Taweel, A.M., Walker, L.D., (1983). Liquid Dispersion in Static In-Line Mixers. *The Canadian Journal of Chemical Engineering*, 527-533.

Alberini, F., Simmons, M. J., Ingram, A., & Stitt, E. H. (2014). Assessment of different methods of analysis to characterize the mixing of shear-thinning fluids in a Kenics KM static mixer using PLIF. *Chemical Engineering Science*, 152-169.

Amirtharajah, A., & Jones, S. (1996). Mixing for coagulation: Organic polymers, static mixers and modelling. *Chemical water and wastewater treatment IV* (pp. 3-15). Berlin: Springer-Verlag.

Amirtharajah, A., & Jones, S. C. (1996). Mixing for coagulation: Organic polymers, static mixers and modelling. *Chemical water and wastewater treatment IV* (pp. 3-15). Berlin: Springer-Verlag.

Anon. (1979). Enter the motionless mixer. *Food technology in New Zealand*, 55-56.

Arratia, P. E., Kukura, J., Lacombe, J., & Muzzio, F. J. (2006). Mixing of shear-thinning fluids with yield stress in stirred tanks. *AIChE J.*, 2310-2322.

Assefa, K. M., & Kaushal, D. R. (2015). A comparative study of friction factor correlations for high concentrate slurry flow in smooth pipes. *Journal of Hydrology and Hydromechanics*, 13-20.

Austvik, T., & Loken, K. P. (1992). Deposition of CO2 on the seabed in the form of hydrates. *Energy conversion and Management*, 659-666.

Avalosse, T. (1996). Numerical simulation of distributive mixing in 3-D flows. *Macromol. Symp*, 91-98.

Buckingham, E., (1921). On plastic flow through capillary tubes. *ASTM Proceeding*, 1154-1161.

Bandyopadhyay, T.K., Sandhibigraha, S., & Das, S.K., (2014). Experimental and CFD analysis of non-Newtonian pseudoplastic liquid flow through vertical helical coil. *American Journal of fluid dynamics*, 56-68.

Bahpaj, R. K., & Reuss, M. (1982). Coupling of mixing and microbial kinetics for evaluating the performance of bioreactors. *Can.J.Chem.Eng.*, 384-392.

Bajpai, P. (1999). Application of enzymes in the pulp and paper industry. *Biotechnology progress*, 147-157.

Berkman, P. D., & Calabrese, R. V. (1988). Dispersion of viscous liquids by turbulent flow in a static mixer. *AlChE*, 602-609.

Bird, R. B. (1956). Correlation of friction factors in non-Newtonian flow. *AlChE*, 1-2.

Bird, R. B., Stewart, W. E., & Lightfoot, E. N. (2002). *Transport Phenomena.* New York: John Wiley & Sons, Inc.

Blenke, H. (1979). Loop Reactors. *Adv.Biochem.Eng*, 121-124.

Boer, R. d., Zomerman, J., Hiddink, J., Aufderheyde, J., Swaaij, W. v., & Smolders, C. (1980). Fluidized beds as turbulence promoters in the concentration of food liquids by reverse osmosis. *J.Food.Sci*, 1522-1528.

Boilyky, L. J. (1981). The mass transferof ozone into water: Energy requirements-State of the art. *Ozone: Science & Engineering*, 181-210.

Bolmstedt, U. (2000). *Viscosity & Rheology: Theoretical and practical considerations in liquid food processing.* Russell Publishing Ltd.

Bor, T. P. (1971). Kenics static engineering. *Food trade review*, 25-28.

Boss, J., & Czastkiewics, W. (1982). Principles of scale-up for laminar miixng process of Newtonian fluids in static mixer. *Int.Chem.Eng*, 362-367.

Braun, H., Hoeren, A., .Schneiders, T., Vortmeyer, K., & Pfost, H. (1998). Measurement of the mixing quality in premix combustors. *Energy conversion and management*, 1991-1999.

Buckingham, E. (1921). On plastic flow through capillary tubes. *ASTM Proceeding*, 1154-1161.

Burke, J. C. (1996). *Effectiveness of static mixers for enhanced coagulation.* Atlanta: Georgia Institute of Technology.

Barber, C.D., Brown, B.H., & Freeston, I.L., (1983). Imaging Spatial Distribution of Resistivity Using Applied Potential Tomography. *Electron.Lett*, 933-935.

Bauman, I., (2001). Solid-Solid Mixing with Static Mixers. *Chem. Biochem. Eng. Q*, 159-165.

Baker, J.R., (1991). Motionless mixers stir up new uses. *Chem Eng Prog*, 32-38.

Cao, Q., Ventresca, A.L., Sreenivas, K.R., Prasad, A.K. (2003). Instability due to viscosity stratification downstream of a centerline injector. The Canadian Journal of Chemical Engineering, 81 913-922.

Copse, A.L., & Middleman, S., (1974). Use of Convection Promotion in the Ultrafiltration of a Gel-Forming Solute. *Ind.Eng.Chem.Process Des.Develop.*, 143-145.

Colebrook, C.F., (1938-1939). Turbulent flow in pipes with particular reference to the transition region between the smooth and rough pipe laws. *Journal of the Institution of Civil Engineering*, 133-156.

Chandra, K. G., & Kale, D. D. (1992). Pressure drop for laminar flow of viscoelastic fluids in static mixers. *Chemical Engineering Science*, 2097-2100.

Chang, G. S., Koo, J. S., & Song, K. W. (2003). Wall slip of vaseline in steady shear rheometry. *Korea-Australia Rheology Journal*, 55-61.

Chella, R., & Ottino, J. M. (1985). Stretching in some classes of fluid Motions and asymptotic mixing efficiencies as a measure of flow classification. *Archive for rational mechanics and analysis*, 15-42.

Chemineer. (n.d.). *Chemineer TM (Reliability and Tehnology in Mixng)*. Retrieved from Chemineer: www.chemineer.com

Cheng, H., & Manas-Zloczower, I. (1998). Distributive mixing in conveying elements of a ZSK-53 co-rotating twin screw extruder. *Polym Eng Sci*, 926-935.

Chilton, R. A., & Stainsby, R. (1998). Pressure loss equations for laminar and turbulent non-Newtonian pipe flow. *Journal of hydraulic engineering*, 522-529.

Chisti, M. Y. (1989). *Airlift bioreactors.* London: Elsevier Science.

Clark, M., Srivastava, R., Lang, J. S., Trussell, R. R., McCollum, L. J., Bailey, D., . . . Stolarik, G. (1994). Selection and design of mixing processes for coagulation. *AWWA Research Foundation.* Denver.

Clements, F. E. (1905). *Research methods in Ecology.* Lincoln: The University Publishing Company.

Colebrook, C. (1938-1939). Turbulent flow in pipes with particular reference to the transition region between the smooth and rough pipe laws. *Journal of the Institution of Civil Engineering*, 133-156.

Colebrook, C. F. (1938-1939). Turbulent flow in pipes with particular reference to the transition region between the smooth and rough pipe laws. *Journal of the Institution of Civil Engineering*, 133-156.

Copse, A., & Middleman, S. (1974). Use of Convection Promotion in the Ultrafiltration of a Gel-Forming Solute. *Ind.Eng.Chem.Process Des.Develop.*, 143-145.

Cybulski, A., & Wermer, K. (n.d.).

Cybulski, A., & Werner, K. (1986). Static mixers: Criteria for applications and selection. *Int.Chem.Eng*, 171-180.

Cymbalisty, L. M. (2005). *Patent No. US6896007 B2.*

Chang, G.S., Koo, J.S., & Song, K.W., (2003). Wall slip of vaseline in steady shear rheometry. *Korea-Australia Rheology Journal*, 55-61.

Chen, G. H., Liu, Z.L., (2013). Numerical research of pressure drop in Kenics static mixer. *Advanced Materials Research*, 547-550.

Clements, F.E., (1905). *Research methods in Ecology.* Lincoln: The University Publishing Company.

Cybulski, A., & Werner, K., (1986). Static mixers: Criteria for applications and selection. *Int.Chem.Eng*, 171-180.

Douroumis, D., & Fahr, A., (2006). Nano- and micro- particulate formulations of poorly water-soluble drugs by using a novel optimized technique. *Eur.J.Pharm.Biopharm*, 173-175.

Derradji, A.F. Bernabeu-Madico, A., Taha, S., & Dorange, G., (2000). The effect of static mixer on the ultrafiltration of a two-phase flow. *Desalination*, 223-230.

Danckwerts, P. V. (1951-3). The definition and measurement of some characteristics of mixtures. *Appl. Sci. Research A3*, 279-296.

Danckwerts, P. V. (1953). Continuous flow systems distribution of residence times. *Chem. Engng Sci.*, 1-13.

De Boer, R., Zomerman, J. J., Hiddink, J., Aufderheyde, J., Van Swaay, W. P., & Smolders, C. A. (1980). Fluidized beds as turbulence promoters in the concentration of food liquids by reverse osmosis. *J.Food.Sci*, 1522-1528.

Dejmek, P., Funeteg, B., Hallstrom, B., & Winge, L. (1974). Turbulence promoters in ultrafiltration of whey protein concentrate. *Journal of food science*, 1014-1017.

Derradji, A. F., Bernabeu-Madico, A., Taha, S., & Dorange, G. (2000). The effect of static mixer on the ultrafiltration of a two-phase flow. *Desalination*, 223-230.

Derradji, A., Bernabeu-Madico, A., Taha, S., & Dorange, G. (2000). The effect of static mixer on the ultrafiltration of a two-phase flow. *Desalination*, 223-230.

Diggle, P. J. (2003). *Statistical analysis of spatial point patterns.* New York: Oxford University Press.

Diggle, P. J., & Matern, B. (1980). On sampling designs for the study of Point-Event Nearest Neighbor Distributions in R2. *Scand.J.Stat.*, 80-84.

Dillon, G. B., & Harris, I. J. (1966). Determination of mass transfer coefficients and interfacial areas in Gas-liquid contacting systems. *The Canadian Journal of Chemical Engineering*, 307-312.

Dillon, G.B., & Harris, I.J., (1966). Determination of mass transfer coefficients and interfacial areas in Gas-liquid contacting systems. *The Canadian Journal of Chemical Engineering*, 307-312.

Dong, Y., Ng, W. K., Hu, J., Shen, S., & Tan, R. B. (2010). A continuous and highly effective static mixing process for antisolvent precipitation of nanoparticles of poorly water-soluble drugs. *Int.J.Pharm.*, 256-261.

Douroumis, D., & Fahr, A. (2006). Nano- and micro- particulate formulations of poorly water-soluble drugs by using a novel optimized technique. *Eur.J.Pharm.Biopharm*, 173-175.

Ess, J. W., & Hornsby, P. R. (1986). Characterization of distributive mixing in thermoplastic composition. *Polymer testing*, 205-218.

Ein Mozaffari, F., Dumont, G.A., Bennington, C.P.J. (2003). Performance and design of agitated pulp stock chests. Appita journal, 56(2), 127-133.

Ein Mozaffari, F., Bennington, C.P.J., Dumont, G. A. (2005). Suspension yield stress and the dynamic response of agitated pulp chests. Chemical engineering science, 60(8-9), 2399-2408.

Fourcade, E., Wadley, R., Hoefsloot, H.C.J., Green, A., & Iedema, P.D., (2001). CFD calculations of laminar striation thining in static mixer reactors. *Chemical Engineering Science*, 6729-6741.

Fan, S., Gretton-Watson, S. P., Steinke, J. H., & Alpay, E. (2003). Polymerization of methyl methacrylate in a pilot-scale tubular reactor: modelling and experimental studies. *Chemical Engineering Science*, 2479-2490.

Fellows, P. (2000). *Food Processing technology: Principles and practice.* CRC.

Fialova, M., Redlich, K., & Winkler, K. (1985). Axial dispersion of the liquid phase in vertical tubular contactors with static mixers. *Collection Czechoalovak Chem. Commun.*, 1925.

Frascari, D. (2008). A pilot-scale study of alkali-catalysed sunflower oil transesterification with static mixing and with mechanical agitation. *Energy & Fuels*, 1493-1501.

Frascari, D., (2008). A pilot-scale study of alkali-catalysed sunflower oil transesterification with static mixing and with mechanical agitation. *Energy & Fuels*, 1493-1501.

Founargiotakis, K., Kelessidis, V.C., & Maglione, R., (2008). Laminar, transitional and turbulent flow of Herschel-Bulkely fluids in concentric annulus. *The canadian journal of chemical engineering*, 676-683.

Grace, H.P., (1982). Dispersion phenomena in high viscosity immiscible fluid systems and application of static mixers as dispersion devices in such system. *Chemical Engineering Communications*, 225-277.

Guegan, D., Leroux,J., (2010). Predicting chaos with Lyapunov exponents : Zero plays no role in forecasting chaotic systems. *Documents de travail du Centre d'Economie de la Sorbonne*, 1-21.

Garcia, E.J., & Steffe, J.F., (1987). Comparison of friction factor equations for non-Newtonian fluids in pipe flow. *Journal of food process Engineering*, 93-120.

Garcia, E.J., & Steffe, J.F., (1987). Comparison of friction factor equations for non-Newtonian fluids in pipe flow. *Journal of food process Engineering*, 93-120.

Garcia, E. J., & F, S. J. (1987). Comparison of friction factor equations for non-Newtonian fluids in pipe flow. *Journal of food process Engineering*, 93-120.

Gassmann, P., List, M., Schweitzer, A., & Sucker, H. (1994). Hydrosols-alternatives for the parenteral application of poorly water soluble drugs. *Eur.J.Pharm.Biopharm*, 64-72.

Gavrilescu, M., & Roman, R. V. (1993). Gas hold-up in bubble column and airlift bioreactors with static mixers. *Biotechnology and Bioengineering*, 2.

Gavrilescu, M., Roman, R. V., & Sauciuc, A. (1992). Oxygen transfer in an airlift bioreactor using static mixers. *Biotechnology and Bioengineering*, 60-63.

Grout, K., & Devellian, R. (1974). *Patent No. US3800985 A*. US.

Gudmundsson, J. S., & Borrehaug, A. (1996). Frozen hydrate for transport of natural gas. *Proceedings of the 2nd International Conference on Natural Gas Hydrate*, (pp. 439-446). Toulouse.

Gyebis, J., & Katai, F. (1990). Determination and randomness in mixing of particulate solids. *Chem.Eng.Sci*, 2843-2855.

Harlow, F.H., & Welch, J.E., (1965). A numerical calculation of time dependent viscous incompressible flow of fluid with free surface. *Phys. Fluids*, 2182-2189.

Hobbs, D.M., Swanson, P.D., & Muzzio, F.J., (1998). Numerical characterization of low Reynolds number flow in the Kenics static mixer. *Chemical Engineering science*, 1565-1584.

Hiddink, J., Kloosterboer, D., & Bruin, S., (1980). Evaluation of static mixers as convection promoters in the ultrafiltration of dairy liquids. *Desalination*, 149-167.

Hobbs, D.M., (1997). *Characterization of a Kenics Static Mixer under Laminar Flow Conditions.* The State University of NewJersey.

Hobbs, D.M., & Muzzio, F.J., (1997). The Kenics static mixer: a three dimensional chaotic flow. *Chemical Engineering journal*, 153-166.

Hobbs, D.M., & Muzzio, F.J., (1998). Optimization of a static mixer using dynamical systems techniques. *Chemical Engineering Science*, 3199-3213.

Hobbs, D.M., & Muzzio, F.J., (1998). Reynolds number effects on laminar miixng in the Kenics static mixer. *Chemical Engineering Journal*, 93-104.

Harvey, R., Gallaher, T., T.L.Small, & Mullikin, R. (1982). *Patent No. CA 1117107 A1*.

Heindel, H. L., Hardy, S. A., Amirtharajah, A., & Arrowood, M. J. (1999). Disinfection of cryptosporidium parvum with static mixers. *Proc. AWWA Water Quality Technology Conf.*, (pp. TU12-16). Denver.

Hessel, V., Hardt, S., Lowe, H., & Schonfeld, F. (2003). Laminar mixing in different interdigital micromixers: I.Experimental characterization. *AlChE*, 566-577.

Hobbs, D., & Muzzio, F. (1997). The Kenics static mixer: a three dimensional chaotic flow. *Chemical Engineering journal*, 153-166.

Hobbs, D., & Muzzio, F. (1997). The Kenics static mixer: a three-dimensional chaotic flow. *Chemical Engineering Journal*, 153-166.

Hobbs, D., Swanson, P., & Muzzio, F. (1998). Numerical characterization of low Reynolds number flow in the Kenics static mixer. *Chemical Engineering science*, 1565-1584.

Hsu, K. H. (1974). Kansas State University.

Hsu, K. H., Erickson, L. E., & Fan, L. T. (1975). Oxygen transfer to mixed cultures in tower system. *Biotechnology and bioengineering*, 499-514.

Iliuta, I., & Larachi, F. (2003). Concept of bifunctional redox iron-chelate process for H2S removal in pulp and paper atmospheric emissions . *Chemical engineering science*, 5305-5314.

Jaffer, S. A., & Wood, P. E. (1998). Quantification of laminar mixing in the Kenics static mixer: An experimental study. *The Canadian Journal of Chemical Engineering*, 516-521.

Junker, Seamans, Ramsubramanyan, Aunins, & Adrian. (1994). Cultivation of Attenuated Hepatitis a Virus Antigen in a Titanium Static Mixer Reactor. *Biotechnology & Bioengineering*, 1315.

Karoui, A., Hakenholz, F., Sauze, N., Costes, J., & Bertrand, J. (1998). Determination of the mixing performance of Sulzer SMV static mixers by Laser Induced Fluorescence. *The Canadian Journal of Chemical Engineering*, 522-526.

Kemblowski, Z., & Pustelnik, P. (1988). Residence time distribution of a power law fluid in Kenics static mixers. *Chemical Engineering Science*, 473-478.

Khan, M. M. (1992). Friction factor and flow characterization of non-Newtonian fluids. *11th Australian Fluid Mechanics Conference* (pp. 1029-1031). Australia: University of Tasmania.

Khinast, J. G., Bauer, A., Bolz, D., & Panarello, A. (2003). Mass-transfer enhancement by static mixers in a wall-coated catalytic reactor. *Chemical Engineering Science*, 1063-1070.

Kilijanski, T. (1989). A method for correction of the wall-slip effect in a Couette rheometer. *Rheologica Acta*, 61-64.

Kiss, N., Brenn, G., Pucher, H., Wieser, J., Scheler, S., Jennewein, H., . . . Khinast, J. (2011). Formation of O/W emulsions by static mixers for pharmaceutical applications. *Chemical engineering science*, 5084-5094.

Komax System. Inc Mixing by Design. (n.d.). Retrieved from Komax: www.komax.com

Kozyuk, O. (2011). *Patent No. WO/2011/071,842*.

Krstić, D., Koris, A., & Tekio, v. (2006). Do static turbulence promoters have potential in cross-flow membrane filtration applications? *Desalination*, 371-375.

Krstic, D., Tekic, M., Caric, M., & Milanovic, S. (2003). Kenics Static Mixer as Turbulence Promoter in Cross-Flow Microfiltration of Skim Milk. *Separation science and technology*, 1549-1560.

Kukukova, A., Aubin, J., & Kresta, S. (2009). A new definition of mixing and segregation: Three dimensions of a key process variable. *Chemical Engineering Research and Design*, 633-647.

Kukukova, A., Aubin, J., & Kresta, S. (2011). Measuring the scale of segregation in mixing data. *The Canadian Journal of Chemical Engineering*, 1122-1138.

Kukukova, A., Noel, B., Kresta, S., & Aubin, J. (2008). Impact of sampling method and scale on the measurement of mixing and coefficient of variaince. *AlChE*, 3068-3083.

Khokhar, A.A., Gudmundsson, J.S., & Sloan, E.D., (1998). Gas storage in structure H hydrates. *Fluid Phase Equilib*, 383-392.

Kukukova, A., Noel, B., Kresta, S.M., & Aubin, J., (2008). Impact of sampling method and scale on the measurement of mixing and coefficient of variaince. *AlChE*, 3068-3083.

Kukukova, A., Aubin, J., & Kresta, S.M., (2009). A new definition of mixing and segregation: Three dimensions of a key process variable. *Chemical Engineering Research and Design*, 633-647.

Kukukova, A., Aubin, J., & Kresta, S.M., (2011). Measuring the scale of segregation in mixing data. *The Canadian Journal of Chemical Engineering*, 1122-1138.

Kalyon, D.M., (2005). Apparent slip and viscoplasticity of concentrated suspensions. *Journal of Rheology*, 621-640.

Krstić, D.M., Koris, A.K., & Tekio, M.N., (2006). Do static turbulence promoters have potential in cross-flow membrane filtration applications? . *Desalination* , 371-375.

Krstic, D.M., Tekic, M.N., Caric, M.D., & Milanovic, S.D., (2003). Kenics Static Mixer as Turbulence Promoter in Cross-Flow Microfiltration of Skim Milk. *Separation science and technology*, 1549-1560.

Kleinermann, F., Avis, N.J., & Alhargan, F.A., (1999). Analytical solution to the three dimensional electrical forward problem for a circular cylinder. *1st World Congress on Industrial Process Tomography*, 189-194.

Kalyon, D. (2005). Apparent slip and viscoplasticity of concentrated suspensions. *Journal of Rheology*, 621-640.

Legrand, J., Morancais, P., & Carnelle, G., (2001). Liquid-liquid dispersion in an SMX-sulzer static mixer. *Trans IChemE*, 949-956.

Lacey, P. M. (1943). Mixing of solid particles. *Trans.Inst.Chem.Eng*, 53-59.

Lam, Y. C., Wang, Z. Y., Chen, X., & Joshi, S. C. (2007). Wall slip of concentrated suspension melts in capillary flows. *Powder Technology*, 162-169.

Lammers, G., Stamhuis, E. J., & Beenackers, A. A. (1993). Continuous production of hydroxypropyl startch in a static mixer reactor. *Starch*, 227-232.

Latimer, R. J., & Amirtharajah, A. (1998). Pilot scale comparison of static mixers and backmix reactors for water tretament. *Proc. Awwa Annual Conf. Denver*, (pp. 705-740). Denver.

Lee, S. S., Erickson, L. E., & Fan, L. T. (1971). Modeling and optimization of a Tower-Type activated sludge system. *Biotechnology and Bioengineeering Symp*, 141-173.

Levenspiel, O. (1972). *Chemical Reaction Engineering.* New York: John Wiley and Sons.

Li, H., Fasol, C., & Choplin, L. (1997). Pressure drop of Newtonian and Non-Newtonian fluids across a Sulzer SMX static mixer. *Trans IChem E*, 792-796.

Li, H., Fasol, C., & Choplin, L. (1998). Heat transfer to Newtonian and non-Newtonian fluids flowing in a sulzer SMX static mixer. *Chem. Eng. Commun*, 1-15.

Li, H., Fasol, C., & Choplin, L. (1998). Residence time distribution of rheologically complex fluids passing through a Sulzer SMX static mixer. *Chemical Engineering Communications*, 1-15.

Lammers, G., Stamhuis, E.J., & Beenackers, A.A.C.M., (1993). Continuous production of hydroxypropyl startch in a static mixer reactor. *Starch*, 227-232.

Lowe, E., & Durkee, E.L., (1971). Dynamic turbulence promotion in reverse osmosis processing of liquid foods. *Journal of food science*, 31-32.

Li, T., & Manas-Zloczower, I. (1995). A study of distributive mixing in counterrotating twin screw extruders. *International polymer processing*, 314-320.

Li, T., & Manas-Zloczower, I. (1995). Evaluation of distributive mixing efficiency in mixing equipment. *Chem.Eng.Commun.*, 223-231.

Lin, C. F., Wu, C., Fang, H., Kuo, T., & Hu, C. (1976). Oxygen transfer and mixing in a tower cycling fermenter. *Biotechnology Bioengineering*, 1557-72.

Liu, S., Hrymark, A. N., & Wood, P. E. (2006). Laminar mixing of shear thinning fluids in a SMX static mixer. *Chemical Engineering Science*, 1753-1759.

Loren, K. P., & Austvik, T. (1993). Deposition of CO2 on the seabed in the form of hydrates, Part II. *Energy Conversion and Management*, 1081-1087.

Lowe, E., & Durkee, E. L. (1971). Dynamic turbulence promotion in reverse osmosis processing of liquid foods. *Journal of food science*, 31-32.

Lin, C.H., Fang, B.S., Wu, C.S., Fang, H.Y., Kuo, T.F.,& Hu, C.Y., (1976). Oxygen transfer and mixing in a tower cycling fermenter. *Biotechnology Bioengineering*, 1557-72.

McKenna, C.J., Humble, D.E., & Hobson, K.L., (1986). Static mixer performance for chlorine mixing. *Proc. Water Pollution Control Federation Annual Conf.* Washington,D.C.

McLaughlin, C.M., & Rushton, J.H., (1973). Interfacial areas of liquid-liquid dispersions from light transmission measurements. *AlChE*, 817-822.

Merchuk, J.C. (1986). Hydrodynamics and Hold-up in Air-Lift Reactors. In N.P.Cheremisinoff, *Encyclopedia of Fluid Mechanics* (pp. 1485-1511). Houston: Gulf Publishing.

Mohamadi, B., Pironneau, O., (2001). *Applied Shape Optimization for Fluids* . Oxford: Oxford Univ. Press.

Madupu, A., Mazumdar, A., Jinsong, Z., Roelant, D., & Srivastava, R., (2005). Electrical resistance tomography for real-time mapping of the solid-liquid interface in tanks containing optically opaque fluids. *Proceedings of the SPIE - the International Society for Optical Engineering*, 36-46.

Margaritis, A., & Sheppard, J.D., (1981). Mixing time and oxygen transfer characteristics of a double Draft-Tube airlift fermenter. *Biotechnology and Bioengineering*, 2117-2135.

Metzner, A.B., (1957). Non-Newtonian Fluid Flow: Relationship between recent pressure drop correlations. *Industrial and Engineering Chemistry*, 1429-1432.

Metzner, A.B., & Reed, J.C., (1955). Flow of Non-Newtonian fluids-Correlation of the laminar, transition and turbulent-flow regions. *AlChE*, 434-440.

Mickaily-Huber, E.S., Bertrand, F., Tanguy, P., Meyer, T., Renken, A., Rys, F.S., & Wehrli, M., (1996). Numerical Simulations of Mixing in an SMRX static mixer. *Chem.Eng.J*, 117-126.

Muzzio, F.J., Swanson,P.D., Ottino, J.M., (1991). The statistics of stretching and stirring in chaotic flows. *Phys.Fluids A*, 822-834.

Montante, G., Mostek, M., Jahoda, M., & Magelli, F., (2005). CFD simulation and experimental validation of homogenization curves and mixing times in stirred Newtonian and Pseudoplastic liquids. *Chem.Eng.Sci*, 2427-2437.

Munch, M., & Klein, R., (2012). CFD at its limits: Scaling issues, Uncertain data and the User's role. In J.Schmidt, *Process and Plant Safety* (pp. 189-212). Wiley-VCH.

Mackley, M. R., & Saraiva, R. (1999). The quantitative description of fluid mixing using Lagrangian-and concnetrated-based numerical approaches. *Chem. Erg. Sci*, 159-170.

Mansour, H., Sohn, M., Al-Ghananeem, A., & DeLuca, P. (2010). Materials for pharmaceutical dosage forms: molecular pharmaceutics and controlled release drug delivery aspects. *International Journal of Molecular Sciences*, 3298-3322.

Margaritis, A., & Sheppard, J. (1981). Mixing time and oxygen transfer characteristics of a double Draft-Tube airlift fermenter. *Biotechnology and Bioengineering*, 2117-2135.

Martin, N., & Galey, C. (1994). Use of static mixer for oxidation and disinfection by ozone. *Ozone.Sci.Eng*, 455-473.

McGarvey, R., Byth, K., Dixon, C. D., Day, R. W., & Feenstra, J. E. (2005). Field trials and simulations of point-nearest-neigbour distance methods for estimating abalone density. *J.Shellfish Res.*, 393-399.

McKenna, C., Humble, D., & Hobson, K. (1986). Static mixer performance for chlorine mixing. *Proc. Water Pollution Control Federation Annual Conf.* Washington,D.C.

McLaughlin, C., & Rushton, J. (1973). Interfacial areas of liquid-liquid dispersions from light transmission measurements. *AlChE*, 817-822.

Mead, R. (1974). Test for spatial pattern at several scales using data from a grid of contiguos quadrats. *Biometrics*, 295-307.

Merchuk, C. (1986). Hydrodynamics and Hold-up in Air-Lift Reactors. In N.P.Cheremisinoff, *Encyclopedia of Fluid Mechanics* (pp. 1485-1511). Houston: Gulf Publishing.

Metzner, A. (1957). Non-Newtonian Fluid Flow: Relationship between recent pressure drop correlations. *Industrial and Engineering Chemistry*, 1429-1432.

Metzner, A., & Reed, J. (1955). Flow of Non-Newtonian fluids-Correlation of the laminar, transition and turbulent-flow regions. *AlChE*, 434-440.

Mickaily-Huber, E. S., Bertrand, F., Tanguy, P., Meyer, T., Renken, A., Rys, F. S., & Wehrli, M. (1996). Numerical Simulations of Mixing in an SMRX static mixer. *Chem.Eng.J*, 117-126.

Middleman, S. (1974). Drop size distributions produced by turbulent pipe flow of immiscible fluids through a static mixer. *Ind.Eng.Chem.Process.Des.Develop*, 78-83.

Mohr, W. D., Saxton, R. L., & Jepson, C. H. (1957). Mixing in laminar-flow systems. *Industrial and Engineering Chemistry*, 1855-1856.

Mooney, M. (1931). *Journal of Rheology*.

Manglik, K.R., (2003). *Heat Transfer Handbook.*

McCue, L.S., Troesch,A.W., (2011). Contemporary Ideas on Ship Stability and Capsizing in Waves. In A. L.S.McCue, *Use of Lyapunov exponents to predict chaotic vessel motions* (pp. 415-432). Springer Netherlands.

Morancais, P., Hirech, K., Carnelle, G., & Legrand, J. (1999). Friction factor in static mixer and determination of geometric parameters of SMX sulzer mixers. *Chemical Engineering Communication*, 77-93.

Myers, J., Bakker, A., & Ryan, D. (1997). Avoid agitation by selecting static mixers. *Chemical Engineering Progress*, 28.

Nigam, K. D., & Vasudeva, K. (1980). Residence Time Distribution In Static Mixer. *The Canadian Journal of Chemical Engineering*, 543-544.

Nauman, E. B., (2002). *Chemical reactor design, optimization and scale-up.* New York: McGraw-Hill.

Ohgaki, K., Takano, K., & Moritoki, M. (1994). Exploitation of CH4 hydrates under the Nankai Trough in combination with CO2 storage. *Kagaku Kogaku Ronbunshu*, 121-123.

Olivier, A., & Oosterhuis, N. (1988). Oxygen mass transfer in Non-Newtonian fermentation. In D.G.Bobichon, & G.Florent, *8th International Biotechnology Symposium* (pp. 398-409). Paris: Societe Franqaise de Microbiologie.

Onken, U., & Weiland, P. (1983). Airlift Fermenters: Construction Behaviour and Uses. In A. a. Mizrahi, *Advances in Biotechnological Processes* (pp. 67-95). New York: Alan R. Liss, Inc.,.

Ottino, J. M. (1983). Mechanical miixng efficiency parameter for static mixers. *AlChE*, 159-161.

Olivier, A.P.C., & Oosterhuis, N.M.G., (1988). Oxygen mass transfer in Non-Newtonian fermentation. In D.G.Bobichon, & G.Florent, *8th International Biotechnology Symposium* (pp. 398-409). Paris: Societe Franqaise de Microbiologie.

Patel, D., Ein Mozaffari, F., Mehrvar, M. (2012). Effect of impeller type on continuous-flow mixing of non-Newtonian fluids in stirred vessels through dynamic tests. The Canadian Journal of Chemical Engineering, 90, 290-297.

Patel, D., Ein Mozaffari, F., Mehrvar, M. (2013). Using a tracer technique to identify the extent of non-ideal flows in the continuous mixing of non-Newtonian fluids. EPJ web of conferences, 50, 01006P1-P7.

Patel, D., Ein Mozaffari, F., Mehrvar, M. (2015). Effect of rheological parameters on non-ideal flows in the continuous-flow mixing of biopolymer solutions. Chemical Engineering Research and Design, 100, 126-134.

Pahl, M., & Muschelknautz, E. (1982). Static mixers and their applications. *Int Chem Eng*, 197.

Paul, D., & Newman, S. (1978). *Polymer Blends.* New York: Academic Press.

Paul, E., V.A.Atiemo-Obeng, & Kresta, S. (2004). *Handbook of industrial mixing .* Wiley Online Library.

Peri, C., & Dunkley, W. (1971). REVERSE OSMOSIS OF COTTAGE CHEESE WHEY 2. Influence of flow conditions. *Journal of food science*, 395-396.

Pitera, E., & Middleman, S. (1973). Convection promotion in tubular desalination membranes. *Ind. Eng. Chem.Process Des. Dev*, 52-56.

Prandtl, L. (1935). The mechanics of viscous fluids. *In: Durand,W.F.(Ed): Aerodynamics Theory*, 34-208.

Pustelnik, P. (1985). Investigation of residence time distribution in Kenics static mixers. *Chemical Engineering and Processing: Process Intensification*, 147-154.

Patankar, S.V., & Spalding, D., (1972). A calculation procedure for heat, mass, and momemtum transfer in 3-D parabolic flows. *Int.J.Heat Mass Transfer*, 1787-1806.

Paul, D.R., & Newman, S., (1978). *Polymer Blends.* New York: Academic Press.

Paul, E.L., Atiemo-Obeng, V.A., & Kresta, S.M., (2004). *Handbook of industrial mixing.* Wiley Online Library.

Rader, R. G., Mutsakis, M., Grosz-Roell, F., & Maugweller, W. (1989). Better Absorption? Try a Static Mixer. *Chemical Engineering*, 137-142.

Rao, I. J., & Rajagopal, K. R. (1999). The effect of the slip boundary condition on the flow of fluids in a channel. *Acta Mechanica*, 113-126.

Ranade, V.V., (2002). *Computational flow modelling for chemical reactor engineering.* San Diego: ACADEMIC PRESS.

Rao, M. A., & Anantheswaran, R. C. (1982). Rheology of fluids in food processing. *Food Technology*, 116-126.

Reardon, S. F., & O'Sullivan, D. (2004). Measures of spatial segregation. *Socio Method*, 121-162.

Regner, M., Ostergren, K., & Tragardh, C. (2006). Effects of geometry and flow rate on secondary flow and the mixing process in static mixers- A numerical study. *Chemical Engineering science*, 6133-6141.

Rodriguez, F., Grotz, L. C., & .Engle, D. L. (1961). Interfacial area in liquid-liquid mixing. *ALCHE Journal*, 663- 665.

Rulyov, N. N. (1999). Application of ultra-flocculation and turbulent micro-flotation to the removal of fine contaminants from water. *Colloids and Surfaces A: Physicochemical and Engineering Aspects* , 283-291.

Rodriguez, F., Grotz, L.C., & Engle, D.L., (1961). Interfacial area in liquid-liquid mixing. *ALCHE Journal*, 663- 665.

Rusnac, L. M., Floarea, O., & Vlades, R. V. (1992). Continuous hydrogenation of vegetable oils in reactors equipped with static mixers. *JAOCS*, 384-386.

Sukhadia, A.M., Datta, A., & Baird, D.G., (1992). Mixing history on the morphology and properties of thermoplastic/LCP blends. *Intern. Polymer Processing VII*, 218-228.

Schulgen,B.F., Amirtharajah,A.,& Jones, S.C., (1996). Effectiveness of static mixers for coagulation in water treatment. *Proc.AWWA Annual conf.*, (pp. 121-147). Denver.

Sarghini, F., Romano, A., & Masi, P., (2013). Effect of different viscocity on optimal shape of static mixers for food industry. *Chemical Engineering Transcations*, 1753-1758.

Song, H-S., Han, S.P., (2005). A general correlation for pressure drop in a Kenics static mixer. *Chemical engineering science*, 5696-5704.

Slijepcevic, S., & Peric, D., (2000). Some aspects of computational modelling of non-Newtonian fluids based on stabilised finite element methods. *European Congress on Computational Methods in Applied Sciences and Engineering*, 1-15.

Saeed, S., F.Ein-Mozaffari, & S.R.Upreti. (2008). Using computational fluid dynamics to study the dynamic behaviour of the continuous mixing of Herschel-Bulkley fluids. *Ind.Eng.Chem.Res*, 7465-7475.

Saji, A., & H.Yoshida. (1992). Fixation of carbondioxide by clathrate-hydrate. *Energy Conversion and Management*, 643-649.

Saji, A., Noda, H., & Takamura, Y. (1995). Dissolution and sedimentation behavior of carbon dioxide clathrate. *Energy Conversion and Management*, 493–496 .

Schulgen, B., Amirtharajah, A., & Jones, S. (1996). Effectiveness of static mixers for coagulation in water treatment. *Proc.AWWA Annual conf.*, (pp. 121-147). Denver.

Sencza, W. (1984). *Patent No. US 4470907 A*.

Shah, N. F., & Kale, D. D. (1991). Pressure drop for laminar flow of non-Newtonian fluids in static mixers. *Chemical Engineering Science*, 2159-2161.

Siadat, B., Lundberg, R., & R.W.Lenz. (1980). Preparation of an ionomer elastomer by continuous sulfonation in an extruder and neutralization in static mixers. *Polymer Engineering & Science*, 530-534.

Siegel, M. H., Hallaile, M., & Merchuck, J. C. (1988). Airlift reactor: Design, operation and applications. In *Upstream processes, equipment and techniques* (pp. 79-124). New York: Alan R. Liss Inc.

Simpson, M. M., & Janna, W. S. (2008). Newtonian and non-Newtonian fluids: Velocity profiles, viscocity data, and laminar flow friction factor equations for flow in a circular duct. *2008 ASME International Mechanical Engineering Congress and Exposition*, (pp. 1-8). Boston.

Sochi, T. (2011). *Slip at fluid-solid interface.* London.

Somnuk, K., Niseng, S., & Prateepchaikul, G. (2014). Optimization of high free fatty acid reduction in mixed crude palm oil using circulation process through static mixer reactor and pilot-scale of two-step process. *Energy conversion and Management*, 374-381.

Song, H.-S., & Han, S. (2005). A general correlation for pressure drop in a Kenics static mixer. *Chemical Engineering Science*, 5696-5704.

Spencer, R. S., & Wiley, R. M. (1951). The mixing of very viscous liquids. *J.Colloid Sci.*, 133-143.

SPX. (2015). Retrieved from www.spx.com

Stejskal, J., & Potucek, F. (1985). Oxygen transfer in liquids. *Biotechnology and Bioengineering*, 503-508.

Sukhadia, A., Datta, A., & Baird, D. (1992). Mixing history on the morphology and properties of thermoplastic/LCP blends. *Intern. Polymer Processing VII*, 218-228.

Sulzer. (n.d.). Retrieved from www.sulzer.com

Tajma, H., Yamasaki, A., & Kiyono, F. (2004). Continuous formation of CO2 hydrate via a Kenics-type static mixer. *Energy and Fuel*, 1451-1456.

Taweel, A. A., Yan, J., Azizi, F., Odedra, D., & H.G.Gomaa. (2005). Using in-line static mixers to intensify gas–liquid mass transfer processes. *Chemical engineering science* , 6378-6390.

Thakur, R., Vial, C., Nigam, K., Nauman, E., & Djelveh, G. (2003). Static mixers in the process industries- A review. *Trans IChemE*, 787.

Thompson, J. C., & He, B. B. (2007). Biodesel production using static mixers. *ASABE 50*, 161-165.

Torres, A.P., & Oliveira, F.A.R., (1998). Residence time distribution studies in continuous thermal processing of liquid foods: a review. *Journal of food engineering*, 1-30.

Thomas,D.G., Griffith,W.L., & Keller, R.M., (1971). The role of turbulence promoters in hyperfiltration plant optimization. *Desalination*, 33-50.

Torres, A., & Oliveira, F. (1998). Residence time distribution studies in continuous thermal processing of liquid foods: a review. *Journal of food engineering*, 1-30.

Tripathi, G., & Mishra, P. (1970). Friction factor & velocity profile correlations for purely viscous non-Newtonian fluids. *Journal of scientific and industrial research*, 397- 402.

Ugwu, C., Ogbonna, J., & Tanaka, H. (2002). Improvement of mass transfer characteristics and productivities of inclined tubular photobioractors by installation of internal static mixers. *Appl Microbiol Biotechnol*, 600-607.

Vanderwaal, M. J., Vandervelden, P. M., Koning, J., Smolders, C. A., & VanSwaaij, W. P. (1977). Use of fluidized beds as turbulence promotors in tubular membrane systems. *Desalination*, 465-483.

Virgil, G., Trice, J., & Rodger, W. A. (1956). Light transmittance as a measure of interfacial area in liquid-liquid dispersions. *AlChE*, 205-210.

Voth, G. A., Haller, G., & Gollub, J. P. (2002). Experimental Measurements of Stretching Fields in Fluid Mixing. *Physical Review Leters*, 2545011-2545014.

Versteeg, H.K., & Malalasekera, W., (2007). *An introduction to computational fluid dynamics: The finite volume method.* England: Pearson Education Limited.

Ventresca, A.L., Cao, Q., Prasad, A.K. (2002). The influence of viscosity ratio on mixing effectiveness in a two-fluid laminar motionless mixer. The Canadian Journal of Chemical Engineering, 80 614-621.

Wang, W., & Manas-Zloczower, I., (2001). Temporal distribution: the basis for the development of mixing indexes for scale-up of polymer processing equipment. *Polymer engineering and science*, 1068-1077.

Waggener, J. P. (1961). Friction factors for pressure-drop calculations. *Nucleonics*, 145-147.

Walters, K., & Webster, M. F. (2003). The distinctive CFD challenges of computational rheology. *International journal for numerical methods in fluids*, 577-596.

Weltmann, R. N. (1956). Friction factors for flow of Non-Newtonian materials in pipelines. *Industrial and Engineering Chemistry*, 386-387.

Wittrup, K. D. (2007, Spring). *Course materials for 10.37 Chemical and Biological Reaction Engineering.* Retrieved 05 7, 2015, from Massachusetts Institute of Technology: http://ocw.mit.edu

Wong, D. (2004). Comparing traditional and spatial segregation measures: A spatial scale perspective. *Urban Geography*, 66-82.

Wong, D. (2005). Formulating a general spatial segregation measure. *The Prof Geogr*, 285-294.

Wong, D. W. (2002). Modelling local segregation: a spatial interaction approach. *Georgr Environ Model*, 81-97.

Wong, T. H., & Manas-Zloczower, I. (1994). Two dimensional dynamic study of the distributive mixing in an internal mixer. *International polymer processing*, 3-10.

Wolf, A., Swift,J.B., Swinney, H.L., Vastano, J.A., (1985). Determining Lyapunov exponents from a time series. *Physica 16D*, 285-317.

Walters, K., & Webster, M.F., (2003). The distinctive CFD challenges of computational rheology. *International Journal for Numerical Methods in Fluids*, 577-596.

Xu, G., Feng, L., Li,Y., & Wang, K., (1997). Pressure Drop of Pseudo-Plastic Fluids in Static Mixers. *Chinese Journal Chemical Engineering*, 93–96.

Xia, B., & sun, D.-W. (2002). Applications of computational fluid dynamics (CFD) in the food industry: a review. *Computers and Electronics in Agriculture*, 5-24.

Yang, H.C., (2007). Mixing characteristics of motionless mixers. *Visualization Society of Japan*, 83-89.

Yang, H., & Park, S. (2004). Pressure drop in motionless mixers. *International Journal*, 526-532.

Yenjaichon,W., Grace, J.R., Lim, C.J., Bennington, C.P.J. (2012). In-line jet mixing of liquid-pulp-fibre suspensions: Effect of concentration and velocities. Chemical Engineering Science, 75, 167-176.

Yenjaichon,W., Grace, J.R., Lim, C.J., Bennington, C.P.J. (2014).Mixing quality in low consistency fibre suspensions downstream of an in-line mechanical mixer measured by electrical resistance tomography., Nordic Pulp and Paper Research Journal, 29 (3), 392-400.

Yoshinaga, M., S.Katsuki, M.Miyazaki, L.liu, S.I.Kihara, & K.Funatsu. (2000). Mixing mechanism of three-tip kneading block in twin screw extruders. *Polym Eng. Sci*, 168-178.

Yamasaki, A., Wakatsuki, M., Teng, H., Yanagisawa, Y., & Yamada, K. (2000). A new ocean disposal scenario for anthropogenic CO2: CO2 hydrate formation in a submerged crystallizer and its disposal. *Energy conversion and management*, 85-96.

Yamasaki, A., Wakatsuki, M., Teng, H., Yanagisawa,Y., & Yamada, K., (2000). A new ocean disposal scenario for anthropogenic CO2: CO2 hydrate formation in a submerged crystallizer and its disposal. *Energy conversion and management*, 85-96.

Zhou, C., & Wang, Z. (2010). *Case study of introducing heavy aromatics in blending diesel fuel.* Sino-Global Energy/Zhongwai Nengyuan.

Zalc, J. M., Szalai, E. S., Muzzio, F. J., & Jaffer, S. (2002). Characterization of flow and mixing in an SMX static mixer. AIChE Journal, 48(3), 427-436

Zalc, J. M., Szalai, E. S., Muzzio, F. J. (2003). Mixing dynamics in the SMX static mixer as a function of injection location and flow ratio. Polym Eng Sci, 43(4), 875-890